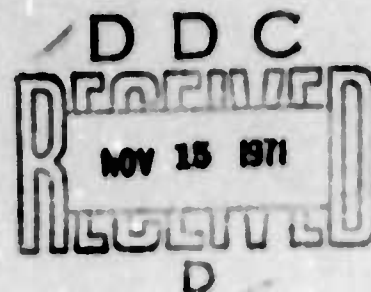AD732284

Faraday Cup Detectors

Prepared by H. H. HILTON and J. R. STEVENS
Space Physics Laboratory

71 JUN 15

D D C

NOV 15 1971

D

Laboratory Operations
THE AEROSPACE CORPORATION

APPROVED FOR PUBLIC RELEASE:
DISTRIBUTION UNLIMITED

126

DOCUMENT CONTROL DATA - R & D

(Security classification of title, body of abstract and indexing annotation must be entered when the overall report is classified)

1. ORIGINATING ACTIVITY (Corporate author)	2a. REPORT SECURITY CLASSIFICATION
The Aerospace Corporation El Segundo, California	Unclassified
	2b. GROUP

3. REPORT TITLE

Faraday Cup Detectors

4. DESCRIPTIVE NOTES (Type of report and inclusive dates)

5. AUTHOR(S) (First name, middle initial, last name)

Henry H. Hilton and John R. Stevens

6. REPORT DATE	7a. TOTAL NO. OF PAGES	7b. NO. OF REFS
71 JUN 15	129	29

8a. CONTRACT OR GRANT NO.	9a. ORIGINATOR'S REPORT NUMBER(S)
F04701-71-C-0172	TR-0172(2260-20)-3
b. PROJECT NO.	
c.	9b. OTHER REPORT NO(S) (Any other numbers that may be assigned this report)
d.	SAMSO-TR-71-222

10. DISTRIBUTION STATEMENT

Approved for public release; distribution unlimited

11. SUPPLEMENTARY NOTES	12. SPONSORING MILITARY ACTIVITY
	Space and Missile Systems Organization Air Force Systems Command Los Angeles, California

13. ABSTRACT

The study of low-energy charged particles, in the range from 1 to 10 keV, through the use of Faraday cup detectors is documented. In 1961, the design of the first Faraday cup was initiated, and the final Faraday cup was placed in orbit in 1968. The development of these instruments is described, and observations from successful launches are discussed.

DD FORM 1473
(FACSIMILE)

LABORATORY OPERATIONS

The Laboratory Operations of The Aerospace Corporation is conducting experimental and theoretical investigations necessary for the evaluation and application of scientific advances to new military concepts and systems. Versatility and flexibility have been developed to a high degree by the laboratory personnel in dealing with the many problems encountered in the nation's rapidly developing space and missile systems. Expertise in the latest scientific developments is vital to the accomplishment of tasks related to these problems. The laboratories that contribute to this research are:

Aerodynamics and Propulsion Research Laboratory: Launch and reentry aerodynamics, heat transfer, reentry physics, propulsion, high-temperature chemistry and chemical kinetics, structural mechanics, flight dynamics, atmospheric pollution, and high-power gas lasers.

Electronics Research Laboratory: Generation, transmission, detection, and processing of electromagnetic radiation in the terrestrial and space environments, with emphasis on the millimeter-wave, infrared, and visible portions of the spectrum; design and fabrication of antennas, complex optical systems, and photolithographic solid-state devices; test and development of practical superconducting detectors and laser devices and technology, including high-power lasers, atmospheric pollution, and biomedical problems.

Materials Sciences Laboratory; Development of new materials; metal matrix composites and new forms of carbon; test and evaluation of graphite and ceramics in reentry; spacecraft materials and components in radiation and high-vacuum environments; application of fracture mechanics to stress corrosion and fatigue-induced fractures in structural metals; effect of nature of material surfaces on lubrication, photosensitization, and catalytic reactions; and development of prothesis devices.

Plasma Research Laboratory; Reentry physics and nuclear weapons effects; the interaction of antennas with reentry plasma sheaths; experimentation with thermonuclear plasmas; the generation and propagation of plasma waves in the magnetosphere; chemical reactions of vibrationally excited species in rocket plumes; and high-precision laser ranging.

Space Physics Laboratory; Aeronomy; density and composition of the atmosphere at all altitudes; atmospheric reactions and atmospheric optics; pollution of the environment; the sun, earth's resources; meteorological measurements; radiation belts and cosmic rays; and the effects of nuclear explosions, magnetic storms, and solar radiation on the atmosphere.

THE AEROSPACE CORPORATION
El Segundo, California

14

KEY WORDS

Faraday Cups

Retarding Potential Analyzers

Plasma Probes

Low Energy Particles

Distribution Statement (Continued)

Abstract (Continued)

.

Air Force Report No.
SAMSO-TR-71-222

Aerospace Report No.
TR-0172(2260-20)-3

FARADAY CUP DETECTORS

Prepared by

H. H. Hilton and J. R. Stevens
Space Physics Laboratory

71 JUN 15

Laboratory Operations
THE AEROSPACE CORPORATION

Prepared for

SPACE AND MISSILE SYSTEMS ORGANIZATION
AIR FORCE SYSTEMS COMMAND
LOS ANGELES AIR FORCE STATION
Los Angeles, California

Approved for public release; distribution unlimited

ABSTRACT

The study of low-energy charged particles, in the range from 1 to 10 keV, through the use of Faraday cup detectors is documented. In 1961, the design of the first Faraday cup was initiated, and the final Faraday cup was placed in orbit in 1968. The development of these instruments is described, and observations from successful launches are discussed.
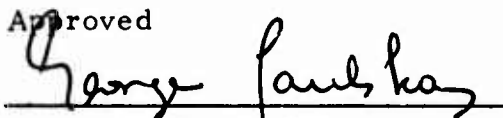
FOREWORD

This report is unusual in that it documents a development program that was not a success. Frustrated by an incredible sequence of launch and satellite failures, and tantalized by glimpses of mysterious phenomena, this line of development of low-energy particle detectors was overtaken and bypassed by new developments in detector technology and was terminated. This report is thus a historical record of years of effort and a monument to persistence.

This report, which documents research carried out from July 1962 through June 1970, was submitted for review and approval on 7 July 1971 to Capt Ronald P. Fuchs, SYAE.

Approved

G. A. Paulikas, Director
Space Physics Laboratory

Publication of this report does not constitute Air Force approval of the report's findings or conclusions. It is published only for the exchange and stimulation of ideas.

Ronald P. Fuchs, Capt, USAF
Project Officer

-ii-

CONTENTS

CONTENTS (Continued)

FIGURES

TABLES

I. INTRODUCTION

Since its inception in 1961, the Aerospace Space Physics Laboratory
has been engaged in the study of particles in the earth's radiation belts,
auroral zones, and polar caps. It was apparent from the beginning, however,
that a complete understanding of such phenomena would be possible only
when information was available on particle behavior over a wide range of
energies.

This report documents a study of low-energy charged particles, in
the range from 1 to 10 keV, that has been conducted since 1961 when design
of the original Faraday cup detector was initiated. Improvements to the
Faraday cup detector were made during this period, but recent electronic
advances have replaced it with the low-energy electrostatic analyzer for
these ranges.

In 1968, the final three Faraday cup detectors and the first pair of
low-energy electrostatic analyzers developed by Aerospace were flown on
three Air Force satellites that were conducting low-energy particle
experiments.

A general description of the Faraday cup detector is presented in
Section II. Section III contains a history of the various instruments and the
satellites used to obtain the measurements. The development, calibration,
and testing of these instruments is detailed in Sections IV and V. Observa-
tions from successful launches are presented in Section VI, and the conclu-
sions resulting from this study are presented in Section VII.

II. DESCRIPTION OF FARADAY CUP DETECTORS

A. GENERAL OPERATION

The Faraday cup detector is an instrument designed to measure the directional differential energy spectra of low-energy protons and electrons. Two important characteristics of the detector are its large geometric factor and its low-energy thresholds for charged particles.

Faraday cups are known by many names — plasma probes, plasma cups, ion traps, and retarding potential analyzers. The simplest configuration (Fig. 1) consists of a collector, located behind an entrance grid, that is held at a potential V relative to the spacecraft (and presumably relative to the plasma being observed). This potential prevents charged particles of certain energies from reaching the collector. For example, with a positive retarding voltage V applied to the collector, the current at the collector will be proportional to the flux of positive ions whose parallel energy per unit charge $E_{\parallel}$ is greater than eV. This current will also be proportional to the flux of electrons (and negative ions) of all energies.

An important factor to be considered is the concept of parallel energy per unit charge $E_{\parallel}$. The electric field produced by the voltage difference between the grid and the collector acts only on the component of velocity parallel to the field. The transverse component is unaffected; hence,

$$E_{\parallel} = 1/2 \ MV_{\parallel}^2/|Z|$$

$$= E \cos^2\theta/|Z| \tag{1}$$

where θ is the angle between the instrument normal and the velocity vector.

The plasma probe used on Explorer X (Fig. 2) (Bridge, et al., 1963) was a more complex instrument and employed four grids. At the front of the probe, the outer grid G_4 was held at the potential of the satellite skin to limit the

-3-
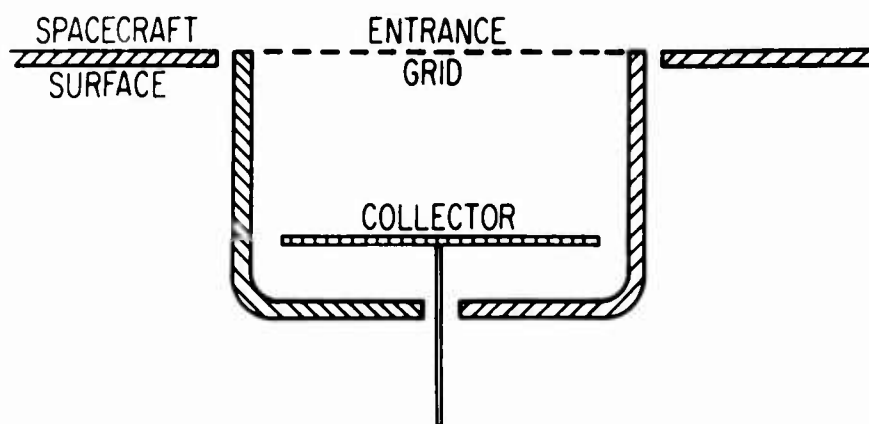
Fig. 1. Simple Faraday Cup Detector
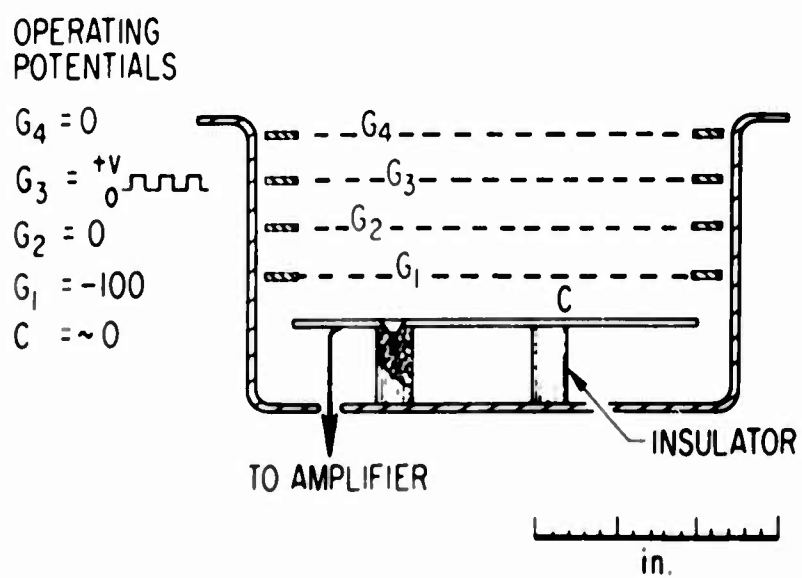
Fig. 2. Plasma Probe on Explorer X

fringing fields of the instrument. A square-wave potential, with values O and V, was applied to grid G_3. Thus, the modulated current at the collector was proportional to the flux integrated from essentially zero energy per unit charge to the limits of $E_{\parallel}$ given by Eq. (1). Grids G_2 and G_1 reduced capacitive coupling between the modulating grid G_3 and the collector C. Grid G_1 was at -100 V with respect to the collector C. This voltage suppressed both the photoelectric current from the collector due to ultraviolet radiation and the secondary emission current from the collector due to the impact of positive ions. On Explorer X, six different amplitudes of the modulating voltage were used; hence, five values of a differential energy spectrum could be obtained by successive subtractions.

The first Faraday cup detector of the Space Physics Laboratory, which evolved from the original design of Mozer, et al. (1962), was flown on USAF satellite 1964-45A. Although many improvements have been made in the electronic circuitry, construction, and reliability since the original flight, the basic concept has remained relatively unchanged. The instrument (Fig. 3) uses seven grids. Grid G_1 is at ground to contain the field due to grid G_2 within the instrument. Grid G_3 is at ground and serves to shield the two high-voltage grids G_2 and G_4 from one another. Grids G_5 and G_6 at ground potential and grid G_7 at -90 V serve to attenuate the electrostatic coupling between grid G_4 and the collector C. In addition to serving as an electrostatic shield, grid G_7 serves to suppress photoelectrons caused by ultraviolet and secondary electrons as a result of particle impact on the collector.

The critical parts of the instrument for energy analysis of incident particles are the two high-voltage grids G_2 and G_4, with G_2 at a positive potential and G_4 at a negative potential. The role of these grids inter-changes, depending upon whether the instrument is in the proton or electron mode. In the proton mode, the positive high-voltage grid G_2 becomes the control grid, and the negative high-voltage grid G_4 becomes the repelling grid. A square-wave voltage, which oscillates between the values $V + v/2$

INCIDENT FLUX

```
          G₁  — — —
          G₂  — — —  — — + HIGH VOLTAGE
          G₃
          G₄  — — —  — — − HIGH VOLTAGE
          G₅
          G₆
          G₇  — — —  — — − 90 V SUPPRESSOR
                              VOLTAGE
```

TO PREAMPLIFIER
AND
SYNCHRONOUS DETECTOR
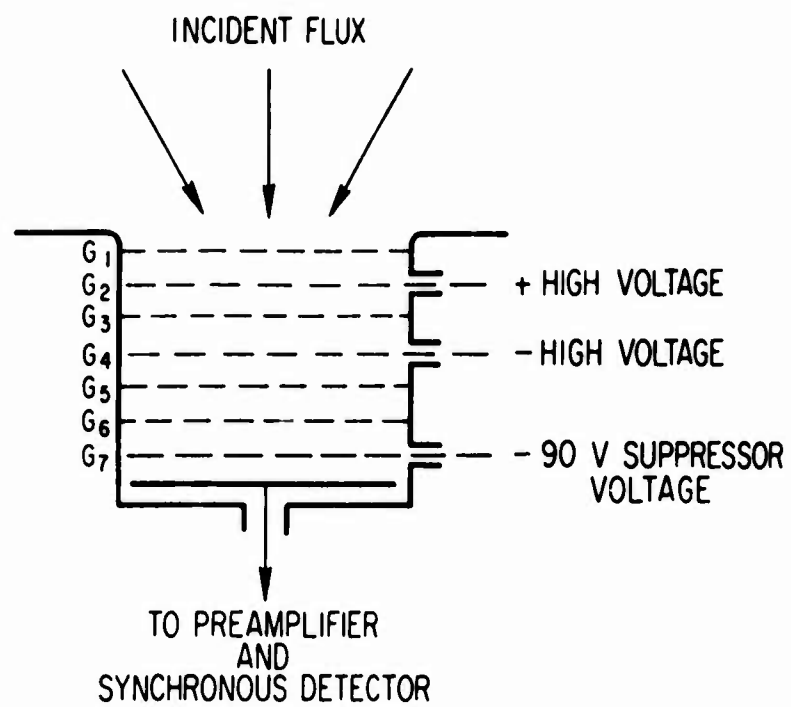
Fig. 3. Typical Faraday Cup Detector of
the Space Physics Laboratory

and $V - v/2$ at a frequency of 2 kHz, is applied to grid G_2. Positively charged particles, whose parallel energy per unit charge $E_{\parallel}$ is less than $V - v/2$, cannot reach the collector, while those with $E_{\parallel}$ greater than $V + v/2$ are unaffected by the modulating voltage and contribute only a direct current to the collector. Hence, the flux of positive ions, whose parallel energy per unit charge is between $V - v/2$ and $V + v/2$, is chopped at the modulating frequency and contributes an alternating current at the collector. This alternating current is converted to a voltage that is amplified, synchronously demodulated, and telemetered. The negative high-voltage grid G_4 is maintained at a high constant voltage V_r and acts as a repelling grid. Its purpose is to repel all negatively charged particles whose $E_{\parallel}$ is less than $|V_r|$ and thus decrease the direct current at the collector. The DC component of the current at the collector is proportional to the algebraic sum of the negatively charged particles whose $E_{\parallel}$ is greater than $|V_r|$, the positively charged particles whose $E_{\parallel}$ is greater than $V + v/2$, and the photoelectrons from G_4 and G_7. A minimum current is desirable to improve the sensitivity of the instrument. This will be discussed in the section that follows.

In the electron mode, the roles of the positive and negative grids are reversed. The modulating voltage is applied to the negative high-voltage grid G_4, and a high constant voltage V_r is applied to the positive high-voltage grid G_2.

B. AC MODULATION AND SYNCHRONOUS DETECTION

Use of the modulating voltage and the accompanying synchronous detector has two distinct purposes. First, it permits direct measurement of the differential flux of charged particles without the problems associated with dc drifts. Second, the synchronous detection of the signal improves the signal-to-noise ratio of the system by effectively narrowing the bandwidth.

Let us examine the modulation and detection system by means of a Fourier analysis. As shown in Fig. 4, the modulation on the control grid V_g,
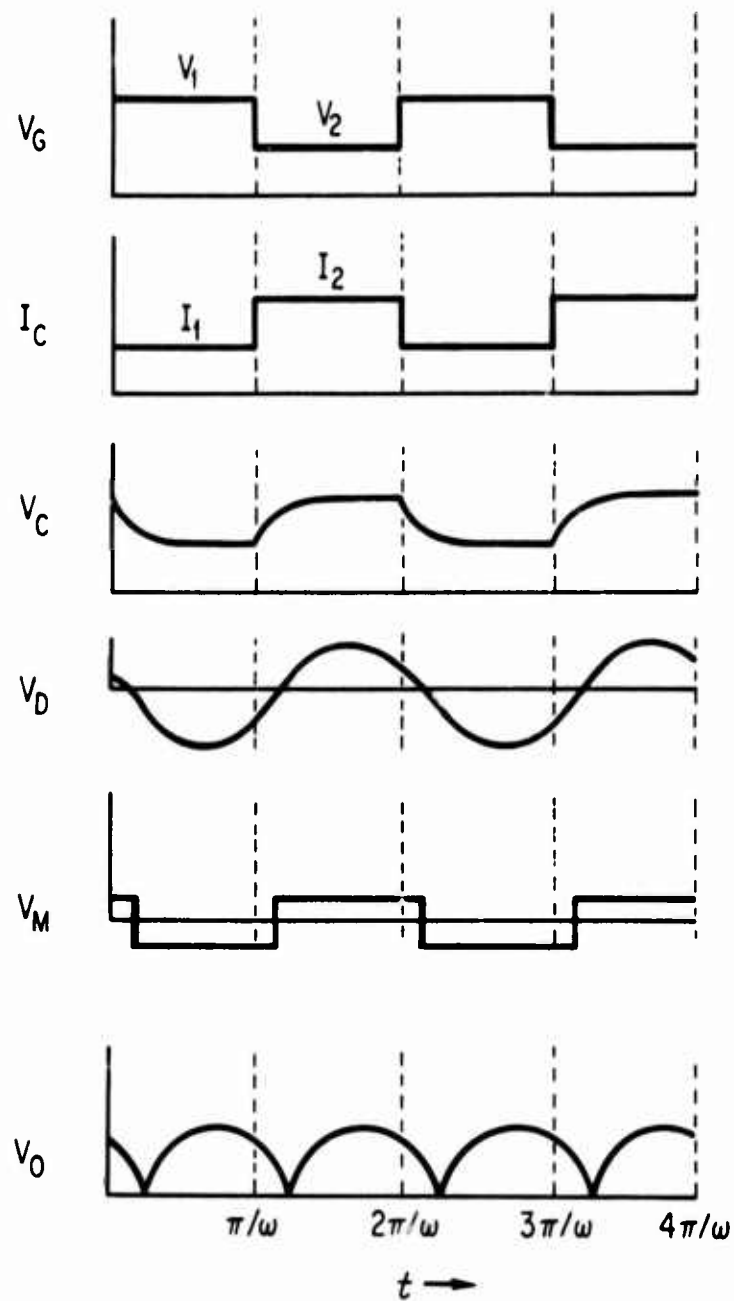
Fig. 4. Voltage and Current Waveforms
that Pertain to Modulation and
Synchronous Detection

-8-

is a square wave whose values are V_1 and V_2. Then the current at the collector will also be a square wave with values I_1 and I_2. The Fourier expansion for this current is:

$$I_c = \frac{I_1 + I_2}{2} + \frac{2}{\pi} (I_1 - I_2) \sum_{n=0}^{\infty} \frac{1}{(2n+1)} \sin \left[(2n+1) \frac{2\pi t}{T} \right] \qquad (2)$$

There is an effective resistance at the preamplifier to convert the incident current to a voltage, and associated with this resistance is a stray capacitance. As shown in Fig. 5, a voltage V_c is developed across the parallel combination of R and C due to the current I_c. This voltage V_c is:

$$\frac{V_c}{R} = \frac{I_1 + I_2}{2} + \frac{2}{\pi} (I_1 - I_2) \sum_{n=0}^{\infty} \frac{\sin \left[(2n+1) \frac{2\pi t}{T} - \tan^{-1} (2n+1) \frac{2\pi \tau}{T} \right]}{(2n+1) \left[1 + \left((2n+1) \frac{2\pi \tau}{T} \right)^2 \right]^{1/2}}$$

$$(3)$$

where $\tau = RC$.

In the system being discussed, neither the DC component of the signal nor the higher harmonics are amplified; therefore, the output voltage V_D before demodulation is given by:

$$\frac{V_D}{R} = A \cdot \frac{2}{\pi} (I_1 - I_2) \frac{\sin \left[\frac{2\pi t}{T} - \tan^{-1} \frac{2\pi \tau}{T} \right]}{\left[1 + \left(\frac{2\pi \tau}{T} \right)^2 \right]^{1/2}} \qquad (4)$$

where A is the voltage gain of the system.

The stray capacitance contained in the time constant τ has two effects: It introduces both a phase delay in the signal by an amount $\tan^{-1} 2\pi\tau/T$ and a

decrease in gain by the factor $\left[1 + \left(\frac{2\pi\tau}{T}\right)^2\right]^{1/2}$. For these reasons, it is desirable to keep τ as small as possible.

This signal is mixed with the modulating voltage V_M, the original modulating voltage delayed by an amount $\tan^{-1} 2\pi\tau/T$. The result produces the full-wave rectified voltage V_o, which, when filtered, produces a DC output voltage proportional to the original flux. In fact, this output voltage V_F, which is found when the voltage V_o is averaged over a half-cycle, is:

$$\frac{V_F}{R} = A \cdot \frac{4}{\pi^2} \frac{I_1 - I_2}{\left[1 + \left(\frac{2\pi\tau}{T}\right)^2\right]^{1/2}}$$

This demodulation is shown schematically in Fig. 6. For noise considerations, it is of interest to consider the frequency response of this system when the demodulating current $S(t)$ is $\sin \omega_o t$, and the signal current $I(t)$ is $I_o \sin \omega t$. Then the resulting current is the product of these two, $I_o \sin \omega_o t \sin \omega t$, and the output voltage is:

$$\frac{V}{R} = \frac{I_o}{2} \left\{ \frac{\cos\left[(\omega - \omega_o) t - \tan^{-1} (\omega - \omega_o)\tau\right]}{\left[1 + (\omega - \omega_o)^2 \tau^2\right]^{1/2}} - \frac{\cos\left[(\omega + \omega_o) t - \tan^{-1} (\omega + \omega_o)\tau\right]}{\left[1 + (\omega + \omega_o)^2 \tau^2\right]^{1/2}} \right\}$$

$$(6)$$

Thus, the output voltage is the sum of two voltages whose frequencies are the sum and the difference of the signal frequency and the demodulating frequency. It is clear that maximum output will result when $\omega \sim \omega_o$. Also, at these frequencies the term with frequency $\omega + \omega_o$ may be neglected
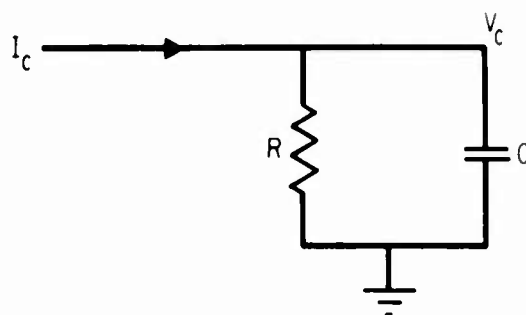
Fig. 5. Idealized Preamplifier Input
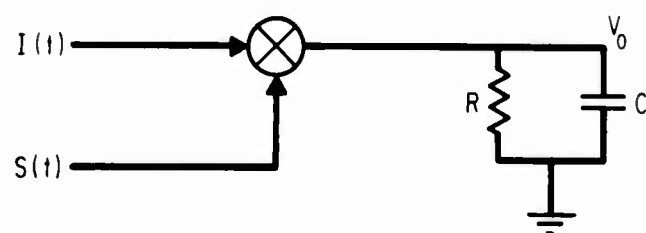
Fig. 6. Idealized Demodulator
and Output Filter

in comparison with the term with frequency $\omega - \omega_o$ because of their respective denominators. In fact, this system acts as a filter of center frequency ω_o and bandwidth $B = (2\tau)^{-1}$.

This result is important as the noise sources are proportional to the bandwidth. The shot noise generated in the preamplifier is:

$$\overline{i_s^2} = 2qIB \tag{7}$$

where I is the drain current of the input field effect transistor, q is the electronic charge, and B is the bandwidth. For I = 1 mA, the shot noise current is 1.8×10^{-11} A/cycle$^{1/2}$.

The thermal, or Johnson, noise current due to a resistance R is:

$$\overline{i_j^2} = 4kTB/R \tag{8}$$

where k is the Boltzmann constant (1.38×10^{-23} J/°K), T is the temperature in degrees Kelvin, and B is again the bandwidth. For an input resistance of 1 MΩ, the Johnson noise current is 1.3×10^{-13} A/cycle$^{1/2}$.

From the foregoing discussion, it would appear that the noise from these two sources can always be reduced to an insignificant value by reducing the bandwidth. The relationship derived from Eq. (6), $B = (2\tau)^{-1}$, shows, however, that decreasing the bandwidth is accomplished by increasing the output time constant. For maximum information retrieval through the spacecraft telemetry system, the output time constant should be between one-quarter and one-half the sampling period. In most cases, this was one sample/sec. Consequently, a time constant of 0.5 sec was chosen, which resulted in an instrument bandwidth of 1 Hz. The previous noise current analysis clearly indicates that care must be taken to measure currents of 10^{-12} A or less.

C. GEOMETRICAL FACTORS

The current detected by a Faraday cup detector is related to the incident flux by the following expression:

$$I = q \int nt \, dA \, d\Omega \, dE \tag{9}$$

where

I = collector current (A)

q = electronic charge (coulombs)

n = differential flux (particles cm^{-2}-sec^{-1}-sr^{-1}-keV^{-1})

t = transmission factor of all the grids

dA = differential area of the collector (cm^2)

$d\Omega$ = differential solid-state angle (sr)

dE = differential energy (keV).

In general, for particles in the magnetosphere, the differential flux is a complicated function of the energy of the particles and of their angles with respect to the magnetic field. Thus, in a coordinate system fixed in the instrument, the differential flux is a function of the polar angle θ, with respect to the axis of the instrument, and the azimuthal angle ϕ about this axis. Because of the finite thickness of the grids, the transmission factor t is a function of the angle θ, decreasing as θ increases, and may be expressed as:

$$t = t_o f(\theta) \tag{10}$$

This expression is the transmission factor for all the grids. Finally, for a detector whose control grid is modulated between two values V_1 and V_2,

-13-

the energy of particles accepted E_{acc} is a function of the angle θ and is

$$\frac{|q|V_1}{\cos^2\theta} \leq E_{acc} \leq \frac{|q|V_2}{\cos^2\theta} \tag{11}$$

Mathematically, the simplest case to analyze is when the solid angle subtended by the collector is small. Then we have

$$I = qnt_o \Delta A \Delta\Omega \Delta E$$

or

$$n = \frac{I}{qt_o \Delta A \Delta\Omega \Delta E} \tag{12}$$

The Faraday cup detector is useful, however, because of its large geometric factor; hence, the integration of Eq. (9) must be done more precisely. Mathematically, it is easier to treat distributions whose energy and angular dependences are separable. Distributions that are either uniform in energy or a delta function of energy (monoenergetic flux) over the range of interest, or that are uniform in angle or a delta function of angle (unidirectional flux) can be analyzed in a straightforward manner.

Two cases are of particular interest. The first case involves a flux that is uniform in energy and angle over the energy and angular acceptances of the detector. This approximates conditions in many regions of the magnetosphere. If we refer to Fig. 7 and use Eqs. (9), (10), and (11), we may write:

$$I = qn_o t_o \Delta E_o \int \frac{f(\theta) dA_1 dA_2}{d^2} \tag{13}$$

-14-
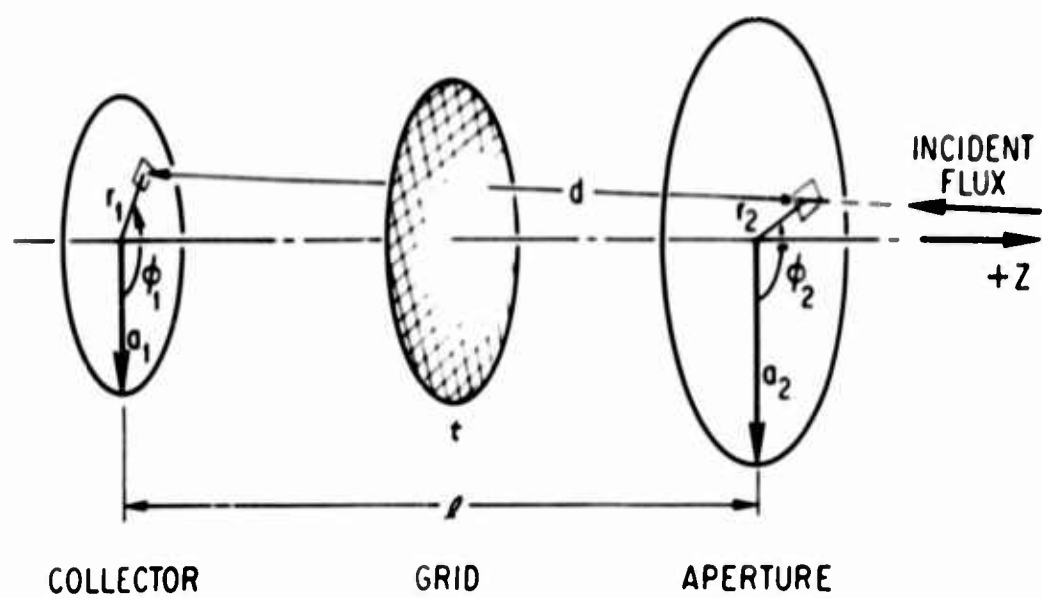
Fig. 7. Faraday Cup Geometry for Calculating
Geometrical Factors

where

$$\Delta E_o = q(V_2 - V_1).$$ (14)

If we note that $l = d \cos \theta$, and let $x_1 = r_1/a_1$, $x_2 = r_2/a_2$, $\alpha_1 = a_1/l$, and $\alpha_2 = a_2/l$, we have:

$$I = q n_o t_o \Delta E_o G_o F$$ (15)

where G_o is the first-order geometric factor and is given by:

$$G_o = \frac{A_1 A_2}{l^2}.$$ (16)

F is a correction factor given by:

$$F = \frac{1}{\pi^2} \int f(\theta) \cos^2\theta \; x_1 \; dx_1 x_2 \; dx_2 \; d\phi_1 \; d\phi_2$$ (17)

where

$$\cos^2\theta = \frac{1}{1 + x_1^2\alpha_1^2 + x_2^2\alpha_2^2 - 2x_1 x_2 \alpha_1 \alpha_2 \cos(\phi_2 - \phi_1)}.$$ (18)

The integration over ϕ_2 may be performed, which results in:

$$F = \frac{2}{\pi} \iiint f(\theta) \cos^2\theta x_1 \; dx_1 x_2 \; dx_2 \; d\phi$$ (19)

-16-

where

$$\cos^2\theta = \frac{1}{1 + x_1^2\alpha_1^2 + x_2^2\alpha_2^2 - 2x_1x_2\alpha_1\alpha_2\cos\phi} \qquad (20)$$

In general, the instruments described in this report have equal collector and aperture radii, and the angular dependence of the transmission factor is small. Figure 8 is a graph of the factor F versus the ratio r/l, assuming $f(\theta) = 1$. The instruments described in this report fall into two groups: those with $r/l \sim 0.25$ and those with $r/l \sim 0.50$. This factor is significant in the later case.

The second case of particular interest is that of a unidirectional flux. This approximates the situation found in the solar wind and in laboratory calibrations. The Faraday cups of this laboratory were designed for the study of radiation belt physics, not for solar wind measurements. In the laboratory, calibrations are made with monoenergetic particles and with one of two beam distributions. The first distribution is a beam that is uniform over an area larger than the entrance aperture, and the second is a beam localized over an area that is small compared with the aperture area.

For a unidirectional flux, Eq. (9) may be rewritten as:

$$I = q\int n_A t \, dA_p \, dE \qquad (21)$$

where

    I = collector current (A)

    q = electronic charge (coulombs)

    n_A = directional differential flux (particles cm^{-2}-sec^{-1}-keV^{-1})

    t = transmission coefficient of all the grids
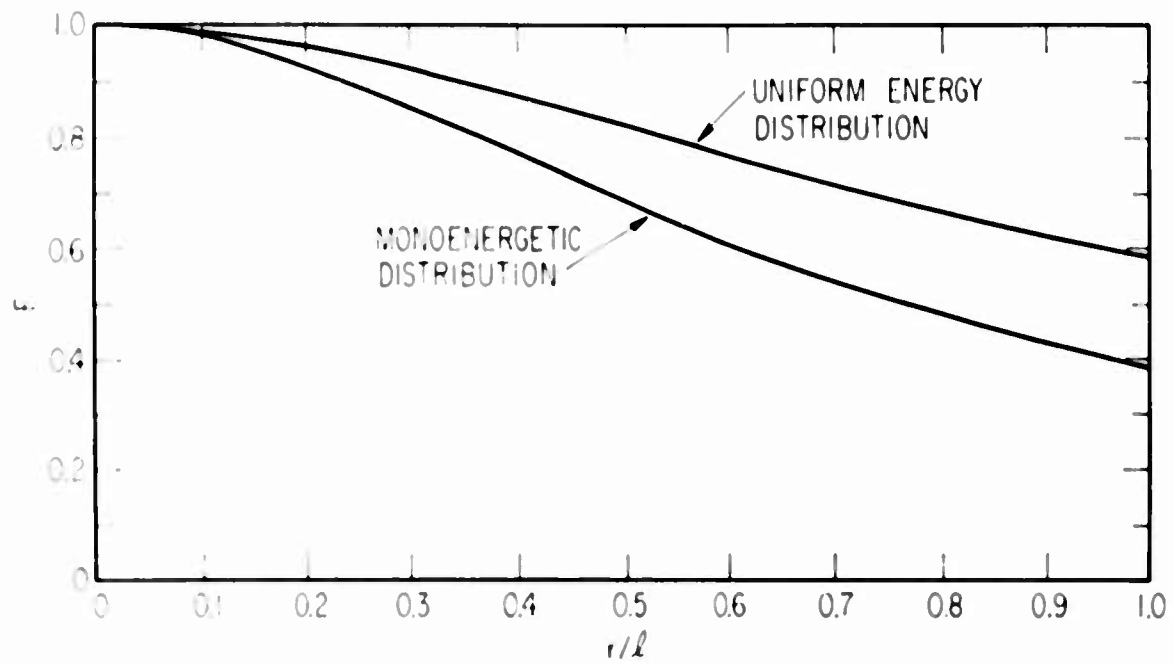
Fig. 8. Correction Factor F as a Function of r/ℓ for
Instruments Having Equal Aperture and Collector
Radii

dA_p = projected differential area of the collector (cm^2)

dE = differential energy (keV).

For a monoenergetic flux, we may perform the integral over dE as follows:

$$N_A = \int n_A \, dE \tag{22}$$

where N_A is the number of particles cm^{-2}-sec^{-1} at an energy E_o. Then, if $t = t_o f(\theta)$ as in Eq. (10), we have:

$$I = qN_A t_o A_M F_1(\theta). \tag{23}$$

A_M is the smaller of two areas: the area of the collector (A_1) or the area of the aperture. E_o must be between the limits as set by Eq. (11). $F_1(\theta)$ is given by:

$$F_1(\theta) = \frac{1}{A_M} \int f(\theta) \, dA_p, \tag{24}$$

which gives the fraction of the projected area as a function of the angle θ.

Let us again refer to Fig. 7 and assume that the collector radius a_1 is less than the aperture radius a_2. Then $A_M = \pi a_1^2$. Thus, after a certain amount of geometry, we find the following expressions for $F_1(\theta)$ for a uniform beam:

$$F_1(\theta) = f(\theta) \cos \theta \text{ for } 0 \le \tan \theta \le \frac{a_2 - a_1}{\ell}$$

$$F_1(\theta) = f(\theta) \cos \theta \left\{ \left(1 - \frac{\alpha_1}{\pi}\right) + \frac{\sin \alpha_1 \cos \alpha_1}{\pi} \right.$$

$$\left. + \frac{a_1^2}{a_2^2} \left[\left(\frac{\alpha_2}{\pi}\right) - \frac{\sin \alpha_2 \cos \alpha_2}{\pi} \right] \right\} \tag{25}$$

for

$$\frac{a_2 - a_1}{\ell} \le \tan \theta \le \frac{a_1 + a_2}{\ell}$$

where

$$\alpha_1 = \cos^{-1} \left(\frac{a_2^2 - a_1^2 - \ell^2 \tan^2 \theta}{2 a_1 \ell \tan \theta} \right)$$

and

$$\alpha_2 = \cos^{-1} \left(\frac{a_2^2 - a_1^2 + \ell^2 \tan^2 \theta}{2 a_2 \ell \tan} \right)$$

$$F_1(\theta) = 0 \text{ for } \frac{a_1 + a_2}{\ell} \le \tan \theta.$$

This function is shown in Fig. 9 for geometries in which a_1 and a_2 are equal, and $f(\theta)$ is 1.
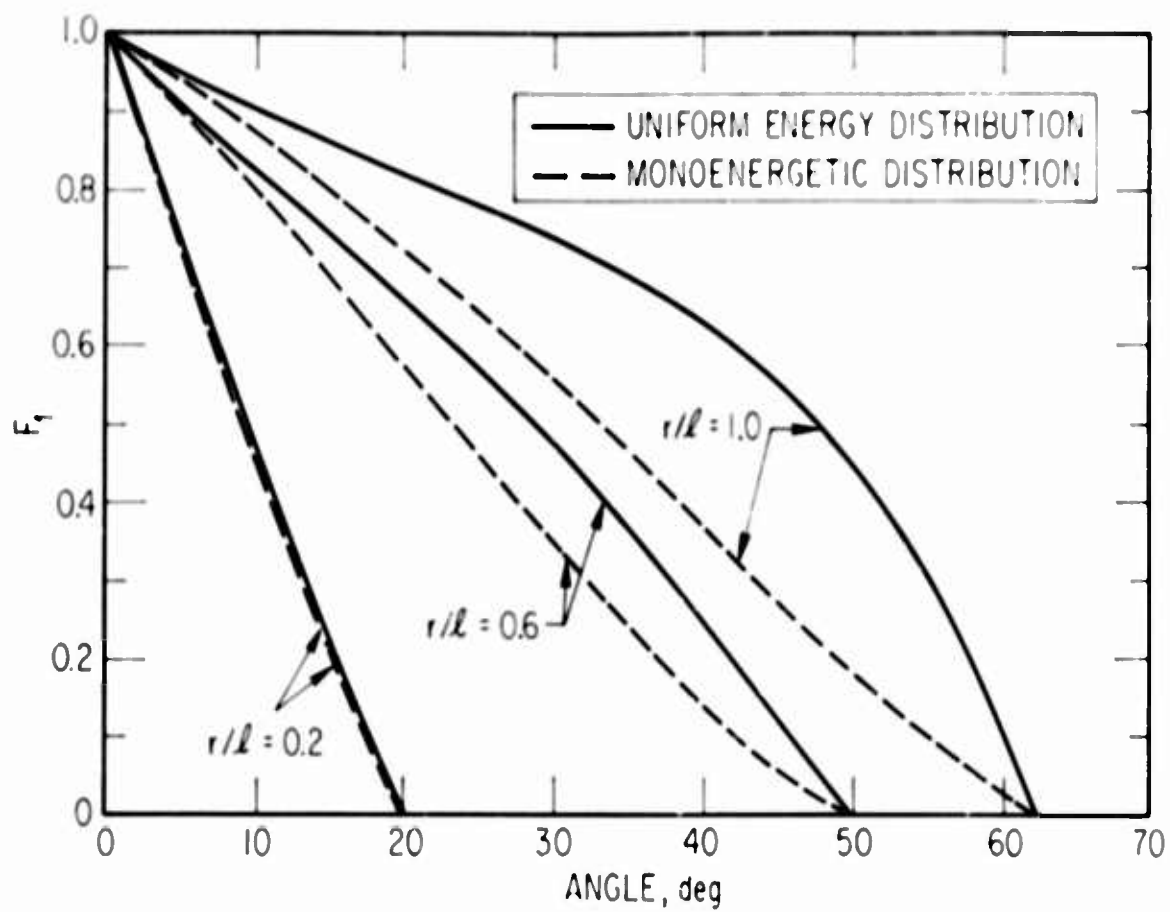
Fig. 9. Correction Factor F_1 as a Function of the Incidence Angle θ for Instruments Having Equal Aperture and Collector Radii

In this case, where the radii of the aperture and collector are equal, the foregoing expressions are simplified considerably. In fact, one finds

$$F_1(\theta) = f(\theta) \cos \theta \left| 1 - \frac{2}{\pi} \left[\sin^{-1} Z + Z (1 - Z^2)^{1/2} \right] \right| \qquad (26)$$

for

$$0 \leq \tan \theta \leq \frac{2a}{l}$$

and

$$F_1(\theta) = 0$$

for

$$\frac{2a}{l} \leq \tan \theta$$

where

$$Z = \frac{l}{2a} \tan \theta.$$

III. HISTORY

A. SUMMARY

When design of the Faraday cup detector began in 1961, essentially no measurements near the earth existed of particles with energy between 1 and 10 keV. Measurements had been made outside the magnetosphere, however, by Gringauz, et al. (1960), Bader (1962), Hoffman, et al. (1962), and Bonetti, et al. (1963). Hoffman, et al., used detectors aboard Explorer 12 to measure the flux of protons with 0.1 to 1.69 MeV energy and the flux of electrons with 10 to 35 keV energy. One-half hour after the sudden commencement of a storm on 30 September 1961, this instrument measured the maximum flux of protons — 2×10^5 protons-cm^{-2}-sec^{-1}-sr^{-1} with energy greater than 140 keV. Peak electron flux was observed one minute prior to the storm's commencement and consisted of a flux of 3×10^6 electrons-cm^{-2}-sec^{-1}-sr^{-1} in the 10 to 35 keV energy interval. These measurements were made at 12 earth radii near local noon. Bader's measurements were also made on Explorer 12. His instrument was a quadraspherical electrostatic analyzer that analyzed protons with 0.1 to 20 keV energy. The proton flux never exceeded the sensitivity threshold for the instrument. This placed an upper limit of 3×10^6 protons-cm^{-2}-sec^{-1}-sr^{-1} -0.1E^{-1} on the proton flux. Gringauz, et al., measured the integral flux of super thermal particles on Lunik 2. Their detectors were capable of measuring plasma density, and observations revealed particles fluxes of 2×10^8 positive ions-cm^{-2}-sec^{-1} with E > 20 eV. This measurement was in interplanetary space and was essentially a measure of the solar wind. The observations of Bonetti, et al., who used a Faraday cup-type detector, were made out to 42 earth radii. At large distances from the earth, fluxes of 10^8 positive ions-cm^{-2}-sec^{-1} with energy between 0 and 800 eV were observed. These were not solar wind measurements. Immediately after launch near the earth, the instrument outputs were dominated by a large flux of positive ions with energy less than 5 eV. No values of flux were determined because of difficulties in understanding the data.

The only measurement inside the magnetosphere that had been reported was by McIlwain (1960). This experiment was flown on a rocket through a visual aurora and employed as the detector a crystal scintillator covered by a thin foil. The instrument was capable of measuring protons with 45 to 2500 keV energy. Flux intensities of 5×10^{10} electrons-cm^{-2}-sec^{-1}-sr^{-1} for electrons with 6 keV energy were detected in a bright, active auroral arc.

The importance of these low-energy protons and electrons in space was unknown. If the energy of spectra continued to increase as particle energy decreased, these low-energy particles could have been the major cause of atmospheric heating and atmospheric optical phenomena. Because of the potential significance of low-energy particles, we decided to measure this component of the near-earth radiation environment. The main reason that this energy region was unexplored was the extreme difficulty involved in detecting the low-energy particles. As discussed previously, we felt that the use of phase-sensitive demodulation would increase current-measurement sensitivity by a factor of 10 or more over existing Faraday cup-type instruments. The original Faraday cup instrument of the Space Physics Laboratory was designed by Mozer, et al. (1962), in 1961. This instrument was similar to that of Explorer X, but it was designed to measure both protons and electrons from 1 to 50 keV. By 1962, the first flight Faraday cup prototype had been constructed. By 1963, successful laboratory tests had been performed, and a flight instrument had been constructed. This instrument measured the differential energy flux of both protons and electrons with energy between 1 and 11 keV. Between 1962 and 1968, 15 Faraday cups with three separate mechanical designs were built for flights on 11 satellites. Of the 11 flights, five provided data. A listing of the various flights for which Faraday cups were built is presented in Table I. The expected or achieved orbit is listed under the heading "Orbit." Under the heading "Experiment" is included the energy range and other

Table I. Flight History of the Faraday Cup

Year	Satellite	Orbit	Experiment	Comments
1964	1964-45A 14 August	140 × 2050 n mi, 96-deg inclination, spin stabilized 62 rpm	0.3 to 11 keV protons and electrons, 20-deg half-angle	Anomalously large proton fluxes observed; electrons present in burst
1965	1602 2 September	92 × 120 n mi, near polar earth oriented	0.1 to 8 keV protons and electrons, 45-deg half angle, insulators shielded from solar uv	Booster destroyed during launch
	OV2-1 15 October	300 × 4000 n mi, 35-deg inclination, spin stabilized	0.1 to 3 keV protons and electrons, correlation with photometer	Trans-stage spun to pieces
	OV2-3 21 December	21,000 n mi; circular, synchronous, equatorial; spin stabilized with active orientation	0.4 to 8 keV protons and electrons; two instruments with grid positions reversed to observe geometry effects on plasma	Separation from truss never occurred
1966	1966-70A (OV3-3) 4 August	200 × 2800 n mi, 81-deg inclination, spin stabilized 9 rpm	0.3 to 11 keV protons and electrons; check if anomalously large proton fluxes were real	Instrument failed after second acquired perigee pass
1967	OV1-11 27 July	298 × 298 n mi, 120-deg inclination gravity gradient	0.2 to 6 keV protons and electrons; three sensors oriented up, down, and parallel to velocity	OV1 injection motor failed to ignite
1968	1968-26B (OV1-14) 6 April	282 × 5370 n mi, 100-deg inclination, spin stabilized 9 rpm	0.3 to 8 keV protons and electrons; check to see if anomalously large proton fluxes were real	Power system failed after 30 orbits; large flux of keV protons was not present; auroral electrons were observed
1968	1968-59A (OV1-15) 11 July	75 × 1000 n mi, 90-deg inclination, spin stabilized 5 rpm, active orientation	0.9 to 6 keV protons and electrons; in-flight comparison of Faraday cup results with ESA results	Faraday cup measured fluxes were con- sistent with ESA measurements; flux was seldom above the Faraday cup threshold
	1968-81A (OV2-5) 26 September	18,956 × 19,308 n mi; equatorial, synchronous; spin stabilized 2 rpm	0.5 to 8 keV protons and electrons; correlation with Lyman - all-sky scanner	Partial satellite failure; Faraday cup measured solar uv; low-electron flux observed
1969	1969-25A (OV1-17) 18 March	217 × 253 n mi, 99-deg inclination, gravity gradient	0.2 to 6 keV protons and electrons, two oriented sensors; one toward zenith and one parallel to velocity	Faraday cups were replaced with electrostatic analyzers
	1969-25C (OV1-19) 18 March	254 × 3129 n mi, 105-deg inclination, spin stabilized 9 rpm	0.2 to 6 keV protons and electrons; check for the anomalously large proton fluxes	Faraday cups were replaced with electrostatic analyzers

instrument-oriented parameters of interest. A brief description of the measurements observed or the problems encountered with the flight is presented in the column headed "Comments." In the paragraphs that follow, each of the planned flights is described in detail, including the experiment objective, instrument parameters, and flight results.

B. DESCRIPTION BY SATELLITE

1. 1964-45A

The Faraday cup was designed to measure the energy spectrum of protons and electrons with energy between 1 and 10 keV. It covered this energy region in four steps centered at 1, 4, 7, and 10 keV, with each step 1.8 keV wide. This left three gaps 1.2 keV wide between the energy measurements. A photograph of this instrument is shown in Fig. 10. The instrument was flown on a satellite in an elliptical polar orbit that was chosen to allow coverage of the inner radiation zone, as well as the polar regions. With the proposed inclination, the line of apsides would process southward at a rate of 2 deg/day. This allowed global coverage of all attainable altitudes at various latitudes every three months. A successful launch took place on 14 August 1964.

Freeman (1962) observed energy deposits as large as 50 ergs-cm^{-2}-sec^{-1}-sr^{-1} in a CdS total energy detector on Injun I. These fluxes were attributed to positive ions with energies above 500 eV. The Faraday cup measured fluxes of positive ions in the same regions of space as Injun I that were consistent with the flux intensity quoted by Freeman. There was no obvious influence of the sun on the data, and the flux at low altitude decreased in inverse proportion to the increase in atmospheric density. The angular dependence of the data was difficult to determine because of the high satellite spin rate and the rapid intrinsic variations of the flux. It was difficult to believe the extremely large flux values that were encountered on almost every orbit. The lack of an internal calibration led us to suspect that the sensitivity of the instrument had changed subsequent to final experimental calibration.

Theoretical work by Prag, et al. (1966), indicated that the observed flux of low-energy protons was at least an order of magnitude too large to account for the observed midlatitude limit of Hα intensity or the temperature of the neutral atmosphere at night.

The electron data was sporadic and appeared to exhibit a seasonal dependence. These measurements by themselves were reasonable, but if the sensitivity of the instrument had changed for protons, it should also have changed for electrons. Because of this possibility, it was doubtful that determination of the absolute flux values for the electron bursts could ever be achieved.

2.   1602

In order to substantiate the results from the Faraday cup on 1964-45A, an improved Faraday cup was built. Instead of measuring the flux in four noncontinuous energy intervals, the measurement was made over a continuous energy range. Several in-flight tests were planned to determine if the flux measurements were dependent on grid voltages or grid geometry in unexpected ways. On 1964-45A, all flux outputs were frequently saturated. The possibility of output saturation was reduced, extending the range of the instrument a factor of 20 toward reduced sensitivity. The overall sensitivity of the instrument was improved by increasing the area of the collector. A photograph of an instrument similar to the one used on the flight is shown in Fig. 11.

Because of the expected atmospheric optical effects caused by large fluxes of protons and electrons with 1 to 10 keV energy striking the atmosphere, a multicolor night-airglow photometer was also flown on this satellite. Thus, correlations of particle flux variations with optical intensity variations in the wavelength regions of 3914 Å, 5577 Å, and 6300 Å were possible. Flux measurements from this instrument could have been compared directly with the results from 1964-45A that was still operating when 1602 was launched. This inflight comparison would have settled the question as to whether the large proton fluxes of 1964-45A were real or instrumental.

Fig. 10. The 1964-45A Faraday Cup
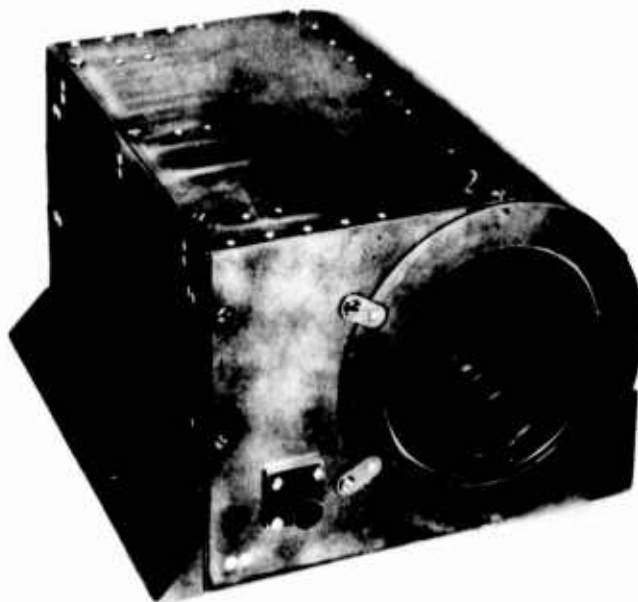
Fig. 11. The 1602 Faraday Cup Before Launch

The launch took place on 2 September 1965, and it was successful until winds drove the booster out of the safety corridor. The range safety officer destroyed the vehicle and the spacecraft at an altitude of approximately 30,000 ft. A photograph of the recovered instrument is shown in Fig. 12.

3.   OV2-1

The OV2-1 vehicle presented another opportunity to verify the existence of the large fluxes of low-energy protons observed on 1964-45A. The proposed orbit traversed the inner radiation zone near the equator. Thi orbit would have made possible the simultaneous measurement of proton fluxes observed on 1964-45A at apogee with measurements of proton flux from the Faraday cup on OV2-1. Should large proton fluxes have existed, one would expect to observe enhanced equatorial night-airglow. An optical photometer sensitive to the 6300 Å red line of atomic oxygen was attached to the Faraday cup. This photometer could detect the tropical red arcs and, along with the Faraday cup, determine whether or not the arcs were caused primarily by protons or electrons with energies of several keV. From previous measurements on 1962 BO1, no correlation between the flux of protons with several MeV energy and the tropical arcs had been observed (Elliott, et al., 1963).

This Faraday cup could measure protons and electrons with energy from 0.1 to 3.0 keV. The energy region was covered by six proton and four electron steps, and the differential energy windows were large enough to allow continuous coverage of the energy interval. Six additional steps were incorporated to look for unexpected interactions between grid potentials and the plasma or between the grid potentials and the solar UV.

The spacecraft was launched on a Titan IIIC from Cape Kennedy on 15 October 1965. One engine on the trans-stage failed to shut down, and the entire trans-stage and spacecraft were spun to pieces. The instrument is similar to that shown in Fig. 11.
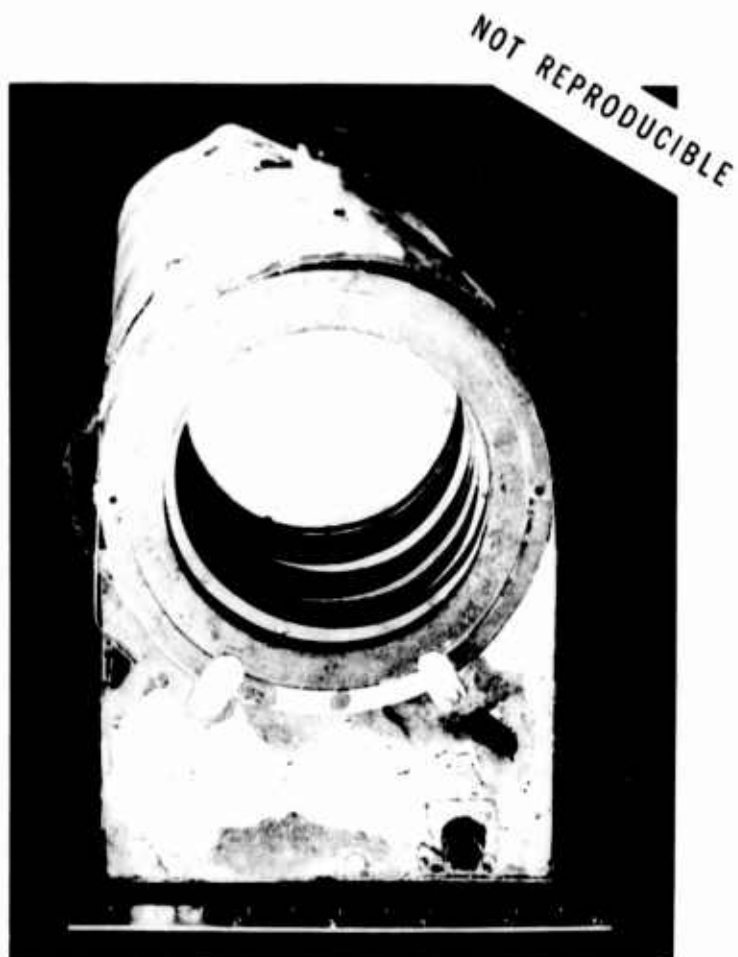
Fig. 12. The 1602 Faraday
Cup After Launch

4.   OV2-3

This satellite gave members of the Space Physics Laboratory their first opportunity to monitor the solar-induced geomagnetic activity and to measure the corresponding variations of the particle flux at synchronous altitude. Had it been successful, the OV2-3 would have been the first United States scientific research satellite in synchronous orbit.   The measurements from 1964-45A indicated a substantial flux of positive ions at an L of 1. 7 in agreement with the measurements of Freeman (1962).   It seemed reasonable to expect that the proton flux would be measurable at synchronous altitudes.   These protons could be a major component of the particle environment at synchronous altitudes.   By means of a spherical electrostatic analyzer, Vernov, et al. (1965), had observed a radiation zone of low energy, 0. 1 to 10 keV electrons, outside the inner radiation belt.   Therefore, it was thought that electrons with several keV of energy could be a major constituent of the synchronous environment. The peak fluxes of 10^9 electrons-cm^{-2}-sec^{-1}-keV^{-1} that were measured on Electron II would have registered midscale on the OV2-3 Faraday cup.

The experiment on OV2-3 consisted of two Faraday cup detectors capable of measuring the flux of protons and electrons with energy from 0. 4 to 8. 0 keV.   One instrument was designated the proton instrument and the other the electron instrument; however, each instrument measured both particles. Essentially, the instruments differed in the relative position of the two high-voltage grids.   In the proton instrument, the positive high-voltage grid was closest to the vehicle skin; while in the electron instrument, the negative high-voltage grid was closest to the skin.   The purpose of this interchange of grids was to determine if the grid position was affecting our results through electrostatic coupling with the plasma near the vehicle or through secondary emission from solar UV striking some grid.   Measurement of the particle flux was achieved in 11 intervals by covering the region from 0. 4 to 8 keV, after which the cup was calibrated.   One calibration step measured the background, and the remaining four steps checked the effect of grid position on the flux measured.   These four steps were synchronized so that both cups were measuring

the same particle at the same energy, at the same time. The instruments are similar to that shown in Fig. 11.

The spacecraft was launched on a Titan IIIC from Cape Kennedy on 21 December 1965. The launch was successful, with three of the four spacecrafts being successfully ejected from the truss into orbit. No ejection signal was received by the OV2-3 spacecraft, and the spacecraft remained passive on the truss.

5.   OV3-3

The Faraday cup on this satellite was intended to substantiate the proton observations from satellite 1964-45A, which had a similar orbit. An improved Faraday cup (Fig. 11) was used to measure the differential flux of protons and electrons with energy from 0.3 to 11 keV. The satellite achieved a successful launch on 4 August 1966, and data from the Faraday cup were obtained for the first three tape-recorded orbits. During the third orbit, an electronic component in the collector circuit failed, and the current sensitivity of the instrument was reduced by a factor of 150. No large fluxes of protons were observed prior to instrument failure. The instrument failed near perigee, at which time the flux outputs were large but negative, and the voltage on the positive high-voltage grid was reduced due to current loading from thermal electrons. Sensitivity of the Faraday cup to solar UV was observed during the electron mode of operation. Limited observations from the OV3-3 Faraday cup during two orbits indicated that the proton observations on 1964-45A should be treated with utmost skepticism.

Outputs were observed in the electron measuring mode that were almost periodic at the spin rate of the vehicle. In most cases, these outputs occurred when the instrument was in the sun and can be attributed to solar UV. Because of the initial tumbling motion of the satellite, however, definite identification of these observations with solar UV were not obtained. The absence of electron flux comparable to that measured on 1964-45A does not invalidate the electron measurements from that satellite because of the

random occurrence of the previous observations. According to the previous electron measurements, the probability of observing an electron burst that exceeded the earlier instruments sensitivity threshold is less than 3 percent for an entire orbit. Hence, the fact that an intense electron burst was not observed on OV3-3 during three orbits was not unexpected. The low flux observed over the auroral zone is below the sensitivity threshold of the 1964-45A instrument. The instrument is shown mounted on the spacecraft in the center of Fig. 13.

6.   OV1-11

This satellite provided us with an opportunity to measure precipitating auroral fluxes from an earth-oriented satellite and to compare these observations with night-airglow measurements. This instrument was sensitive to protons and electrons with energy from 0.2 to 6 keV. The energy interval was covered in seven steps for each particle, with variable step widths proportional to the central energy. Three Faraday cups were used as sensors on the spacecraft, and these detectors looked along the zenith, the nadir, and the anti-velocity direction. Measurements of the sensors were synchronized by a logic circuit in a junction box, and each sensor was programmed to measure the same particle and energy at the same time. Outputs from the three sensors could be switched to a separate IRIG channel by ground station command to obtain a faster time response than was available in the commutated data link. The photometer with which optical correlation had been planned was a multicolor night-airglow photometer sensitive to four wavelength intervals centered at 3914, 5535, and 5577, and 6300 Å.

Launch took place on 27 July 1967. After ejection, the OV1-11 propulsion module failed to burn, and the spacecraft never achieved earth orbit.

7.   OV1-14

This satellite was the third in the series of radiation belt monitoring satellites and again was designed to measure the flux of protons and electrons in the region of space covered by the 1964-45A flight. The instrument used on this satellite was the large aperture cup shown in Fig. 14, with recessed insulators between the high-voltage grids. The instrument measured protons and electrons with energy between 0.3 and 8 keV in seven energy intervals. A complete energy spectrum of protons and electrons was alternately measured. Each energy measurement normally lasted 8 sec. A complete spectrum for both proton and electrons required 128 sec. If a nominal spin period of 10 sec is assumed, each energy interval included sufficient measurements for a pitch angle distribution. The angular distribution enabled us to determine whether the output was due to particles trapped on a magnetic field line or to some spurious signal. Outputs due to solar UV or ram effects were characterized by an angular distribution with one peak for each revolution of the spacecraft, while trapped particles produced two peaks for each revolution.

It was a successful launch, and the satellite functioned properly for several days. The instrument performed correctly, giving calibration signals and occasional outputs. Failure of the satellite was due to overcharging and the subsequent rupture of the battery, but sufficient data had been obtained prior to this failure for us to know that the Faraday cup was functioning properly. The outputs, however, were not consistent with the results from 1964-45A observations. In fact, the proton flux was below the threshold of sensitivity for the entire flight. Outputs were observed in the electron mode that were primarily unidirectional in character and could be attributed to solar UV or the atmospheric ram effect. Outputs were observed in the electron mode during the four auroral passes of the satellite. The flux was below the sensitivity threshold of the 1964-45A instrument. In Fig. 14, the OV1-14 instrument is shown mounted on the lower right-hand corner of the spacecraft.

Fig. 13. The OV3-3 Faraday Cup Mounted on the OV3-3 Satellite
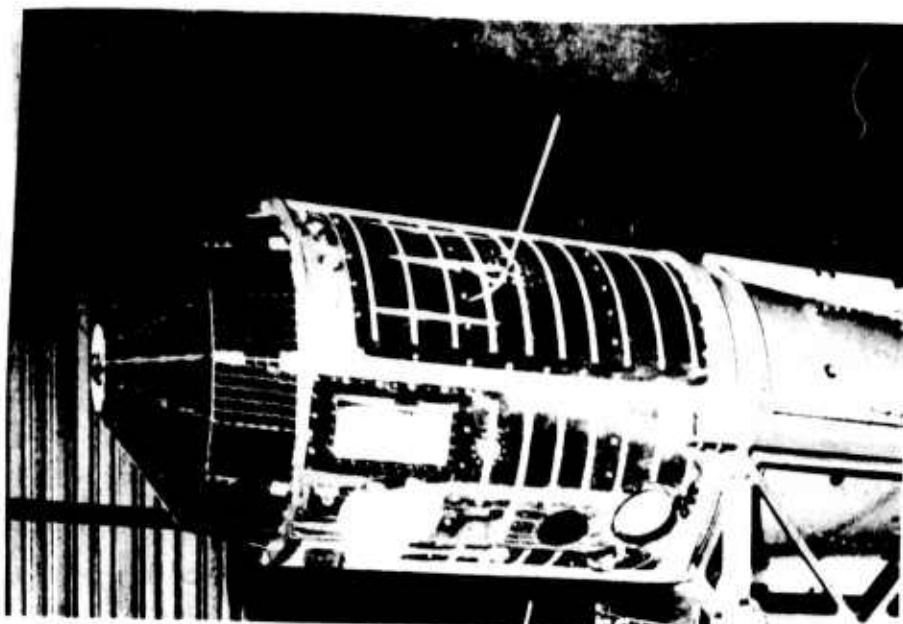
Fig. 14. The OV1-14 Faraday Cup Mounted on the OV1-14 Satellite

8.   OV1-15

The purpose of the OV1-15 spacecraft was to determine atmospheric density and composition. A Faraday cup was included in the payload to determine the contribution to atmospheric heating due to energy loss from precipitating charged particles. Two small electrostatic analyzers were also flown on this flight. Agreement of the data from these two instruments would indicate that both instruments were operating properly. In addition to measuring particle flux scanning atmospheric heating, the instruments measured fluxes in the auroral zones. Both protons and electrons with energy from 0.9 to 7 keV were measured in seven energy intervals. The instrument flown was similar to that shown in Fig. 11.

The satellite was launched successfully on 11 July 1968, and both the Faraday cup and the electrostatic analyzer worked properly. Particles were observed with the electrostatic analyzers during practically every auroral crossing. Only occasionally did the flux attain sufficient intensity to be measured by the Faraday cup. This occurred in the electron mode, and the flux intensities measured by both instruments agreed. This indicated that both instruments were functioning properly and that the flux intensity of the protons was never large enough to exceed the sensitivity threshold of the Faraday cup. The previous anomalous proton measurements on 1964-45A were probably erroneous. The electron flux occasionally exceeded the sensitivity threshold of the Faraday cup, but never attained the intensities observed on satellite 1964-45A. The instrument is shown mounted on the spacecraft in Fig. 15.

9.   OV2-5

This satellite provided a second opportunity to measure the flux of particles with 0.5 to 8 keV of energy at synchronous altitude. In 1965, when these experiments were proposed, the existence of large fluxes of low-energy electrons near an L value of 6 R_e was known (Vernov, et al., 1966). The peak-measured electron flux was 10^9 electrons-cm^{-2}-sec^{-1}-keV^{-1} and was isotropic. An upper limit on the ion flux of 5×10^7 ions-cm^{-2}-sec^{-1}-keV^{-1} was

established, but the effect of solar flares and magnetic disturbances on these particles was unknown. The Faraday cup could measure these electrons and, if the proton fluxes were increased by magnetic disturbances, also measure proton fluxes. Initial indications were that the expected steady-state flux would be comparable to the sensitivity threshold of the instrument.

The satellite was launched successfully in September 1968, and the instrument functioned properly. The observed proton flux never exceeded the sensitivity threshold of the instrument. Trapped electrons were observed, and the electron measurements indicated that the instrument was sensitive to solar UV and earth back-scattered UV. The proton results were consistent with the results of Frank (1967) on OGO-3 in which he observed a steady-state flux of protons. The flux measured by him was at least one order of magnitude less than our threshold of sensitivity.

During the main phase of the July 1966 magnetic storm, the proton flux at synchronous altitude reached 2×10^7 protons-cm^{-2}-sec^{-1}-sr^{-1} in the energy interval from 31 to 49 keV. If the proton flux at 8 keV had changed proportionally to the flux at 40 keV, we could have expected a current of 1.2×10^{-11} A into the instrument during our highest energy measurement. This is only a factor of three above our threshold of sensitivity, and since no magnetic storm occurred during the lifetime of the instrument, we could not expect to observe protons. Because of the Faraday cup's lack of sensitivity, we decided to replace them with electrostatic analyzers on future satellites. The electron channels registered flux during every satellite acquisition, and both the energy spectrum and the angular distribution of the electron were obtained. The instrument is shown mounted on the bottom of the spacecraft in Fig. 16.

10.   OV1-17

After failure of the OV1-11 to achieve orbit, the OV1-17 flight was proposed as a back-up, with the OV1-11 back-up instruments as Faraday cups. The planned orbit was circular polar at low altitude, and the
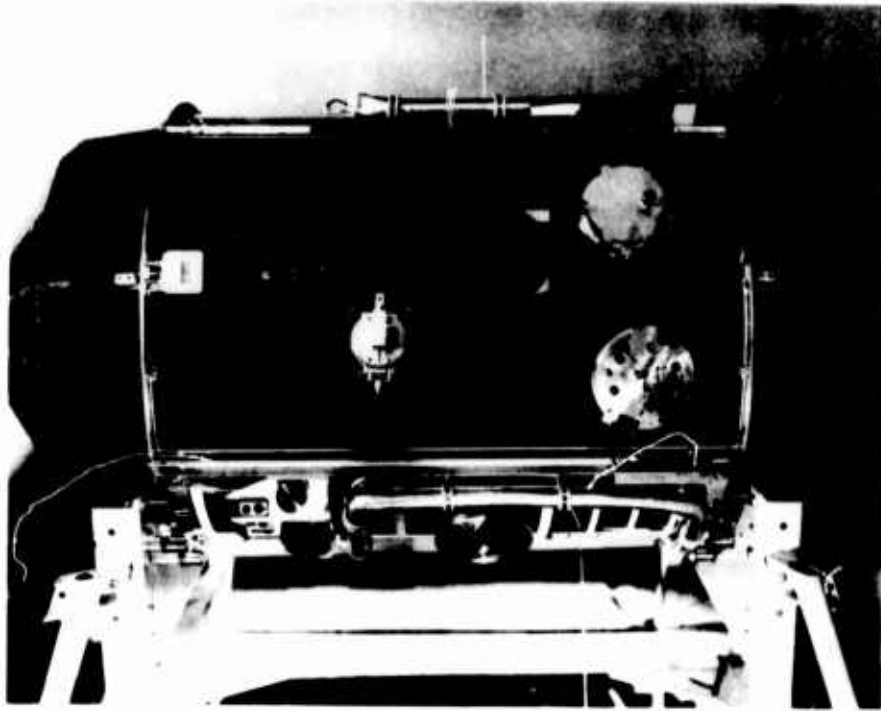
Fig. 15. The OV1-15 Faraday Cup Mounted
on the OV1-15 Satellite
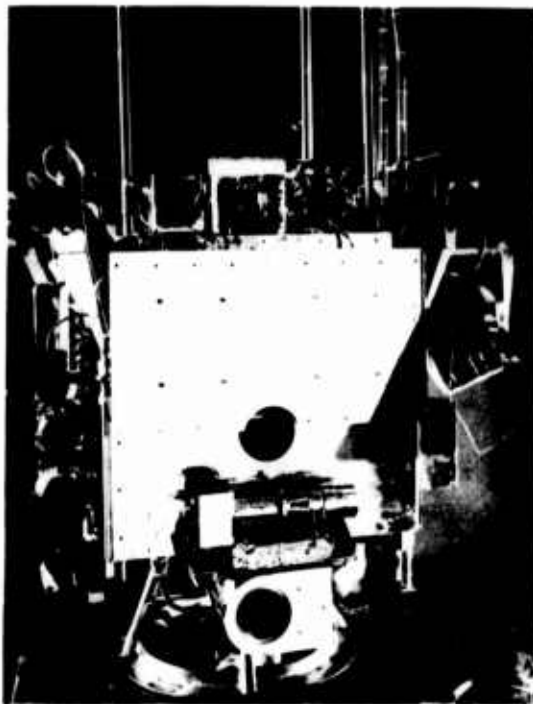
Fig. 16. The OV2-5 Faraday Cup
Mounted on the OV2-5
Satellite

satellite was gravity gradient stabilized. Two sensors were planned for this flight. One would look toward the zenith and the other would look in the anti-velocity direction. In addition to making all the measurements stated for the OV1-11 satellite, the flux of the zenith-directed sensor could be compared with that measured by an electrostatic analyzer that looked in the same direction. The two Faraday cups were replaced by electrostatic analyzers because the flux levels measured by the analyzers on OV1-14 and OV1-15 were several orders of magnitude less than the sensitivity threshold of the Faraday cups.

11.   OV1-19

This satellite was the fourth in the laboratory's series of radiation belt monitoring satellites. A Faraday cup was built for this flight that could measure both protons and electrons with energy between 0.3 and 8 keV. Variations in the precipitating component of the proton flux would be compared with observations from the all-sky Lyman-α scanner. Because of the need for greater sensitivity observations on both the OV1-14 and OV1-15 flights, the Faraday cup was replaced by two electrostatic analyzers. These analyzers measured particles with the same energy as the Faraday cup, but sensitivity was increased by several orders of magnitude.

IV. INSTRUMENT DEVELOPMENT

A. MECHANICAL

1. GENERAL

It is always interesting to compare the final results of a study with the original design objectives. The Faraday cup, which was proposed at Aerospace (Mozer, et al., 1962), was expected to measure the flux of both protons and electrons from thermal to 50 keV energy. Unfortunately, the instruments used to obtain the measurements were seldom capable of analyzing particles with more than 10 keV energy. The proposed weight and power were 2-1/8 lb and 2-1/4 W, respectively, and the achieved values were 6 lb and 3 W. The proposed AC and voltage was 5 to 10 kV peak to peak, and the maximum achieved value was 2 kV peak to peak. Only one proposed design goal was achieved and that was the current sensitivity of the collector. A minimum sensitivity of 10^{-11} A was proposed, and a minimum sensitivity of 10^{-12} A was achieved. The original proposal was ambitious, and a great amount of effort was expended trying to achieve and improve upon the original goals. A major impact on the availability of flights was the excess weight and power required by the final instruments. This eliminated the Faraday cup from competition for payload space on the light scientific satellites that investigated the environment beyond synchronous altitude. This was unfortunate, as most of the useful information that has come from Faraday cup-type instruments has been obtained beyond synchronous altitude.

2. POTTING COMPOUNDS

Because of the need to operate the instrument in the atmosphere as well as in a vacuum, it was necessary to use a potting compound to insulate the various high-voltage supplies against breakdown and to protect them from overloading due to coronal loading. Very little was known about

potting compounds when the Faraday cup project was started. A program was developed by A. L. Vampola of the Space Physics Laboratory to test potting compounds and to determine which compound best suited our needs. Parameters that were important for high-voltage vacuum applications included: volume breakdown potential, surface breakdown potential, flexibility of the cured compound, stability of the compound in vacuum, and stability of the compound to thermal cycling. Fissures were observed around the potted compounds after thermal cycling if the compounds were too inflexible. The flexibility of the compounds should not change within the acceptable thermal extremes and also must not change with the age of the material. It was noticed that certain potting compounds would shrink after prolonged vacuum exposure. The stresses built up at the edges of potted components produced fissures in these potting compounds, and electrical breakdown would occur along the fissures. Finally, after extensive testing, the Epon Resin made by the Shell Chemical Company was chosen. Table II lists the proportions for mixture by weight of the various components. The final entry in the table was the mixture used for all flight Faraday cups.

Table II. Proportions of Epon Resin by Weight

Compound			
828	871	Z	Characteristic
100	---	20	hard
---	100	10	soft
20	80	12.3	too hard
15[*]	90	12.3	useable

[*]Mixture used for all flight Faraday cups.

3. ACOUSTICAL SHIELDING

The collector and preamplifier assembly was extremely sensitive to pickup. In order to reduce the pickup, the collector and preamplifier were built as one unit that was enclosed in an electrostatic shield. A Conetic shield surrounded the preamplifier assembly, and the entire unit was shock mounted to reduce acoustical pickup. The high-voltage grids and their neighboring grounded grids were mounted to minimize the mechanized vibration resulting from electrostatic forces. If the net electrical force on the grids was not zero, the grids could vibrate at the frequency of the ac power supply, and the vibration could acoustically couple with the pre-amplifier to produce unwanted pickup. This problem was eliminated by creating equal space between the high-voltage grid and its two neighboring ground grids and by firmly mounting the grids to inhibit any motion. The transformers in the high-voltage power supplies were mounted inside a Conetic shield to further reduce unwanted pickup.

Once it became apparent that the high-energy limit of the instrument would be caused by the power supply and not the grid insulators, the ceramic insulators were replaced by insulators made of nylon, with an inside diameter of 4.5 in. The insulators between the negative high-voltage grid and the collector were shielded from solar ultraviolet radiation by solid grid holders. The acceptance aperture diameter of the grid holders varied among the instruments and is listed in Table III.

B. ELECTRICAL

1. GENERAL

The Faraday cup circuitry for satellite 1964-45A is shown in Fig. 17. This instrument will be the basis for the discussion of the electronic development of the Faraday cup detector. Although all of the individual circuits have been modified and improved, the basic block diagram has remained virtually unchanged. The major circuits are the

Table III. Calibration Levels and Geometrical Factors

Satellite	Calibrated Output (V)					d_1 (cm)	d_2 (cm)	ℓ (cm)	G_1 (cm^2)[*] (Undirectional)	G_2 (cm^2 - sr)[**] (Isotropic)
	E5	E4	E3	E2	E1					
1964-45A	none	-	-	-	-	2.29	2.29	5.11	4.1	0.594
1966-70A OV3-3	4.39	4.33	2.22	0.72	0.58	8.89	9.14	9.53	62.1	31.80
1968-26B OV1-14	4.90	4.87	1.34	0.63	0.53	5.08	9.14	9.53	20.3	11.38
1968-59A OV1-15	4.91	4.93	1.42	0.52	0.44	2.54	2.54	5.51	5.1	0.766
1968-81A OV2-5	4.91	4.86	1.87	0.62	0.53	7.62	9.14	9.53	45.6	24.21

*The reduction in instrument sensitivity as a result of beam absorbtion by the grids is included in the calibrations of Figs. 24 through 28.

**A small variation of the grid transmission with incident beam angle has not been included in these values.
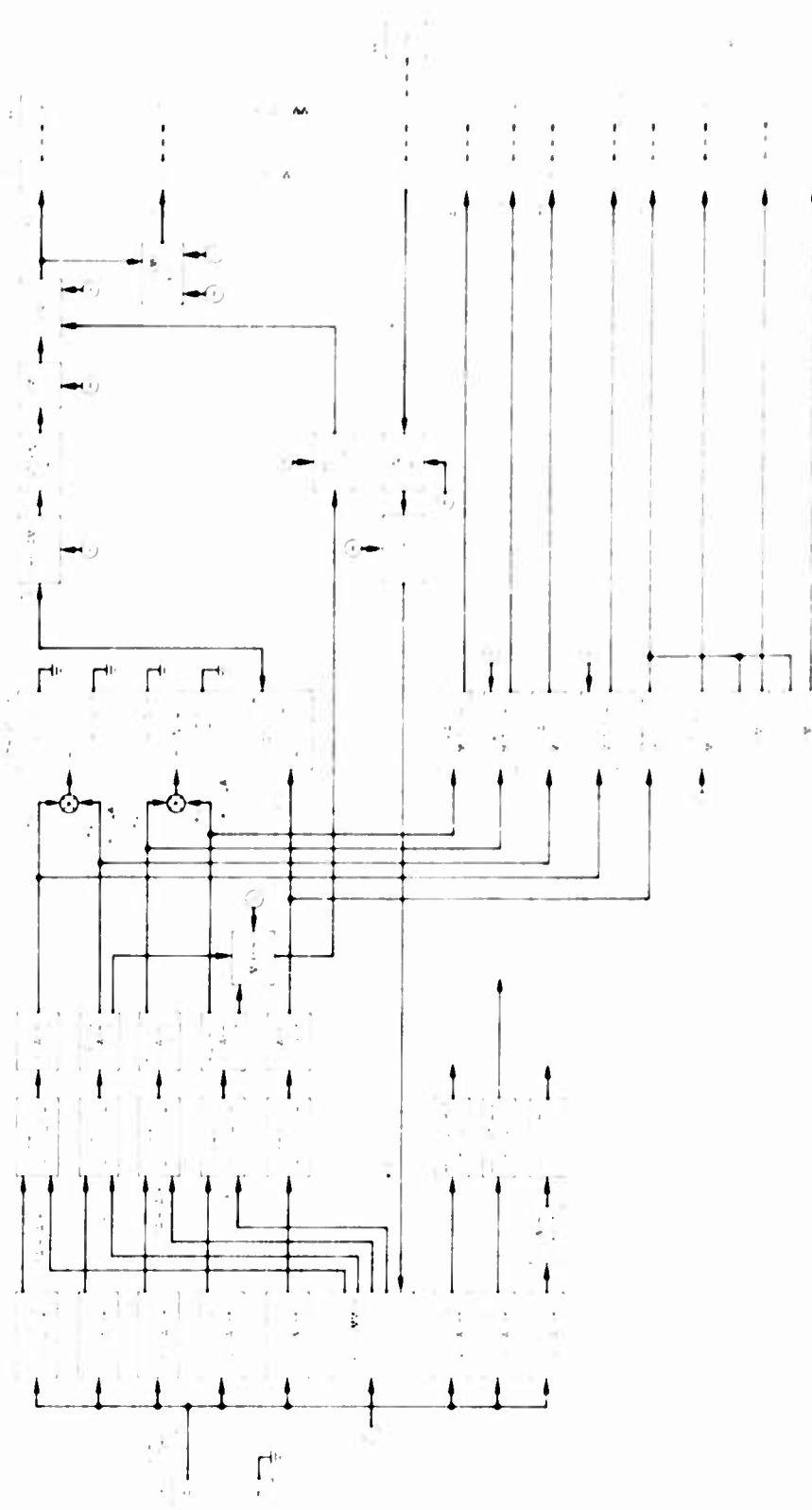
Fig. 17. Faraday Cup Circuitry for Satellite 1964-45A

collector channel electronics, programmer logic, and high- and low-voltage supplies. A brief description of these circuits is presented in the paragraphs that follow.

2. COLLECTOR CHANNEL ELECTRONICS

The collector channel collects the AC current at the collector (this current is proportional to the incident flux) and converts it to a DC analog voltage suitable for the satellite telemetry system. The collector channel (Fig. 18) consists of five circuits: preamplifier, amplifier, synchronous demodulator, dc amplifier, and reference delay.

The first stage of the preamplifier is a P-channel field effect transistor (FET) (2N2500), chosen for its low noise and high-input impedance at 2 kHz. The entire preamplifier has a closed-loop gain of 1000 and an input impedance of 500 kΩ at 2 kHz. Additionally, it incorporates an RC low-pass filter whose half-power point is at 4 kHz. This reduces the contribution of the Johnson and shot noise in the amplifier section before the signal is demodulated.

The amplifier section consists of two stages, each employing a single transistor amplifier and an emitter follower. The total gain is 1000.

The synchronous demodulator converts the 2 kHz signal from the amplifier stage into a DC output with a range from 0 to 5 V. As discussed previously, the demodulator mixes the incoming signal with a delayed reference square wave, so that the output signal has basically two frequencies, a DC level and a signal at twice the modulating frequency. A low-pass filter eliminates the contribution of the second harmonic component in the output.

Additionally, a DC amplifier with a gain of 20 is used to increase the sensitivity of the instrument. This amplifier employs two pairs of matched 5P8414A transistors and two sensitors to attain temperature stability.

Due to stray capacitance at the collector, there is an RC time constant associated with the wave shape at the collector. This delays the various

-46-

Fig. 18. Collector Channel Circuitry

frequency components of the signal relative to the modulation on the grid, in particular the 2 kHz component of interest. Hence, the demodulating signal must be delayed so as to be in phase with the signal. This is accomplished in the reference delay circuit that delays the rising and falling edges of the modulating signal by use of a single one-shot.

3. PROGRAMMER LOGIC

The programmer logic circuit (Fig. 19) takes the satellite commutator sync pulse (1 Hz on 1964-45A) and generates a series of control voltages for the AC and DC high-voltage supplies. It consists of three circuits: isolation stage, countdown flip-flops, and program voltage generator.

The 1 Hz synchronization pulse for satellite 1964-45A was made by physically grounding the input by means of the wiper arm of a mechanical commutator. The input Schmidt trigger stage has a low-input impedance of 4 KΩ and an RC time constant of 50 μsec to inhibit accidental triggering by commutator jitter. This is followed by a one-shot, pulse-shaping circuit to drive the binary flip-flops.

The countdown flip-flops are standard Eccles-Jordon bistable multi-vibrators that operate in the saturated mode and employ two 2N780 transistors. These flip-flops and their associated diodes, resistors, and capacitors are packaged in small epoxy modules. Six flip-flops are used, three to prescale by eight and three for the eight-step program.

In this particular instrument, there are only two values for each of the AC voltages: on or off. Therefore, the AC reference voltages are derived from the final flip-flop of the programmer, where two signals with periods of 64 sec and of opposite phase are generated. The DC reference voltage circuit is designed to produce four increasing voltages that last 8 sec each, and then a 32-sec fixed voltage. Again, the positive and negative voltages are of opposite phase. Three diode AND gates are used to determine the stage of the final three flip-flops (corresponding to steps 0 through 7). For example, at step 0 in Fig. 19, the anodes of diodes D1,
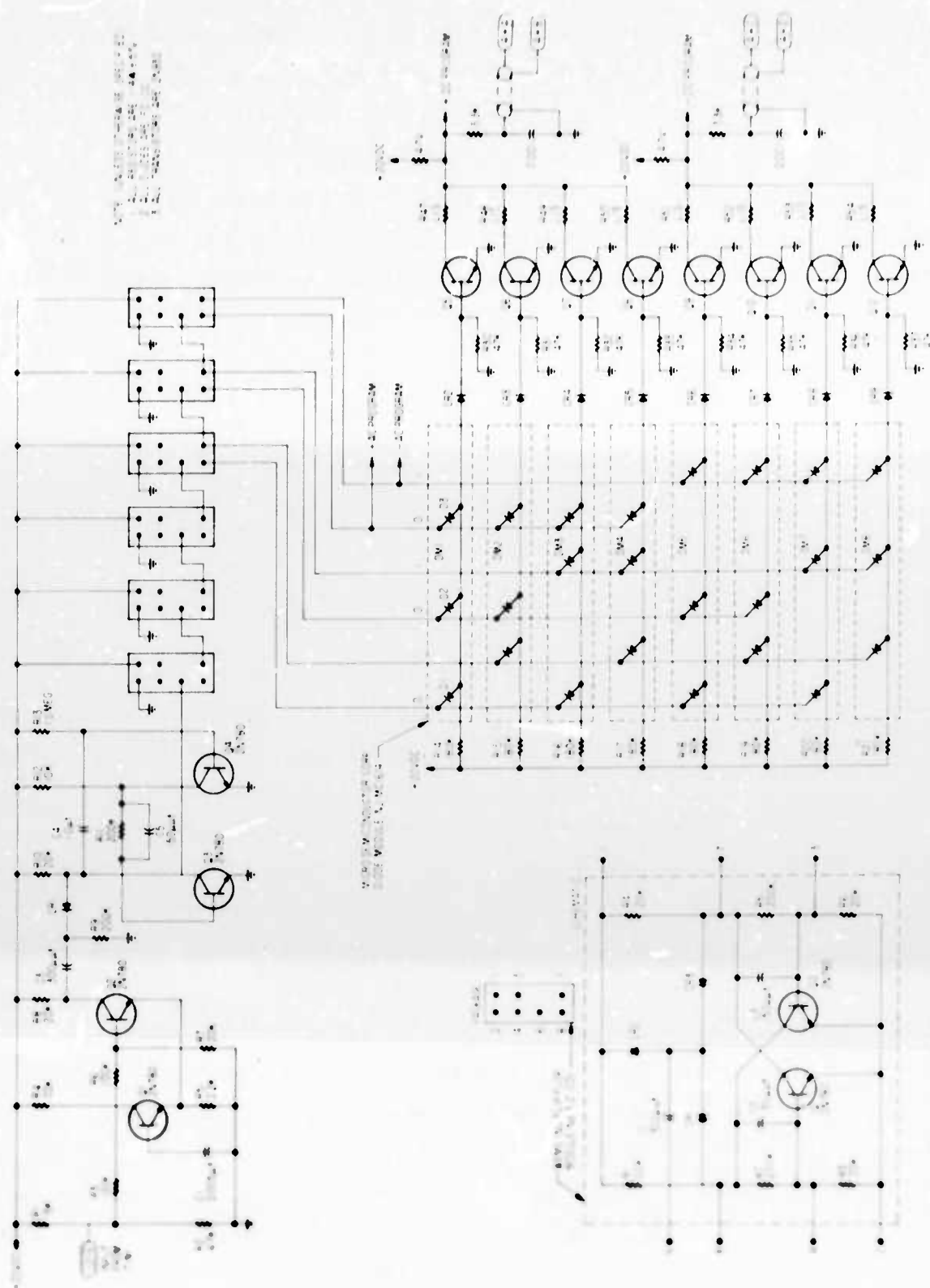
-48-

Fig. 19. Programmer Circuitry

-49-

D2, and D3 are at 20 V, and therefore, transistor Q5 will be on in the
saturated mode, while Q6, Q7, and Q8 will be off. Hence, the +DC program
voltage will be given by the resistance divider 4.7K and R47, and the 20 V
DC supply. For steps 0 to 3, the +DC program voltage will be determined by
R47, R48, R49, and R50; for steps 4 to 7, the +DC program voltage will be
20 V. The -DC program voltage is derived in a similar fashion. Later
instruments used 16-step programmers, with both the AC and DC voltages
being controlled by similar transistor gates.

4.   HIGH-VOLTAGE SUPPLIES

The high-voltage circuitry consists of two AC and two DC supplies
whose control voltages are provided by the programmer logic and whose
outputs are summed and applied to the proper grids. These circuits are
shown in Fig. 20.

The control voltage for the AC power supplies, in this case either
0 or 20 V, is applied to the base of a dual emitter follower (a 2N930,
followed by a 2N1721) to provide the current to drive the magnetically
coupled, free-running multivibrator. This multivibrator consists of a
Magnetics ferrite core, with a turns ratio of 3500/84, and two 2N1717
transistors.

An effective ±20 V on the primary produces a 1.7 kV peak-to-peak
square wave at the output. This signal is capacitively coupled to the grids
through two 200 pf, 6 kV capacitors in series. The AC monitor circuit
monitors the transformer itself, and consists of a 10-turn winding and a
simple diode rectifier. Finally, because there are two free-running, AC
high-voltage supplies (one for the positive grid, the other for the negative),
there is a mixer circuit to derive the signal for the reference delay. This
is necessitated by the fact that the frequencies of the two multivibrators
are not exactly equal.

The control voltage for the DC power supplies, in this case a voltage
between 1 and 20 V, is applied to the base of a dual emitter follower to
provide the current for a Class C oscillator operating at 6 kHz and employing

-50-

Fig. 20. High-Voltage Circuitry

an Arnold ferrite core as the high-voltage, step-up transformer. This particular design was chosen for its low power consumption. The turns ratio is 8000/80; consequently, a 20 V sine wave on the primary produces a 2000 V sine wave at the secondary, resulting in an input to a three-stage Cockeroft-Walton generator that has a DC output voltage of 6 kV. This output, which is coupled to the grid through an 88 MΩ resistor, serves two purposes. It allows operation of the supply with the high-voltage grid grounded without drawing excessive input current, and it provides sufficient output resistance so that the added AC signal is not diminished. The high voltage is monitored directly by means of a 5 kMΩ and a 2.2 MΩ resistor as a 2300:1 voltage divider. With the monitor side of the 2.2 MΩ resistor biased at 0 to 5 V, the positive and negative monitors have outputs from 0 to 5 or 5 to 0 V, respectively.

5. LOW-VOLTAGE SUPPLIES

The low-voltage supplies provide regulated voltages to the circuits previously described. For convenience, the temperature monitors will also be discussed here. The circuits, which are shown in Fig. 21, include the main 20 V supply, programmer 20 V supply, DC amplifier -12 V supply, suppressor -90 V supply, and thermistor monitors.

The 20 V, 200 mA main power supply is a standard series voltage regulator circuit designed to provide a stable 20 V supply from the spacecraft supply, an unregulated 28 V supply that varied ±4 V.

The programmer 20 V supply is similar to the main 20 V supply, and its primary purpose is to provide additional isolation and filtering for the programmer. It has been found that the programmer flip-flops are sensitive to power line noise and to the small amounts of pickup generated by the AC and DC high-voltage supplies.

The DC amplifier requires -12 V for its operation. This is generated by a magnetically coupled oscillator, a bridge rectifier, and standard regulator.

Fig. 21. Low-Voltage Circuitry

The suppressor grid is maintained at -90 V to suppress secondary electrons emitted from the collector by either incoming particles or solar UV. This supply again employs a magnetically coupled oscillator, whose transformer has a 3.25:1 turns ratio, and a single-stage rectifier. Since suppression of electrons is not sensitive to small changes in this voltage, only the primary DC voltage is regulated.

Veco 41D2 thermistors, which have a resistance of 10 KΩ at room temperature, are used to monitor two temperatures: the main 20 V supply and the collector.

C. MODIFICATIONS

As stated previously, the circuits of the Faraday cup detector have been modified and improved over a period of time, although the block diagram of the circuits has not changed significantly. A discussion of these modifications and improvements is presented in the paragraphs that follow.

1. IN-FLIGHT CALIBRATION

Immediately after the flight of 1964-45A and the presumed measurement of large fluxes of low-energy protons, it was clear that an in-flight calibration was necessary. It was desirable to have a source of low-energy particles, both electrons and protons, that could be gated on at frequent intervals to check the operation of the entire instrument. This, however, was difficult to achieve; instead, one step of the programmer was used for calibration. During this step, a square-wave current, derived from the modulating signal and properly delayed, was fed to the input of the pre-amplifier. This current then checked the calibration of the preamplifier, amplifiers, and demodulator, but did not check the operation of the grids.

2. FIXED-FREQUENCY OSCILLATOR

The 1964-45A AC power supplies were free-running, magnetically coupled multivibrators, whose frequency was directly proportional to the

-54-

primary voltage. The frequencies of the positive and negative supply were adjusted to be equal, and a mixer was used so that the demodulator was controlled by the oscillator in use. This type of circuitry prohibited programming the AC voltages, except to turn them on or off. For this reason, we decided to incorporate a fixed-frequency oscillator to control all the modulating and demodulating circuitry. Initially, we attempted to use tuning forks for the frequency control, but these proved to be extremely fragile and unreliable. Finally, an RC oscillator was used as the master oscillator.

3. NARROW BAND FILTER

At the output of the instrument, the bandwidth B_o was equal to $1/\pi\tau$, where τ is the time constant of the output filter. Typically, τ was 0.3 sec; therefore, B_o was 1 Hz. The bandwidth B_i, set by the preamplifier and amplifier, was much larger just prior to demodulation. In the case of 1964-45A, this intermediate bandwidth B_i was 2 kHz. For the noise sources of interest, the rms noise voltage is proportional to the square root of the bandwidth. Hence, for 1964-45A, the rms noise voltage just prior to demodulation was 45 times larger than at the output.

In general, the maximum gain of the instrument is determined by the condition that the internally generated rms noise voltage at the output be equal to the telemetry noise at the output. For 1964-45A, this was 0.1 V; therefore, the rms noise voltage was approximately 4.5 V just prior to demodulation. The maximum nonsaturating signal at this point was 10 V peak to peak; consequently, the noise voltage was close to saturation. Saturation effectively shifts the signal phase with respect to modulation and is undesirable. Saturation in the 1964-45A was prevented by a decrease in the overall gain by a factor of 2. In subsequent instruments, the intermediate bandwidth B_i was decreased. In the OV3-3 instrument, this bandwidth was reduced to 500 Hz; in later models, the bandwidth was reduced to 200 Hz by means of an active filter.

4.   PREAMPLIFIER AND FILTER

The requirements of a narrow bandwidth prior to demodulation and
a low-input capacitance to maximize the signal and to minimize the delay
led to the design of a preamplifier-filter combination. This combination had
an N-channel, 2N3686 low-noise FET as the input transistor, with a feed-
back resistor of 1 MΩ. The feedback loop contained an active twin-T filter
with a Q of 10. Thus, this preamplifier-filter had an effective transfer-
resistance of 10 MΩ and a bandwidth of 200 Hz.

5.   VARIABLE FORMAT

The programmer logic circuit, which was designed to be versatile,
had 16 steps that could be used to measure protons or electrons, or a com-
bination of both particles. Various combinations of particles and particle
energies were chosen, depending on the experiment being performed, with
the duration of each energy measurement altered by varying the number of
countdown flip-flops used. Usually the cycle rate was chosen so that the
instrument made one energy measurement for each rotation of the space-
craft. On several spacecrafts, however, the option of a commandable cycle
rate was included, which permitted the ground station operator to deter-
mine the cycle rate of the instrument. Options of a fast-cycle rate (one
energy measurement for each satellite rotation), a slow-cycle rate (one
energy measurement 16 or 32 times less often), or no cycling (the instru-
ment would remain in one mode until turned off) were available.

6.   BROAD BAND

In order to observe rapid time variations in the particle flux, the five
instrument outputs were combined by means of a range switch. This output
was then telemetered via a subcarrier oscillator that was not shared with
other experiments. When more than one Faraday cup sensor was present
on the satellite, a command was used to determine which sensor would use
the broadband output channel.

V. CALIBRATION AND TESTING

Calibration of the Faraday cups was achieved by the use of collimated, calibrated beams of positive and negative ions. These beams were employed to determine the differential energy intervals and the sensitivity for each instrument. In addition, the effect of a neutralized beam of H^+ and e^- on the Faraday cup was investigated. Sensitivity of the instrument to background in the form of ultraviolet radiation and strong RF fields was checked, and the VLF radiation from the instrument was measured. Prior to launch, the instruments were subjected to extensive thermal, thermal vacuum, vibration, and life tests. Some of the more important aspects of the calibration and testing of Faraday cups are discussed in the paragraphs that follow.

A. THRESHOLD DETERMINATION

The energy thresholds for each step were determined by locking the instrument in a given energy step and varying the energy of the incident particle beam. As the energy of the incident beam increased over the lower threshold, a sharp increase in output was observed; the output decreased sharply as the energy of the beam was increased above the upper limit of the step. The accelerators used for these measurements included: a purchased electron accelerator redesigned by Aerospace personnel; a proton accelerator at the Electronuclear Corporation, Sunnyvale, California; and a proton accelerator built in the Aerospace Space Physics Laboratory. Typical results from the measurement of upper and lower thresholds of one differential energy interval are shown in Fig. 22.

As in most of our measurements, the Faraday cup detected accelerator characteristics that were unknown to the operator prior to beam measurement with the Faraday cup. In Fig. 22 the Aerospace electron accelerator is used as the particle source, and the curve represents the response of step 12 on the OV3-3 Faraday cup to electrons. The lower and upper thresholds are shown at 3.70 keV and 5.54 keV, respectively. The structure of each step 12 (and, incidentally, all steps) should be rectangular and should not contain the step structure
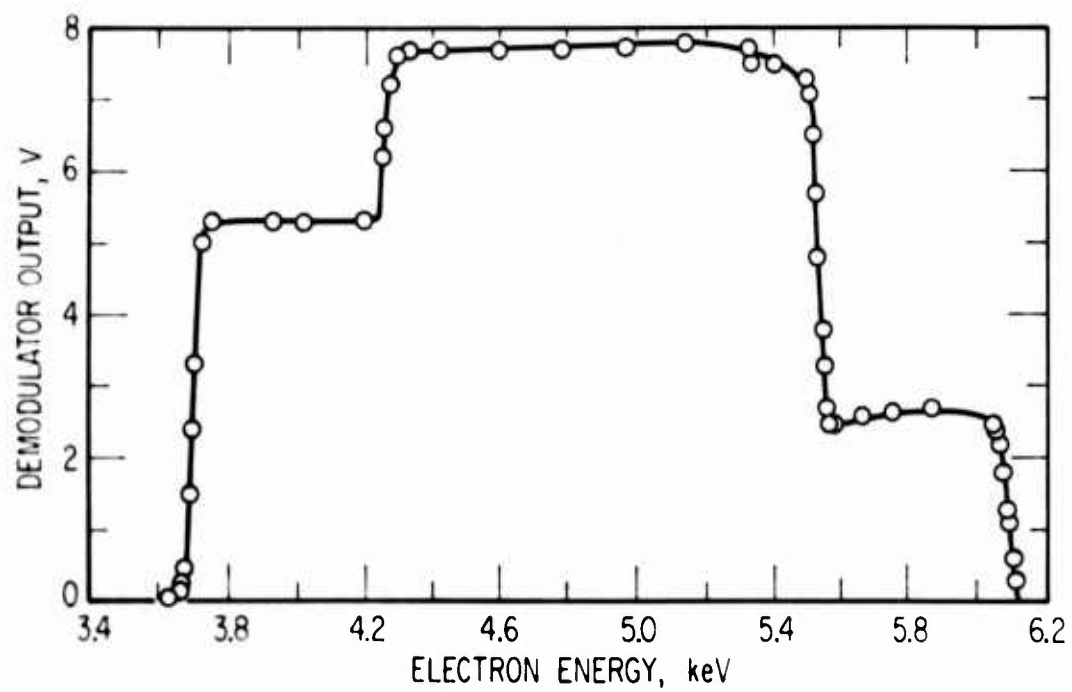
Fig. 22. Response of the OV3-3 Faraday Cup to Electrons
as a Function of Energy

illustrated in Fig. 22. This step structure was due to electrons emitted from the focus electrode in the ion gun that was operated at 600 V lower potential than the hot filament of the ion gun. This electrode produced electrons that were observed by the instrument after the accelerating potential exceeded the instrument's lower threshold by 600 V. The thresholds for the electron steps on all instruments were measured by means of the electron accelerator in the Space Physics Laboratory. These thresholds are listed in Table IV for all the instruments that were successfully orbited.

Determination of the proton thresholds was more difficult, as a proton source did not exist at Aerospace until one was built in 1966. The 1964-45A instrument was calibrated with protons at the Electronuclear Corporation. Their beam was not energy analyzed and, therefore, contained a substantial flux of protons with energy less than the accelerating potential. In addition, the wiring of their ion source made it impossible to obtain a beam with less than 500 eV energy. Because of these difficulties, we were able to obtain the lower threshold of the three highest energy channels quite accurately and the upper edges of all four channels roughly. The widths of each channel were accurately obtained by reversal of the demodulator phase and by means of our electron beam. These widths, combined with the three measured lower edges, gave us sufficient data to calibrate both edges of all four proton steps on the 1964-45A instrument. The proton steps on OV3-3 were measured by introducing air in the vicinity of the hot filament of the electron accelerator and accelerating the positive ions. Proton thresholds on subsequent instruments were measured by means of the analyzed beam of the Space Physics Laboratory's proton accelerator. The thresholds for proton measurements are listed in Table IV.

B. SENSITIVITY

The absolute efficiency of the collector assembly was determined by means of an electron beam. Initially, the incident beam was monitored with a Victoreen electrometer amplifier, but an E-H Research Laboratory electrometer amplifier was used after 1964. Three modes were employed to monitor the beam intensity. In one mode, the beam was sampled intermittently by

Table IV.   Energy Range in keV of Instruments on Successful Satellites

Satellite	Protons			Electrons		
	Step	Lower Edge	Upper Edge	Step	Lower Edge	Upper Edge
1964-45A	0	0.4	2.2	4	0.3	2.1
	1	3.4	5.5	5	3.0	5.2
	2	6.3	8.1	6	5.9	8.0
	3	9.4	11.0	7	9.1	11.2
1966-70A	2	0.37	1.24	9	0.34	1.10
OV3-3	3	0.89	1.83	10	1.18	2.14
	4	2.12	3.06	11	2.28	3.24
	5	2.88	4.72	12	3.70	5.54
	6	4.70	6.60	13	5.42	7.22
	7	5.96	7.82	14	7.80	9.64
	8	7.80	9.66	15	9.06	10.82
1968-26B	2	0.28	1.00	9	0.55	1.03
OV1-14	3	1.06	1.90	10	1.11	1.94
	4	1.82	2.66	11	1.97	2.83
	5	2.40	4.00	12	2.65	4.23
	6	3.68	5.28	13	3.91	5.49
	7	4.74	6.34	14	4.95	6.52
	8	5.96	7.56	15	6.04	7.62
1968-59A	2	0.87	1.57	9	0.92	1.64
OV1-15	3	1.26	2.14	10	1.59	2.47
	4	1.93	2.81	11	2.16	3.05
	5	2.23	3.87	12	2.44	4.07
	6	3.28	4.92	13	3.28	4.93
	7	4.01	5.65	14	4.09	5.71
	8	4.98	6.63	15	4.75	6.40
1968-81A	2	0.55	1.25	9	0.48	0.99
OV2-5	3	1.10	1.96	10	1.14	1.92
	4	1.98	2.86	11	2.09	2.88
	5	2.70	4.35	12	2.65	4.17
	6	4.18	5.85	13	4.07	5.59
	7	5.51	7.17	14	5.29	6.79
	8	6.67	8.34	15	6.24	7.75

inserting a solid collector in the beam. The collector consisted of a copper plate that was inserted between a suppressor grid at -90 V and the instrument. This assembly is shown in Fig. 23a. For the geometry shown, the beam incident on the instrument is equal to that intercepted by the monitor. This monitor geometry was used to calibrate the 1964-45A Faraday cup. Later, improved beam monitoring was achieved with the building of a continuous monitor, which consisted of two beam-limiting apertures and three parallel grids. The assembly is shown in Fig. 23b. This geometry, which was used to calibrate all instruments starting with the 1602 Faraday cup, had the advantage of permitting simultaneous observation of the beam current and the instrument outputs. If the grid transmissions are given by T_i, the ratio of the current incident on the cup to the monitor current is given by I_i/I_m and is:

$$\frac{I_i}{I_m} = \frac{T_3 T_2}{(1 - T_3) + T_3 N_o (1 - T_2)}$$

N_o is the number of electrons emitted from the grid immediately preceding the instrument for each electron that strikes the grid. The edge effect of the last grid is considered small. The ratio of I_i/I_m was measured experimentally after the Faraday cup was replaced with a solid collector and electrometer amplifier. This measured ratio was independent of vacuum below 6×10^{-3} Torr. All of the calibrations were performed with pressures less than 10^{-5} Torr. If the grid transmissions quoted by the Buckbee Mears Company, Minneapolis, Minnesota, of $T_2 = 0.95$ and $T_3 = 0.82$ are used, one obtains a value of 0.9 for N_o. Values of N_o from 0.7 to 1.4 can be obtained if the transmission is permitted to be in error by up to 2 percent. These numbers for N_o are consistent with the expected secondary emission ratios of electrons from nickel. The final monitor assembly used is shown in Fig. 23c. This geometry was used to monitor the proton beam from the proton accelerator. The ratio of the incident current to the monitor current is given by the transmission of the collecting grid.
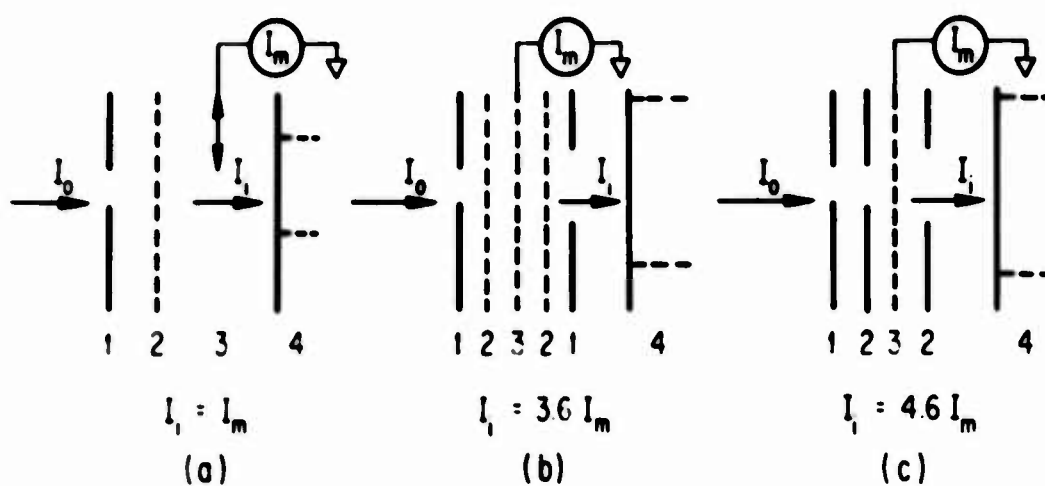
NOTE

    1 CIRCULAR APERTURES

    2 SUPPRESSOR GRIDS WITH 95% TRANSMISSION FOR 2a AND b AND
       APERTURES IN 2c

    3 BEAM COLLECTORS SOLID IN 2a

    4 FARADAY CUPS

Fig. 23. Geometry of Three Beam-Current Monitors

$$\frac{I_i}{I_m} = \frac{T_3}{(1 - T_3)}$$

The calculated value for this ratio was 4.55, and the measured value was 4.6. This was in good agreement with the quoted values for the grid transmission.

The calibration of the two electrometers was checked by passing a known current into them on various scales. Current scales below 10^{-13} A showed large inconsistencies, but these scales were not used during instrument calibration. Measurements made with the three collector geometries and the two electrometer amplifiers were consistent to within 10 percent. The sensitivity calibration accuracy was ±10 percent on the basis of the consistency of the measurements with various monitor geometries and the absolute calibration of the electrometers.

The sensitivity calibration was performed by recording the monitor current and the instrument output as the magnitude of the incident current was varied over the range of the Faraday cup. The incident beam energy was adjusted to the mid-energy of a convenient energy step, and the beam intensity was converted to current incident on the Faraday cup. Plots of current versus output voltage were made. Plots for the five successful flight instruments are shown in Figs. 24 thru 28.

Independent confirmation of these sensitivity calibrations was obtained when we used the facilities of the Electronuclear Corporation in Sunnyvale and of TRW in Redondo Beach, California. The test at Sunnyvale used the 1964-45A Faraday cup and was probably valid only as an order of magnitude check on the absolute sensitivity of the instrument. The fact that the incident proton beam was not energy analyzed made it difficult to correlate the total current with current in a differential energy channel. For example, we observed that with the accelerator operating at 10 kV the total monitored beam was 9×10^{-9} A. The highest energy channel of the Faraday cup registered 2.5×10^{-9} A, and the three lower channels averaged 1×10^{-9} A in each channel. If one assumed that the beam consisted of a 1-keV wide peak containing 2.5×10^{-9} A at the accelerating voltage and a constant 5×10^{-10} A/keV below 9 keV, the integral of the beam observed by the Faraday cup was 7×10^{-9} A. This was in good agreement with the monitored beam of 9×10^{-9} A.
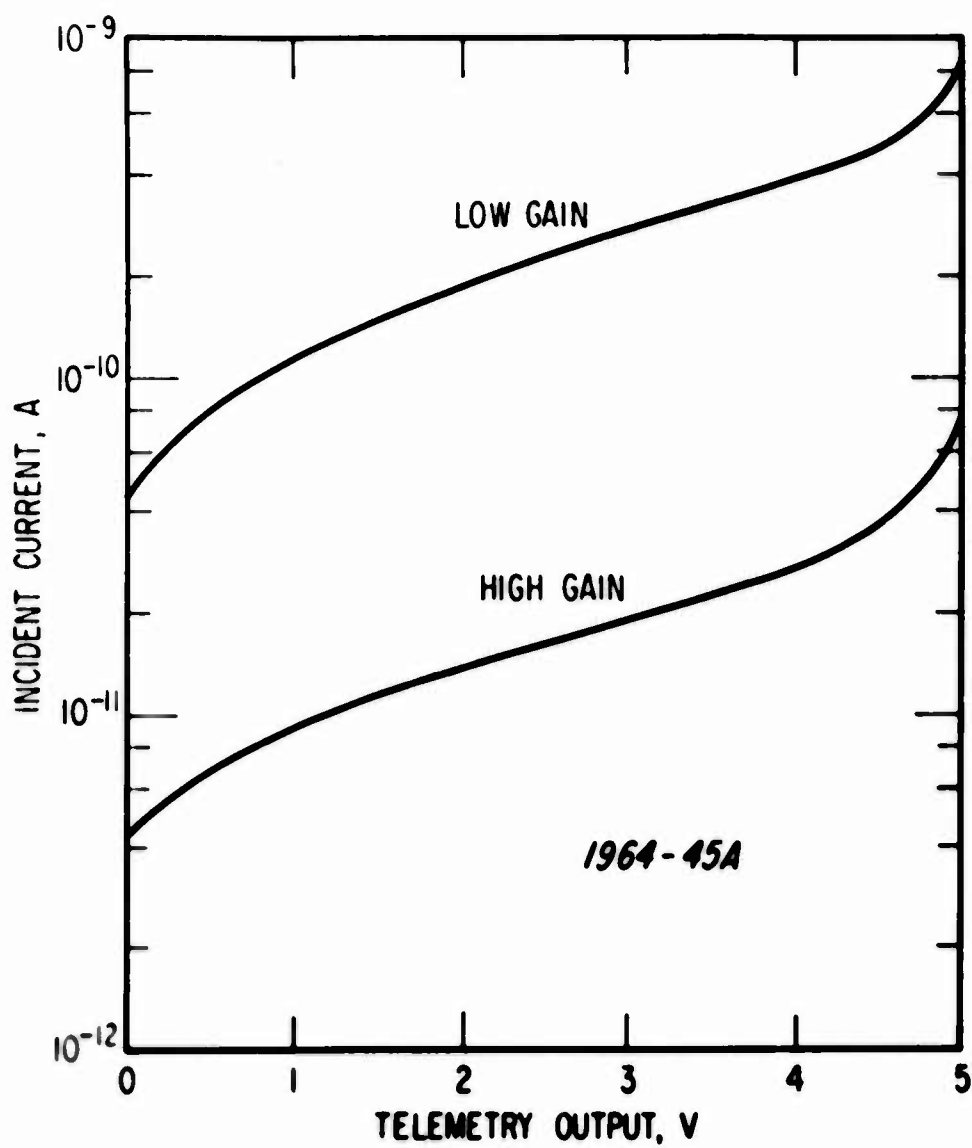
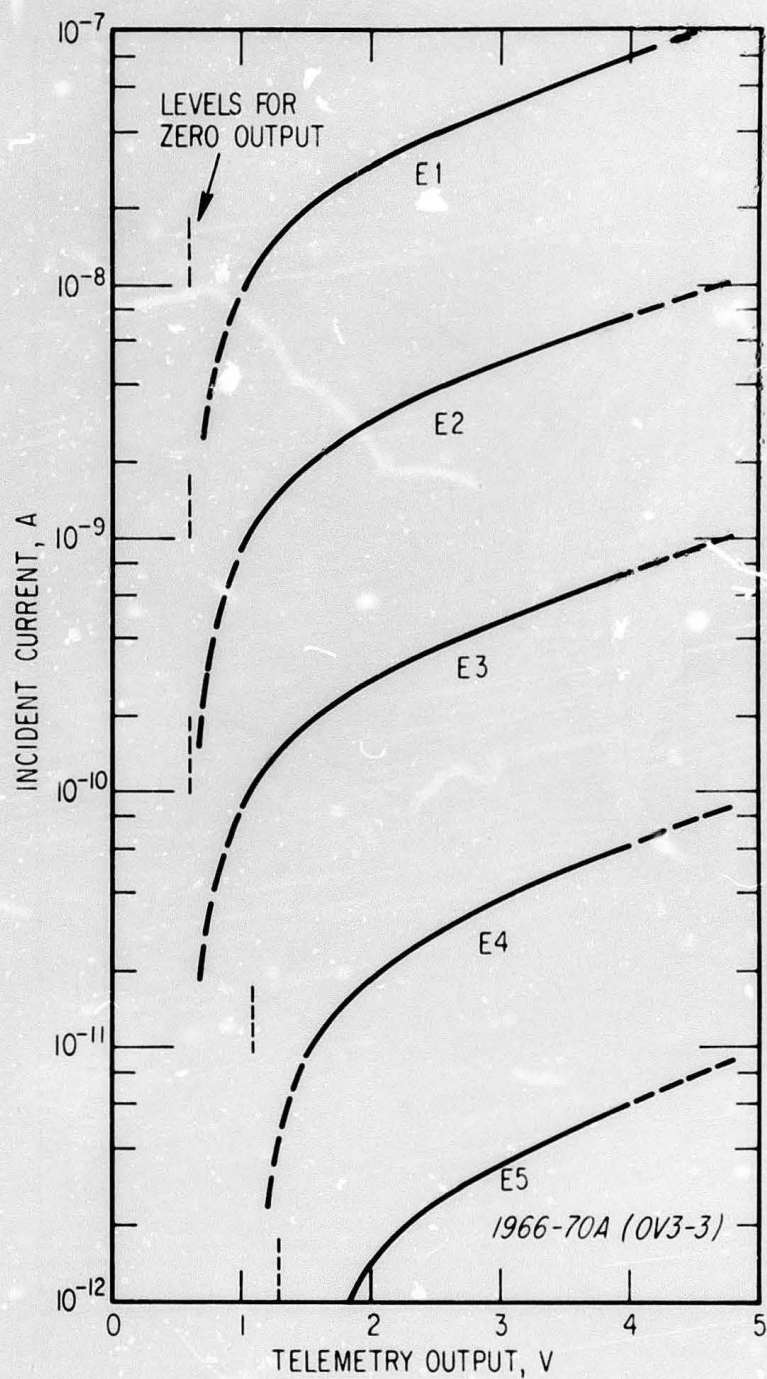Fig. 24. Incident Current Calibration Curves for 1964-45A

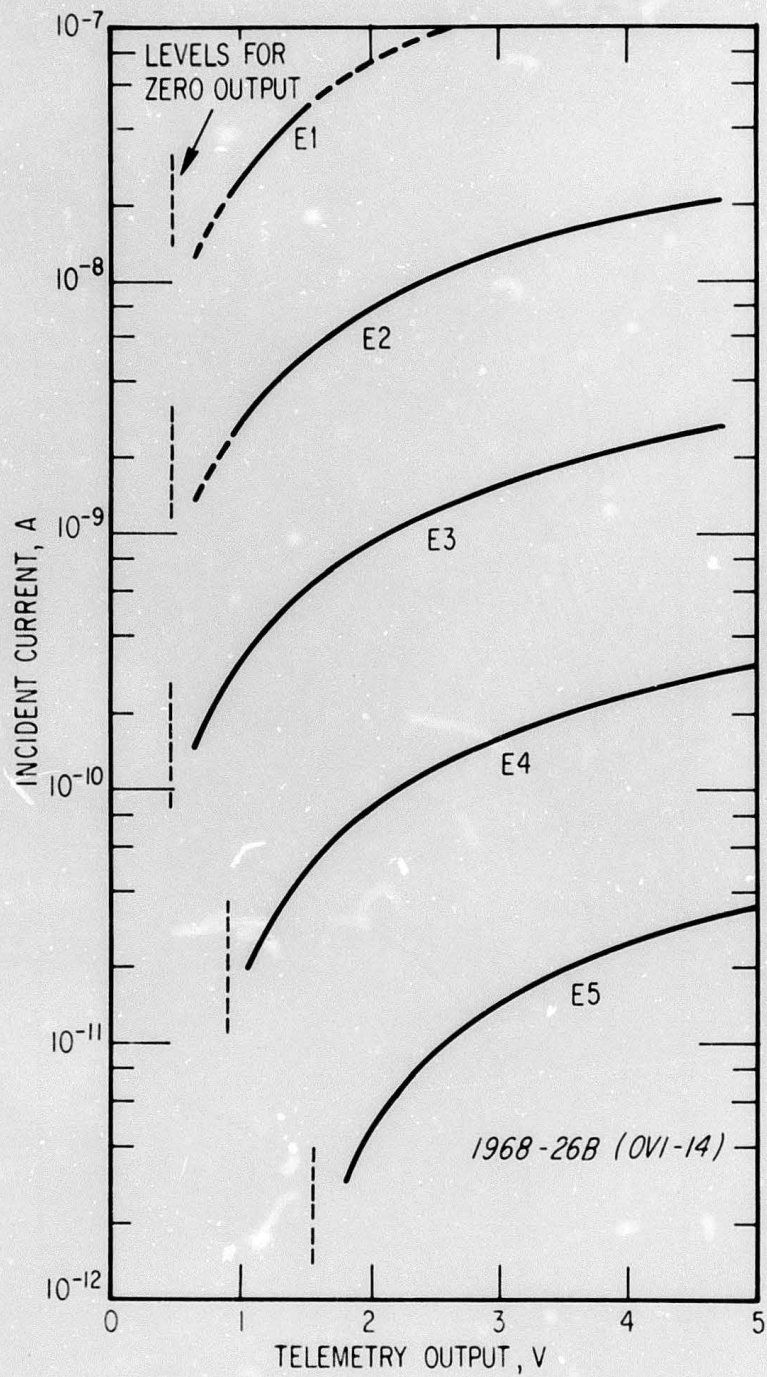Fig. 25. Incident Current Calibration
Curves for OV3-3

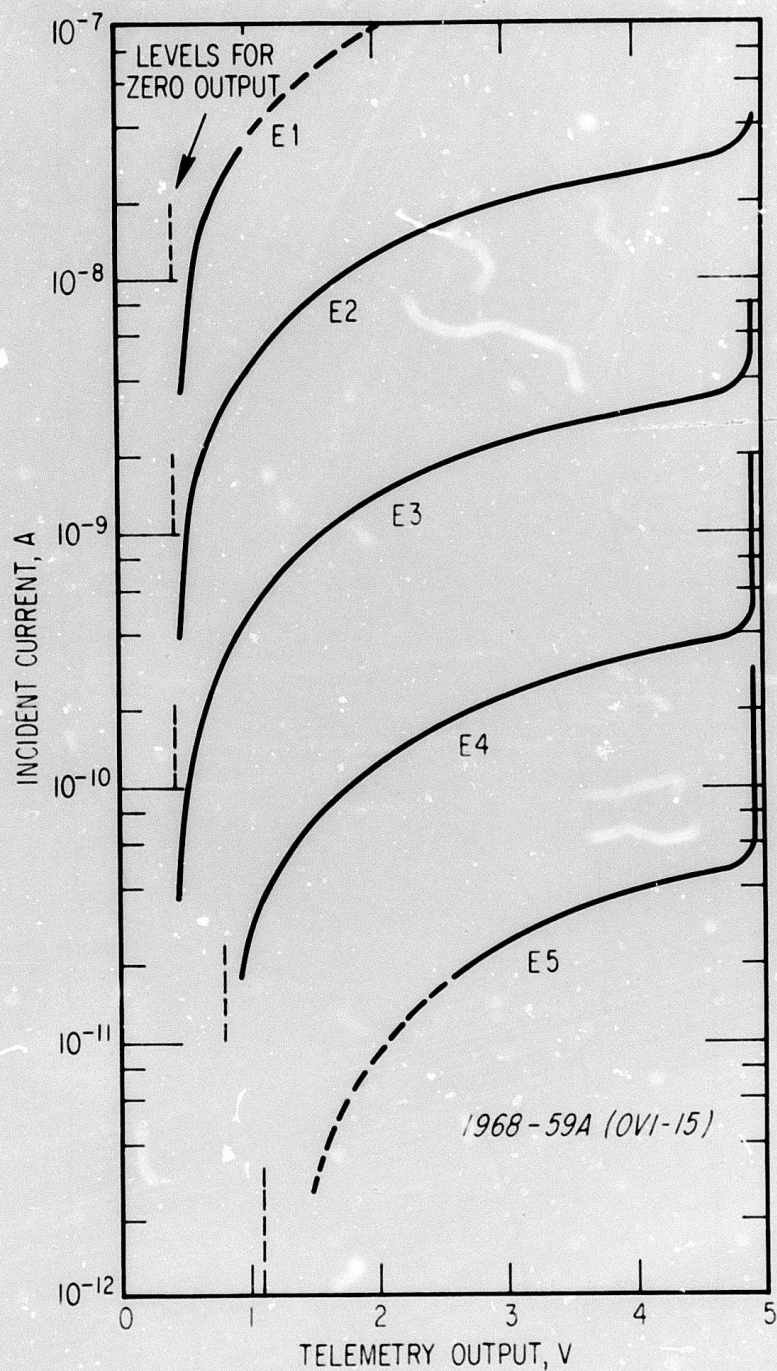Fig. 26. Incident Current Calibration
Curves for OV1-14

Fig. 27. Incident Current Calibration
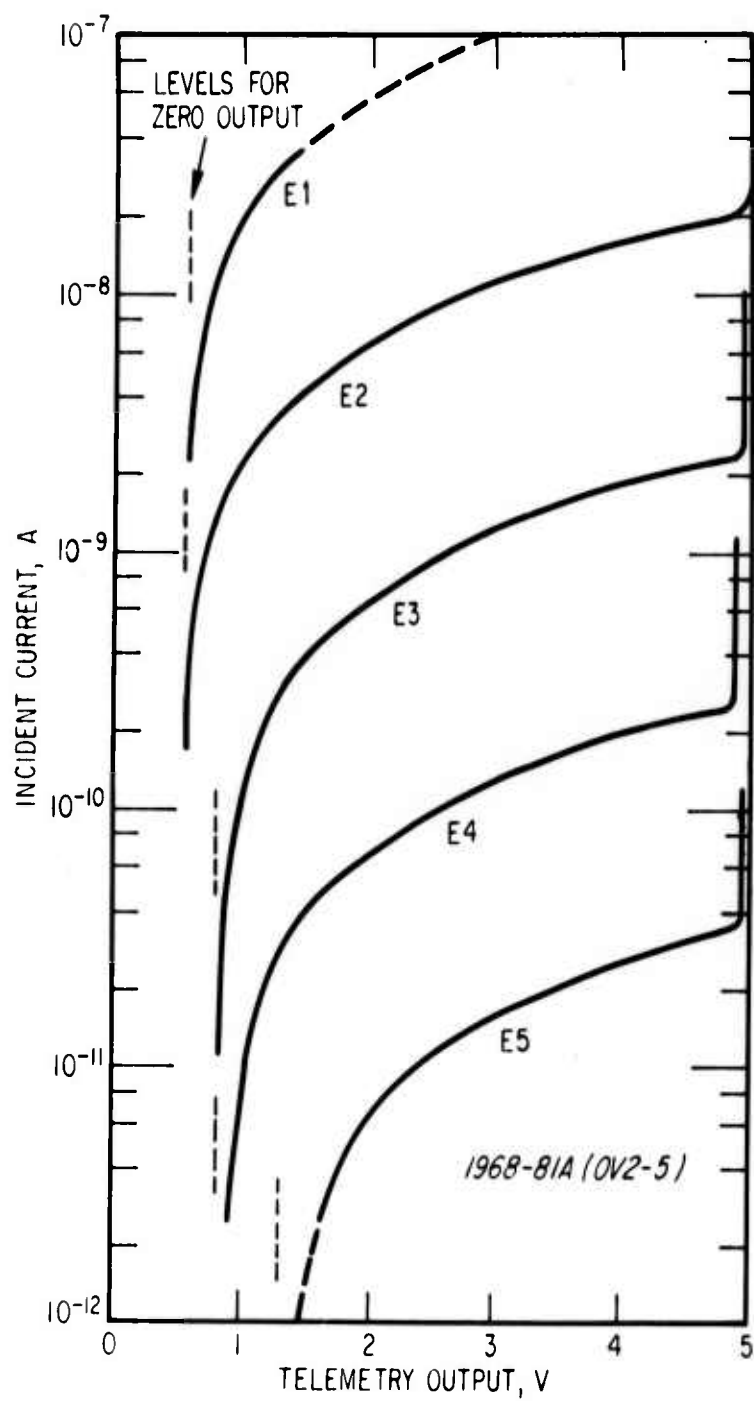Curves for OV1-15

Fig. 28. Incident Current Calibration
Curves for OV2-5

The second confirmation of the Faraday cup's sensitivity calibration was
obtained when we placed the instrument in the exhaust of a TRW ion engine.
The incident beam, which had no net charge, consisted of ionized hydrogen
and electrons. Monitor measurements with the TRW Faraday cup current
collector were a factor of 2.5 less than current measured by the Aerospace
Faraday cup — $\rho(TRW)/\rho(FC) = 0.4$. This difference was partially attributed
to the divergence of the exhaust flow from the engine. The Aerospace Faraday
cup was directly in line with the engine exhaust, whereas the TRW monitor
cup was offset 20 deg from the exhaust direction.

Sensitivity confirmation during flight was achieved through the use of an
internal calibration signal on all successful flights subsequent to the 1964-45A
flight. This signal allowed us to compare the sensitivity of the Faraday cup
collector assembly during flight to the sensitivity measured in the laboratory.
Values of these inflight calibration signals are given in Table III. In order to
convert the sensitivity measurements to flux incident on the instrument, the
geometrical factor of the instrument must be known. Table III also contains
collector dimensions and two geometrical factors. The first geometrical
factor is the effective area of the collector, assuming a plane parallel beam
of incident particles. In the second factor, an isotropic omnidirectional flux
of incident particles is assumed. This second factor was calculated with the
supposition that the collector assembly could be represented by two circular
apertures with areas A_1 and A_2 separated by the distance $l = (A_3/\pi)^{1/2}$.

$$G_2 = \frac{\pi}{2}\left\{ A_1 + A_2 + A_3 - \left[(A_1 + A_3)^2 + (A_2 + A_3)^2 - 2A_1 A_2 - A_3^2 \right]^{1/2} \right\}$$

C. GEOMETRICAL CHARACTERISTICS

Two other characteristics of the Faraday cup were checked during the
tests at TRW. As the instrument is rotated in a parallel beam of particles,
the flux of particles observed should vary with the angle between the beam and
the axis of the Faraday cup θ. The theoretical counting rate (CR) for two

-69-

circular apertures with equal radii r, separated by the distance l, is given by the following expression:

$$CR = CR_o \, T^7(\theta) \, \cos \theta \left\{ 1 - \frac{2}{\pi} \left[\sin^{-1} (Z) + Z(1 - Z^2)^{1/2} \right] \right\}$$

where

$$Z = \frac{l}{2r} \tan \theta$$

and

$$T(\theta) \cong T^{1/2} \left(\frac{T^{1/2} - 1 + \cos \theta}{\cos \theta} \right)$$

The expression $T(\theta)$ is the result of the decrease in transmission of a grid as the angle of the incident beam is moved away from the instrument normal. A comparison of the theoretical expression (solid curve) with the measured values (●) is shown in Fig. 29. A value of 1.07 for $l/2r$ was used, and good agreement was
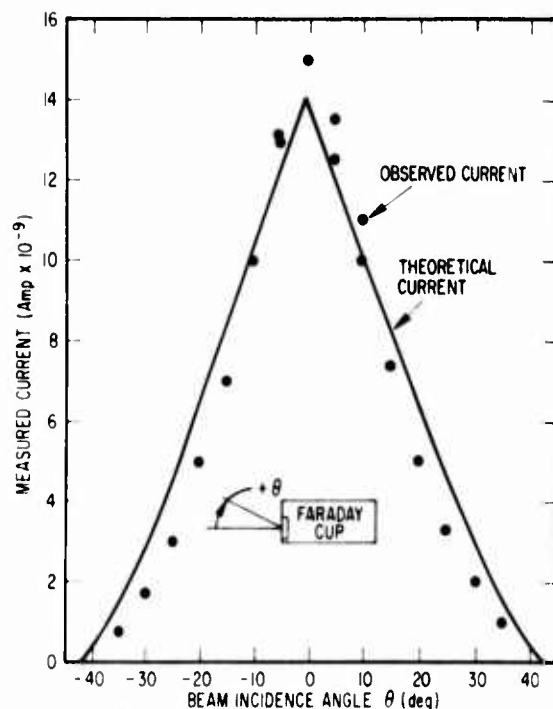

Fig. 29. Measured and Calculated
Angular Response Curves
for a Faraday Cup Detector

achieved between the measured and calculated response. As the Faraday cup is rotated with respect to the incident beam, the energy of the thresholds for the various steps should vary with angle. The instrument analyzes the component of the energy parallel to the axis of the instrument. Therefore, as the angle θ increases, the energy of the incident beam must increase as $(\cos^2 \theta)^{-1}$ in order for the particles to be observed in a given step. The product of $E_t \cos^2 \theta$ should be constant for all θ, where E_t is the threshold energy for a given step. The energy of the lower threshold of one step was measured as a function of the angle between the incident beam and the Faraday cup. A listing of the observed variation of threshold energy with the angle of beam incidence is presented in Table V. The product of $E_t \cos^2 \theta$ is constant to within the accuracy of the measurement. During all the tests at TRW, the Faraday cup rejected the low-energy electrons in the beam and measured the ionized proton current.

Table V. Threshold Dependence on Angle of Incidence

θ (deg)	E_t(eV)	$E_t \cos^2 \theta$
0	1,407	1,407
10	1,434	1,391
20	1,586	1,401
30	1,873	1,405

D.   ULTRAVIOLET SENSITIVITY

Each of the Faraday cups was illuminated in 10^{-6} Torr vacuum with a Pen-Ray lamp, Model 11 SC-1. No response was observed from the lamp in either the proton or electron modes. The lamp emitted 600 μW/cm^2 of 2537 Å light at a distance of 2 in. This is equivalent to the integrated solar emission at 2500 Å in a 300 Å band.

E. VLF SIGNAL

The radiated signal strength between 0.1 to 20.0 kHz was measured by means of a loop antenna at a distance of 1 m from the instrument. This measurement was made to determine the background to the VLF experiment caused by the Faraday cups. Of all the instruments, the Faraday cup and the plasma probe were the primary contributors of background to the VLF experiment. A typical example of the power spectrum generated by the Faraday cup for the OV3-3 flight instrument is shown in Fig. 30, with the various signals labeled by the power supply that caused them. The major contributors to VLF background were the 2 kHz square-wave generators used to determine the differential energy window for each step. In instruments subsequent to OV3-3, the radiated signals from all supplied could be reduced with the exception of the ac supplies. The signal from the AC supplies in orbit cannot be reduced because the beam rejected by the instrument is modulated at 2 kHz. This modulated beam interacts with the plasma near the spacecraft and is coupled by the plasma to other parts of the spacecraft such as the VLF antenna.

F. THERMAL TESTS

All flight instruments were operated at the temperature extremes for which they were designed. During thermal testing, a number of electronic failures occurred, but their causes were eliminated. The high-voltage monitors were always temperature dependent, and the variation of the high-voltage monitor outputs with temperature was recorded. Thermistors were incorporated in the instruments so that the high-voltage monitor values in orbit could be temperature corrected to obtain the proper retarding potentials. A typical thermistor calibration curve is presented in Fig. 31.

G. CONCLUSIONS

Throughout the calibration and thermal tests, the Faraday cups operated in a predictable fashion, and the laboratory tests indicated that the instrument
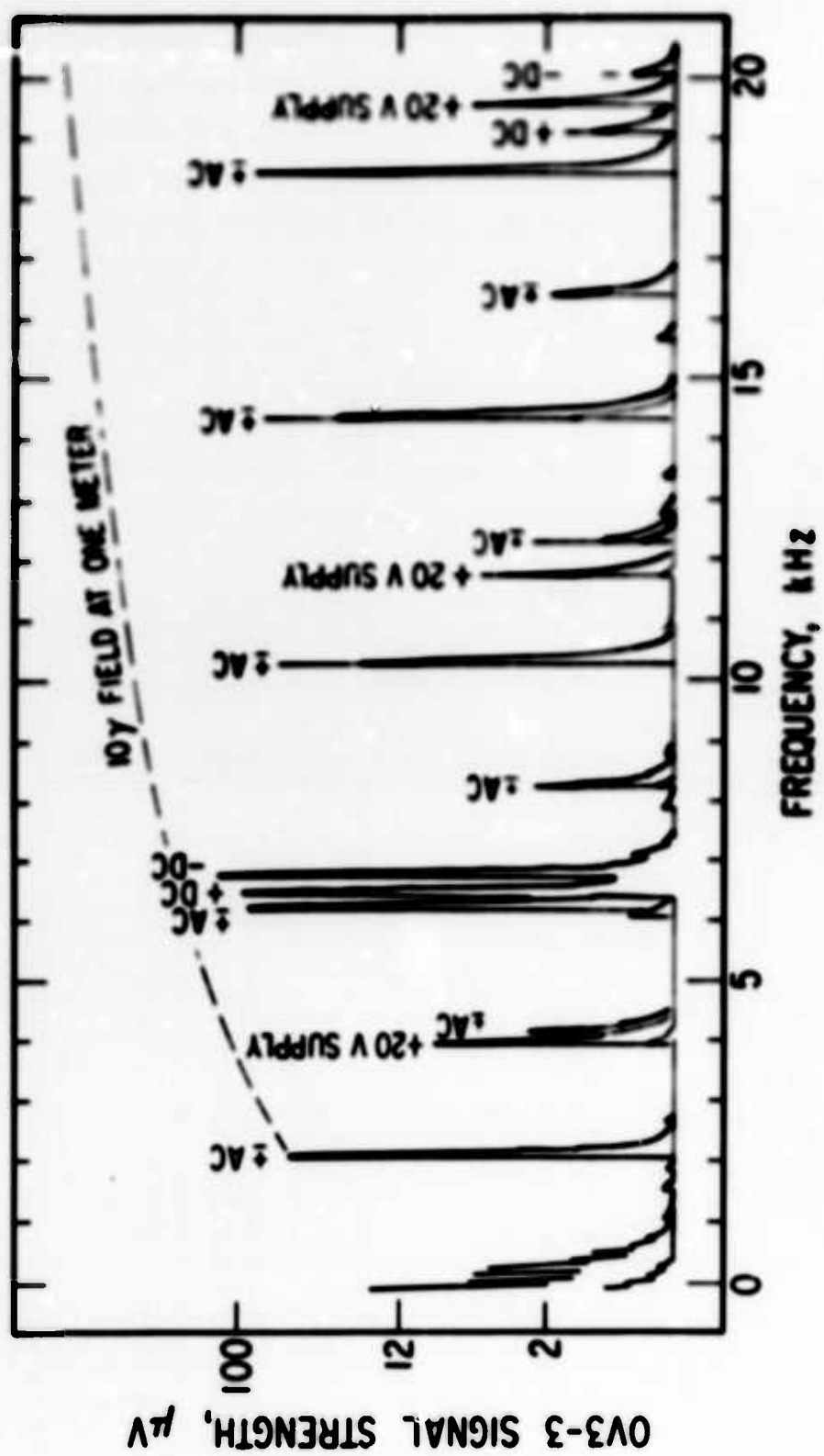
Fig. 30. Radiated VLF Signal from the OV3-3 Faraday Cup Detector

should have functioned properly as a flight instrument. During these tests, the two fundamental unknowns were the effect of the repelled beam of particles on the plasma near the spacecraft and the effect of extreme ultraviolet radiation on the instrument. In a controlled environment, the Faraday cups measured both protons and electrons accurately. The effect of the space environment on the operation of the Faraday cups is discussed briefly in Section VI.
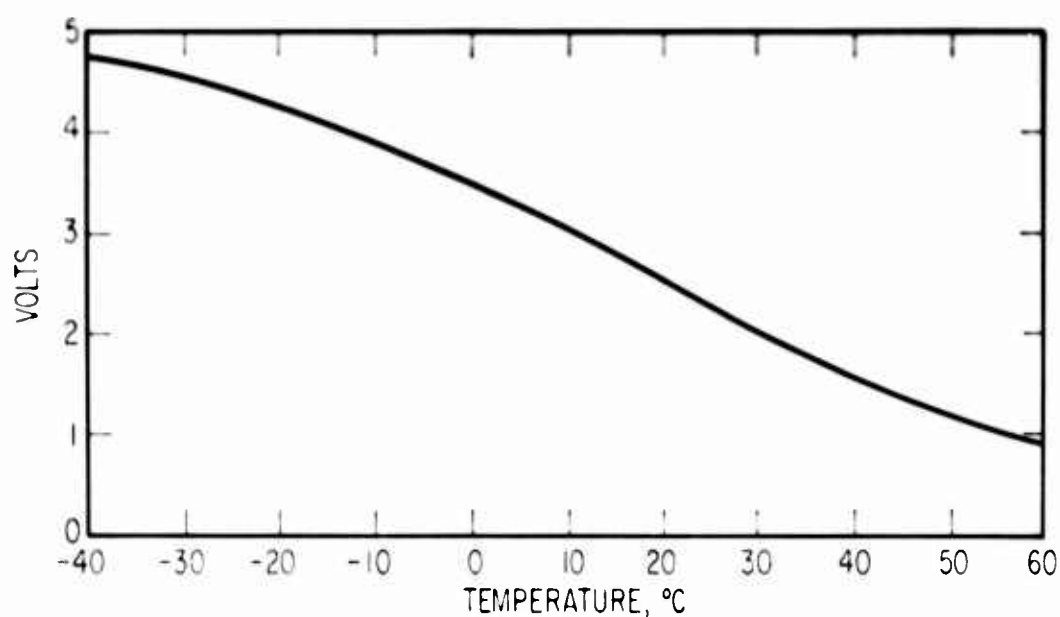

Fig. 31. Temperature Calibration for a
Nominal Thermistor

VI.   OBSERVATIONS

A history of the **Faraday** cup effort was presented in Section III, together with a brief discussion of the five successful flights - 1964-45A, OV3-3, OV1-14, OV1-15, and OV2-5.   Data received from these flights will be examined in the paragraphs that follow.

A.   1964-45A

Although there is doubt as to the validity of the measurements made in 1964, as evidenced by observations made in 1968, a discussion will now be presented of the proton and electron measurements as they appeared to us in 1964 and as they appear at this time.

The instrument was mounted on the spacecraft to look perpendicular to the spin direction.   Initially, the coordinates of this spin vector were declination 77.5 deg N, right ascension 206.5 deg E, and the spin rate was 1 rps. The orbital parameters were apogee 3765 km, perigee 266 km, and inclination 96 deg.   Initially, perigee was 18.2 deg N, which precessed southward at 2 deg/day and occurred at 1:30 a.m. local time (LT).   The orbital period was 127 min.

The first complete orbit of **Faraday** cup data with normal operation was obtained during orbits 9 and 10.   Prior to that time, outgassing of the instrument was responsible for arcing in the high-voltage supplies, which caused random sequencing of the programmer.   The proton data obtained from this orbit is presented in Fig. 32.   The commutator speed was such that 64 revolutions (the cycle period of the **Faraday** cup) took approximately 70 sec.   Each energy was sampled eight times per cycle, but only the last two samples have been plotted.   The most striking feature of this data is the magnitude of the fluxes.   The saturation value of these fluxes is 6×10^9 particles cm^{-2}-sec^{-1}-sr^{-1}, or 10, 40, 70, and 100 ergs -cm^{-2}-sec^{-1}-sr^{-1} for 1, 4, 7, and 10 keV protons, respectively.   As can be seen from Fig. 32,
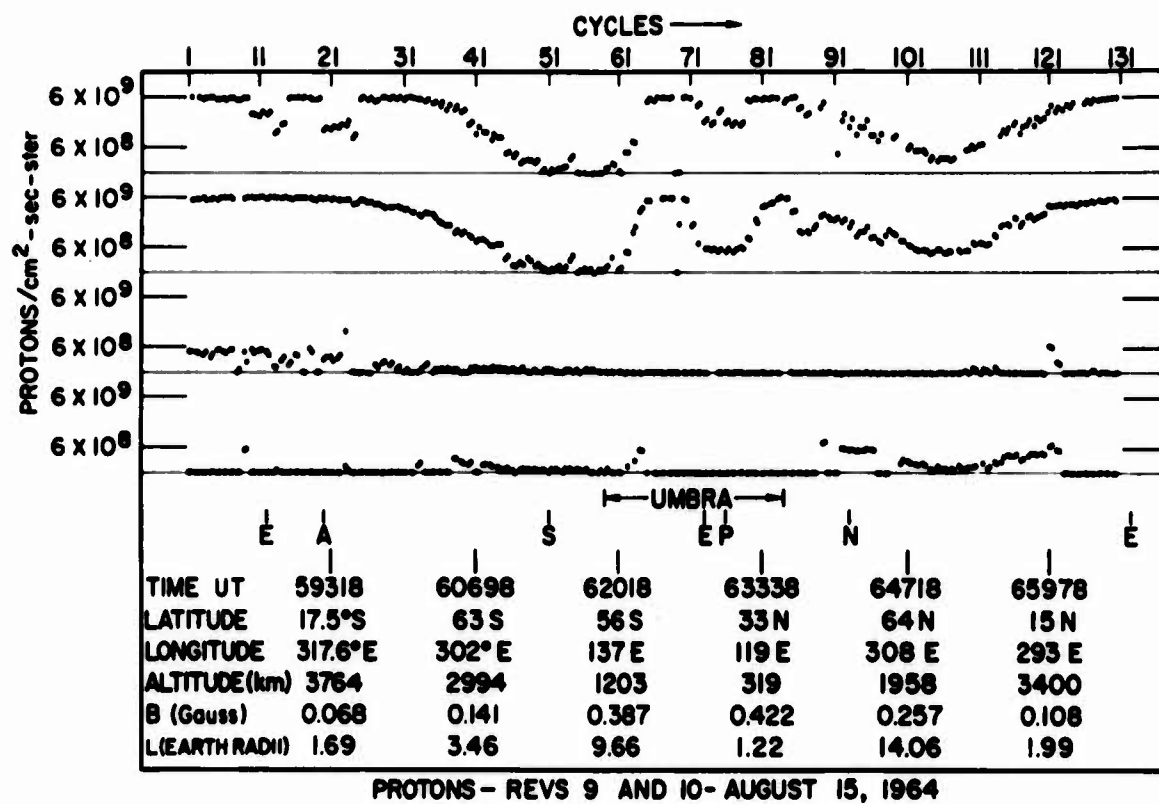
Fig. 32. A Complete 1964-45A Orbit

these large fluxes occur during a significant fraction of the orbit; they occur near apogee in the equatorial regions and near perigee until atmospheric density limits them.

During the apogee portion of the pass, the saturation flux of 1 and 4 keV protons continues through cycle 40, where it has fallen to about half the saturation value, and then commences again at cycle 117. The B, L, and λ (geomagnetic latitude) values of the spacecraft at these times were 0.125 gauss, 2.93, and 42.7 deg S; and 0.155 gauss, 2.89, and 44.6 deg N, respectively. At apogee, these coordinates were 0.068 gauss, 1.68, and 5.1 deg N.

Several apogee passes have been examined, and the most common situation is the one just described. Saturation fluxes of 1 and 4 keV protons were observed between 40 to 45 deg S and 40 to 45 deg N geomagnetic, where apogee has B values of 0.06 to 0.10 gauss and L values of about 1.7. Measurements by Freeman (1962) on Injun 1 with a CdS total energy detector indicate fluxes of protons greater than 1 or 2 keV of 50 to 70 ergs/cm^2-sec-sr at B $\sim$ 0.17 gauss and L $\sim$ 1.3 at altitudes of 1000 km. These measurements appear consistent.

The perigee portion of the pass (Fig. 32), cycles 61 to 101, exhibits large fluxes of 1 and 4 keV protons that diminish as the altitude decreases at perigee, then increases as the spacecraft rises again. It is evident that the atmosphere must play a dominant role in this phenomenon and that B-L coordinates, due to the offset of the dipole field, will be unsatisfactory in a discussion of these results. Hence, we have plotted our data on altitude-L plots, as shown in Fig. 33. The L parameter was chosen to correlate with the source of the particles and the altitude to correlate with the atmosphere. Figure 33 shows the several features that are characteristic of the perigee passes we have examined. These features include the decrease of flux with altitude, the apparent insensitivity of the instrument to sunlight as indicated by the points labeled "S," and the lack of flux at altitude 500 km, and L = 1.5. Figures 34 through 42 show nine additional perigee passes and indicate the quality and consistency of the data obtained.
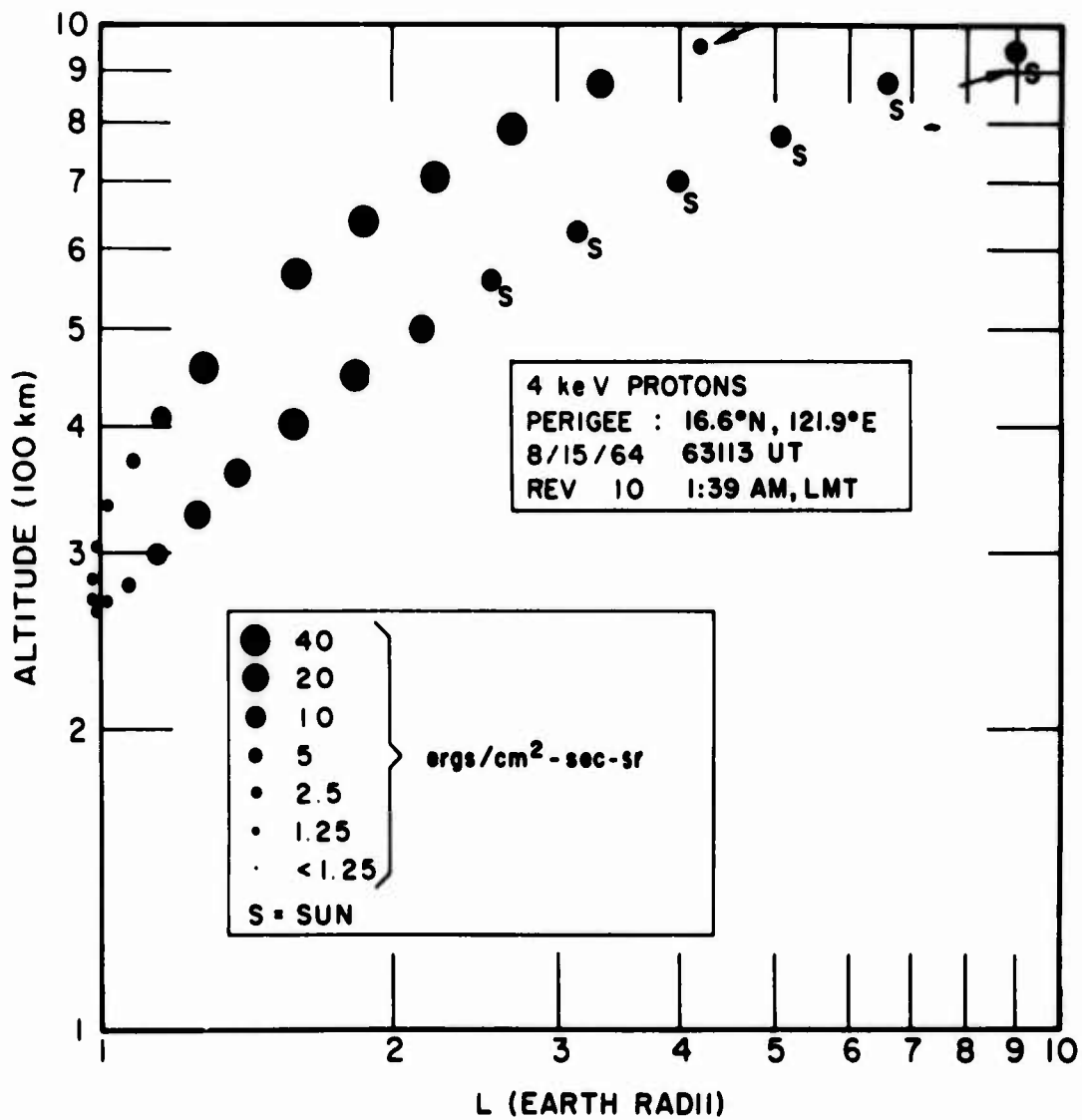
Fig. 33. Flux of 4 keV Protons on an Altitude-L Parameter
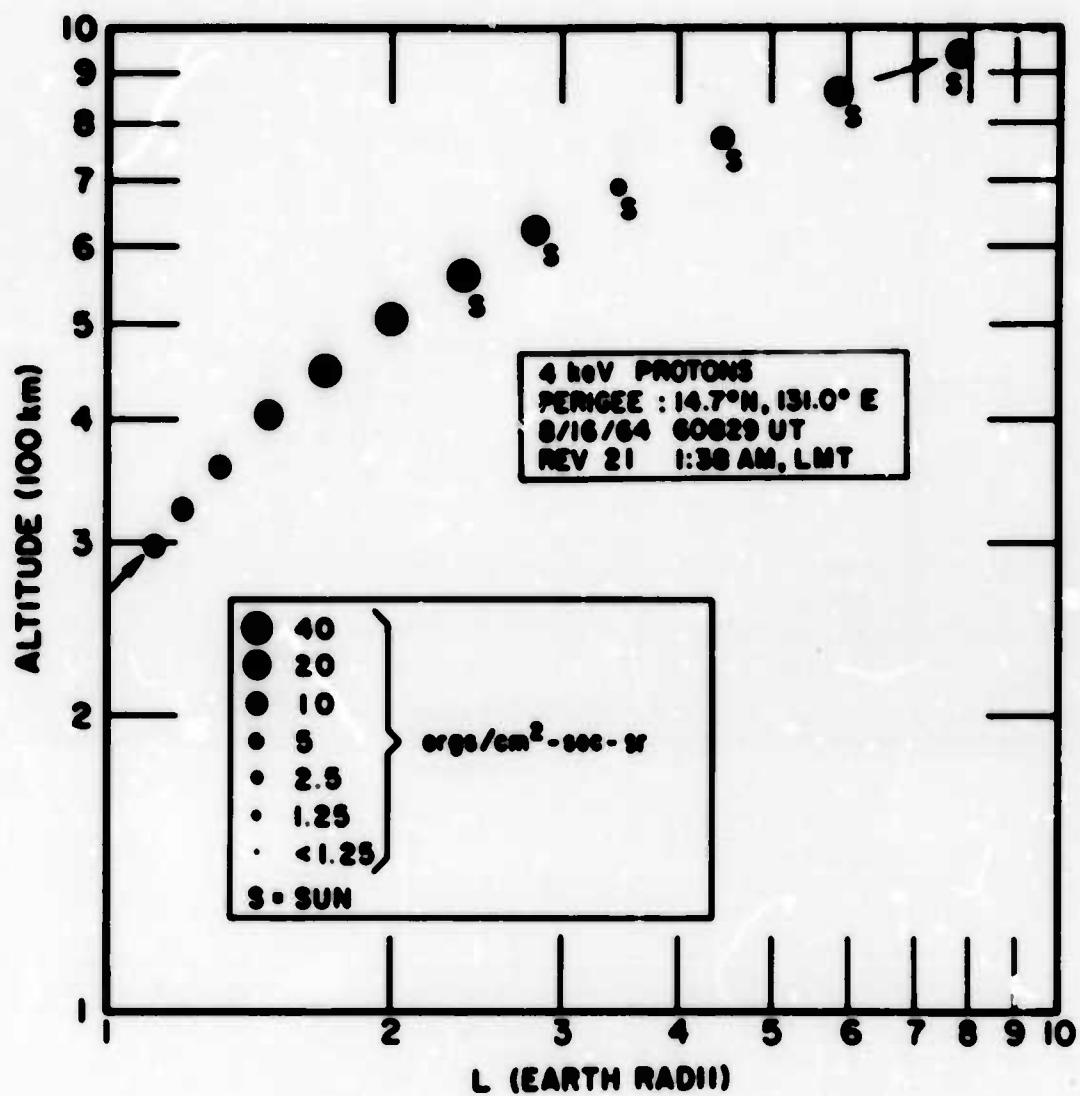Plot for Orbit 10

Fig. 34. Flux of 4 keV Protons on an Altitude-L Parameter Plot for Orbit 21
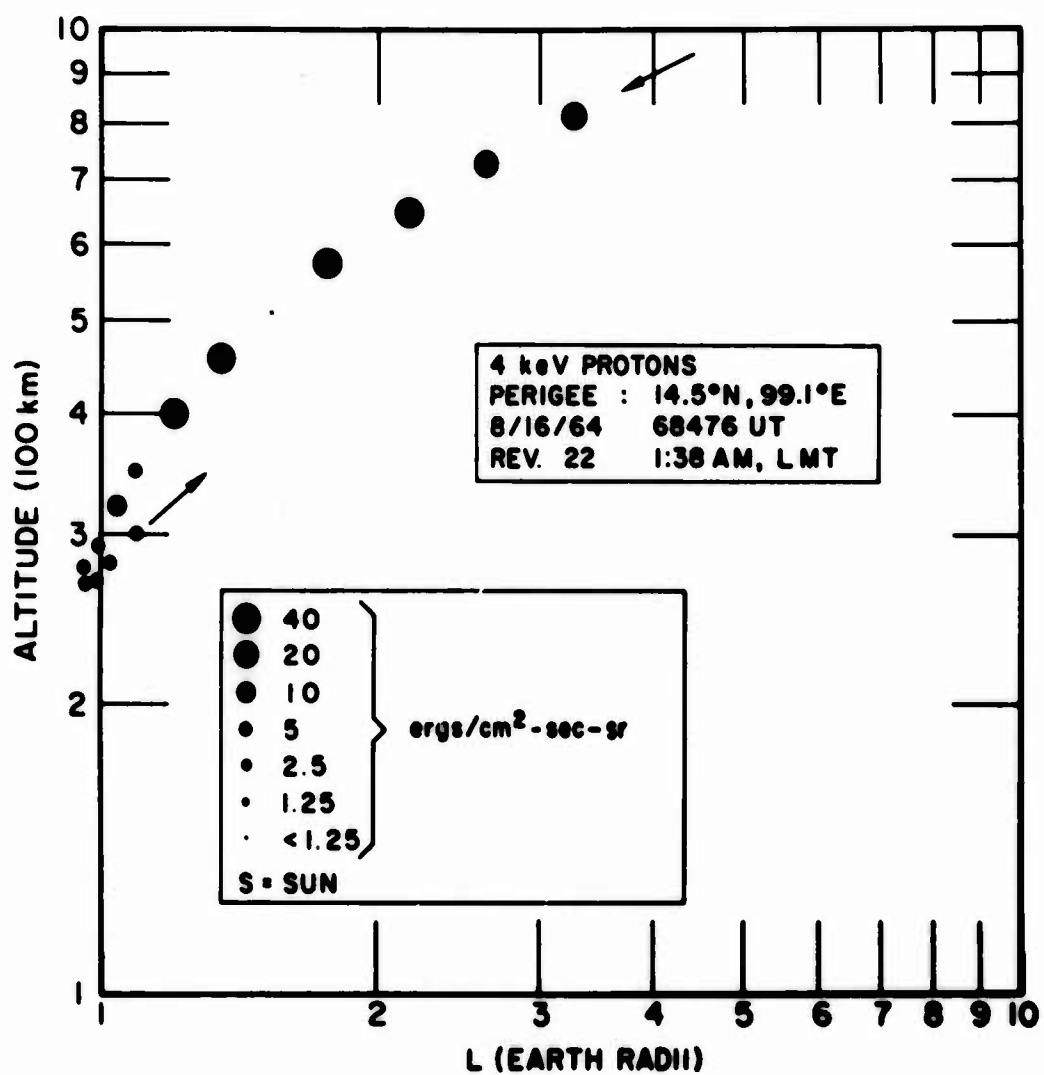
Fig. 35. Flux of 4 keV Protons on an Altitude-L Parameter
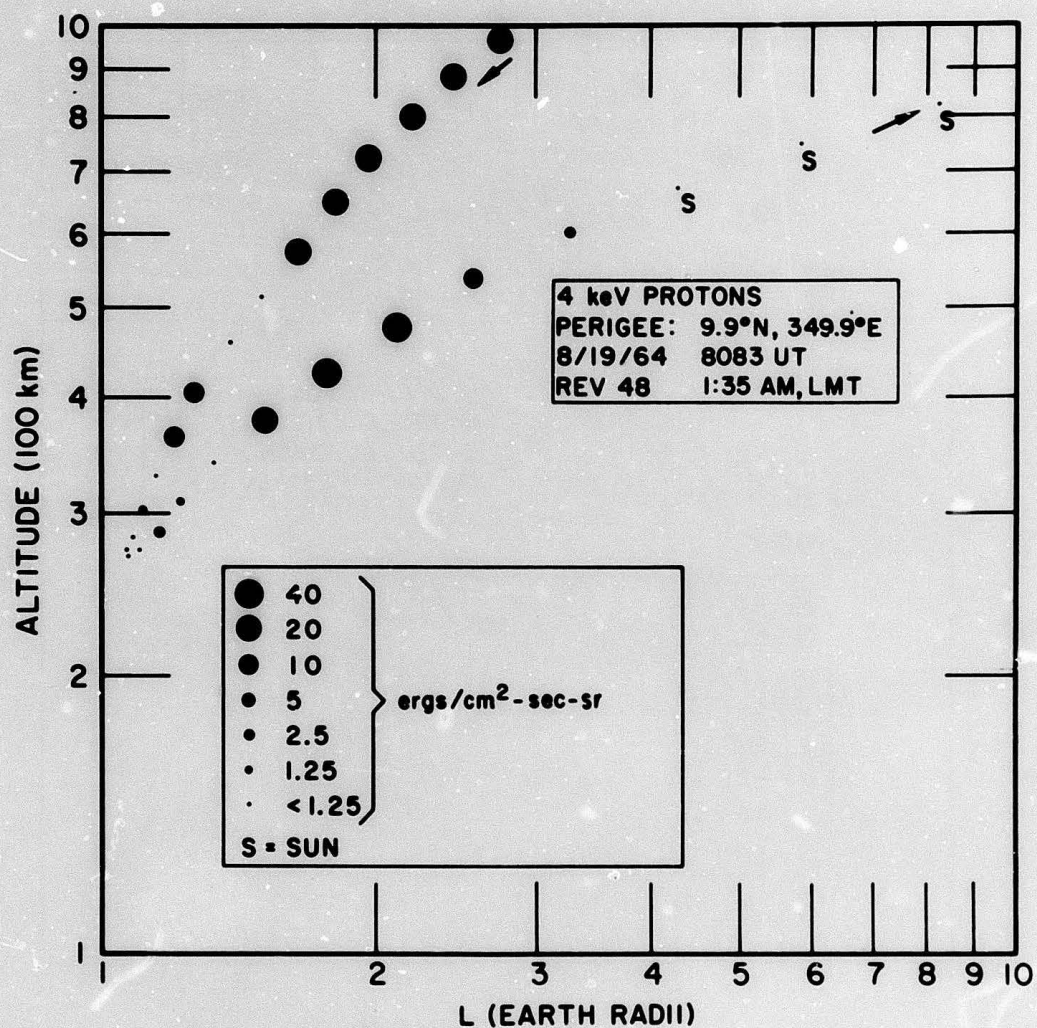Plot for Orbit 22

Fig. 36. Flux of 4 keV Protons on an Altitude-L Parameter
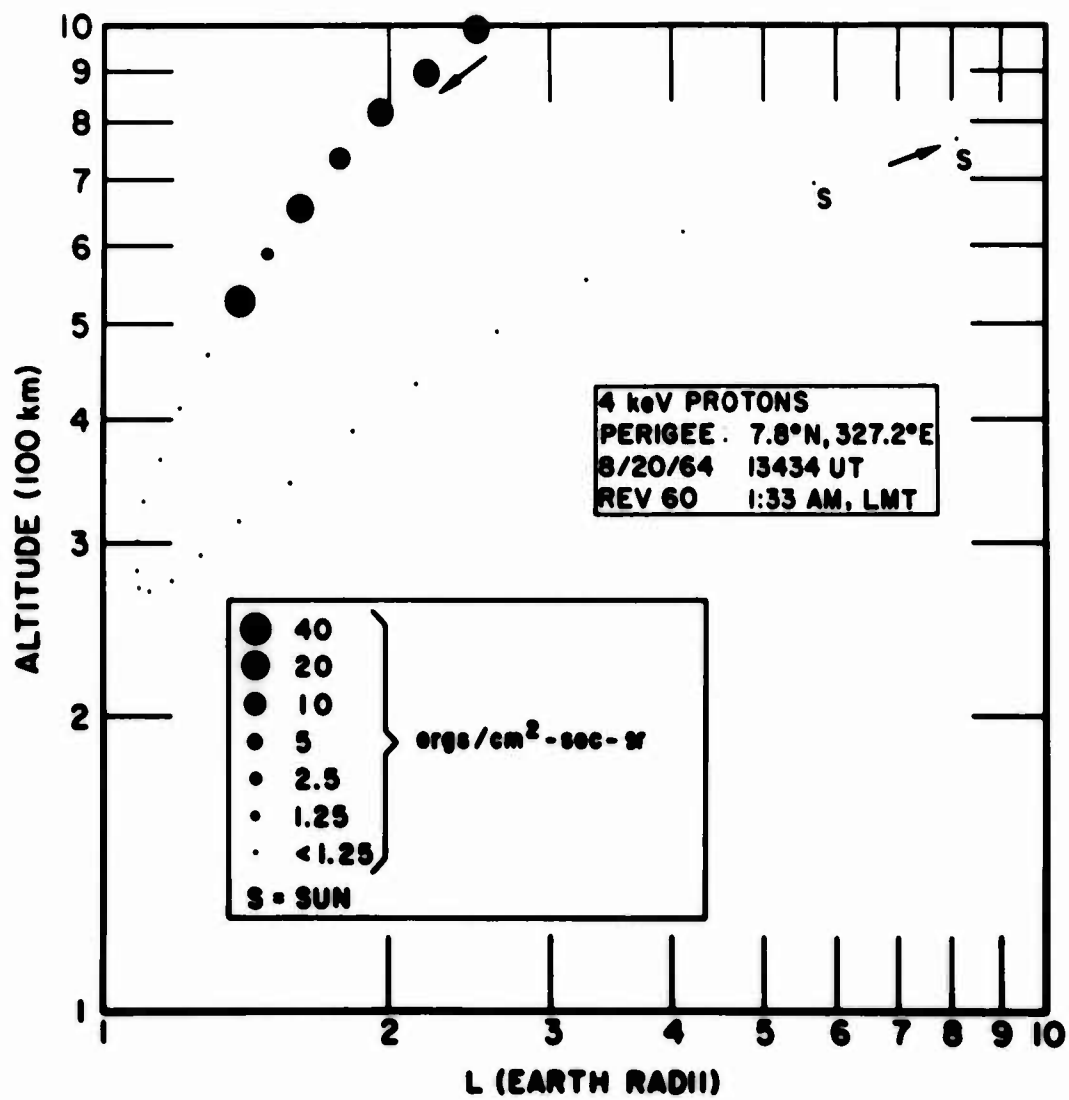   Plot for Orbit 48

Fig. 37. Flux of 4 keV Protons on an Altitude-L Parameter Plot for Orbit 60
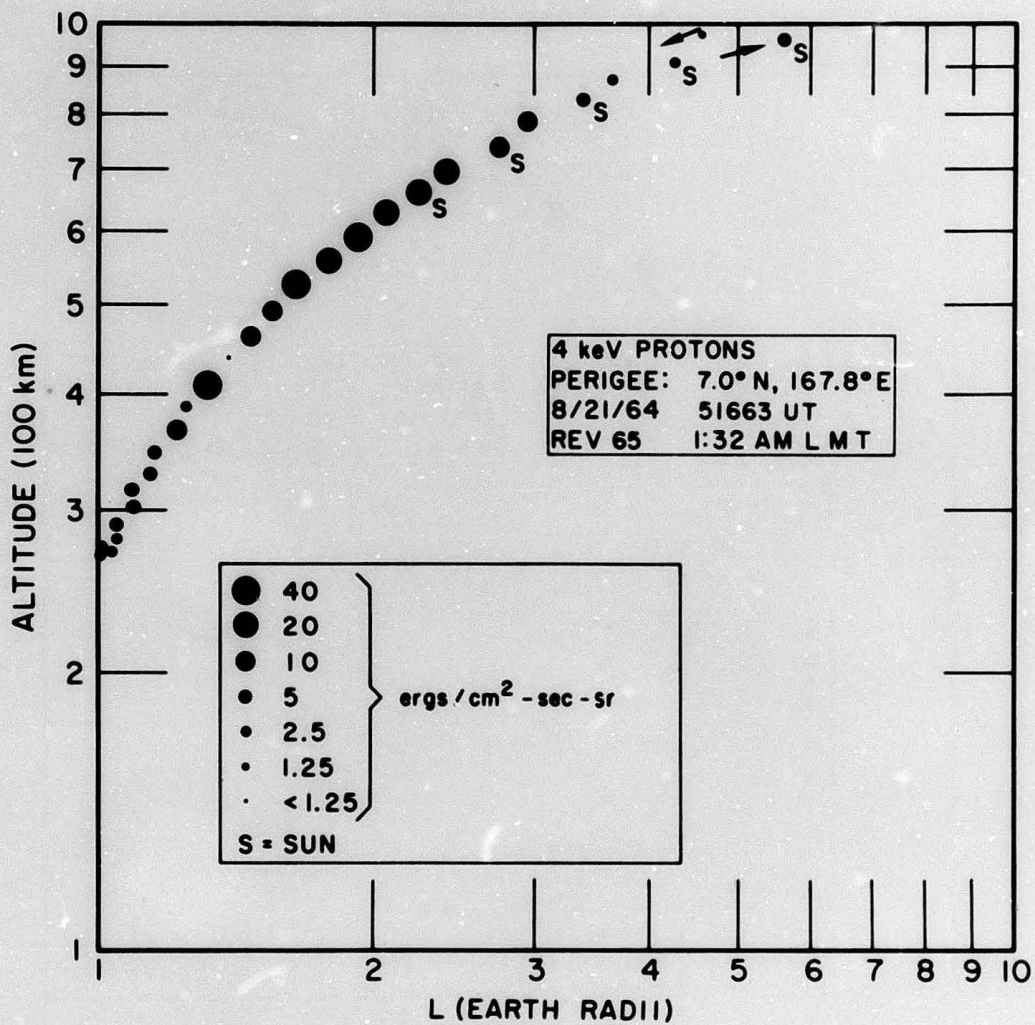
Fig. 38. Flux of 4 keV Protons on an Altitude-L Parameter
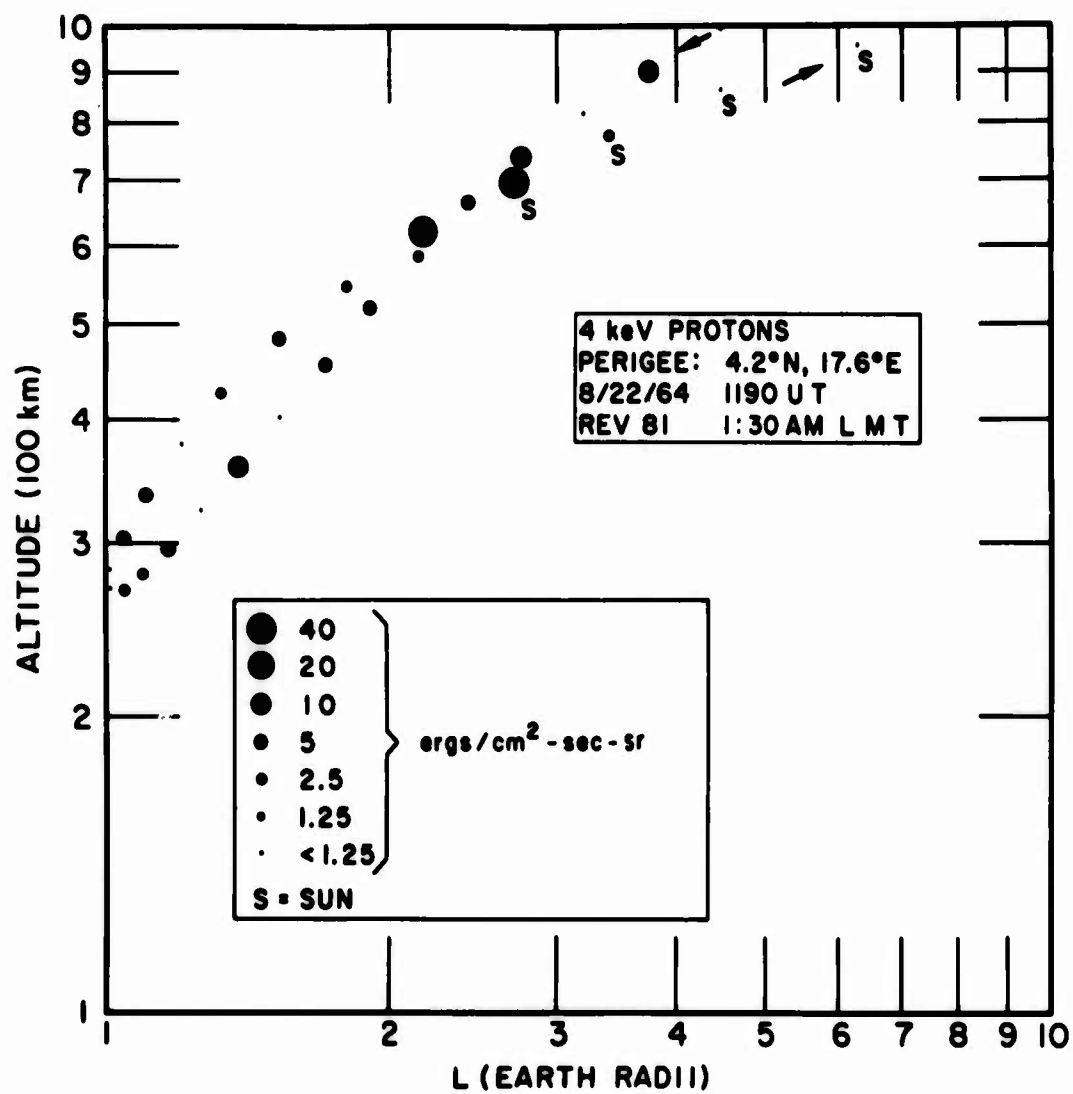Plot for Orbit 65

Fig. 39. Flux of 4 keV Protons on an Altitude-L Parameter Plot for Orbit 81

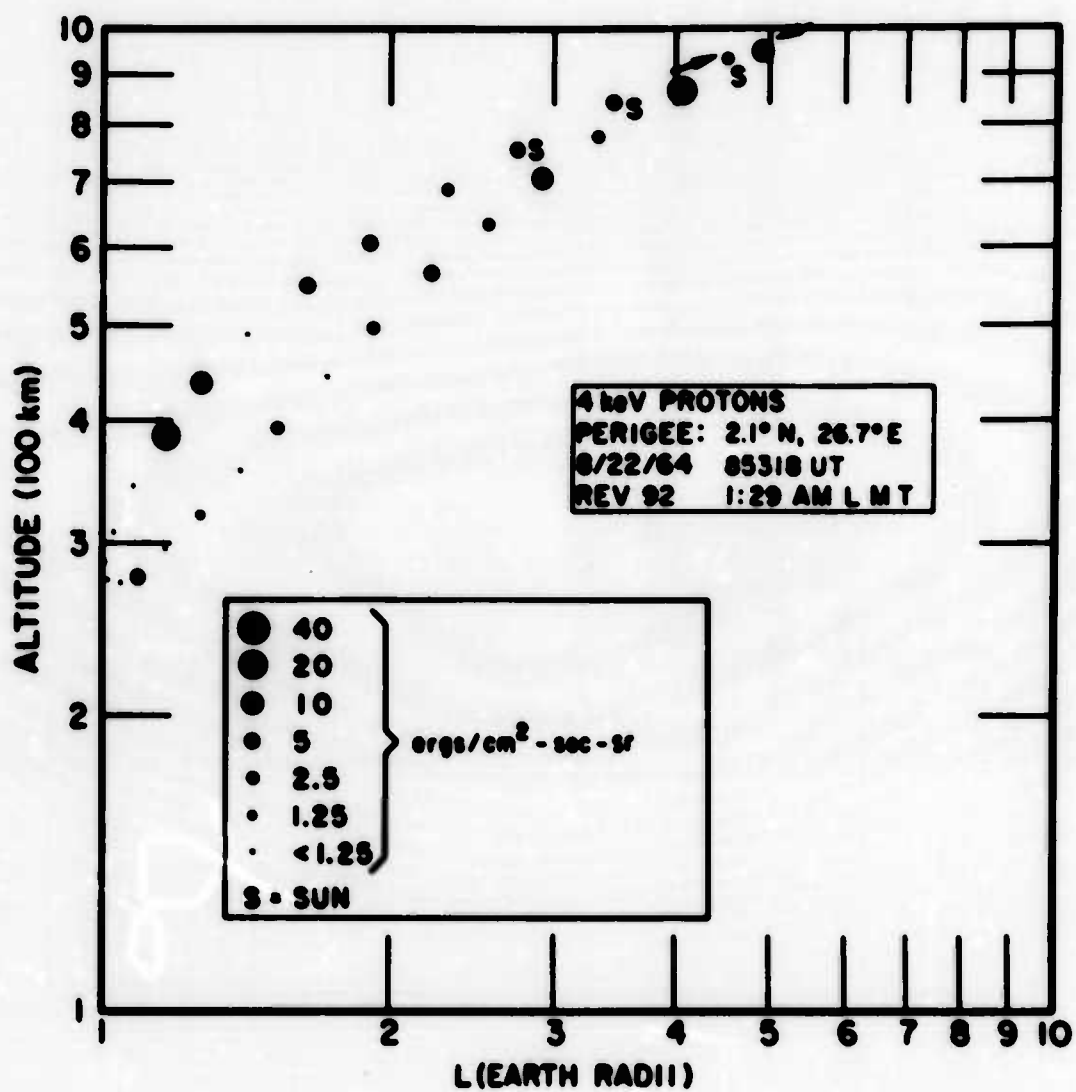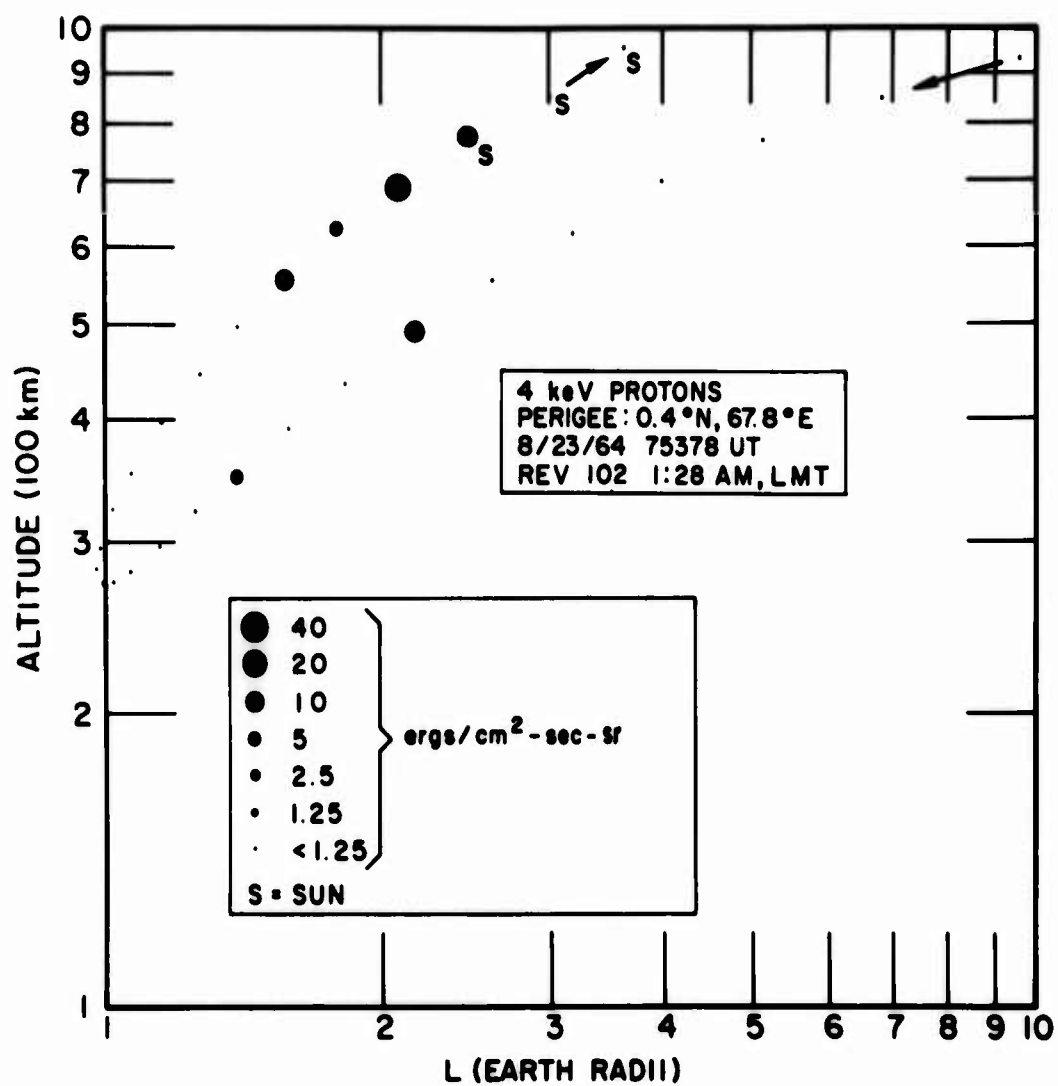Fig. 40. Flux of 4 keV Protons on an Altitude-L Parameter
Plot for Orbit 92

Fig. 41. Flux of 4 keV Protons on an Altitude-L Parameter
Plot for Orbit 102

4 keV PROTONS
PERIGEE : 28.7°S, 174.8°E
9/7/64   48432 UT
REV 267   1:06 AM, LMT

ALTITUDE (100 km)

● 40
● 20
● 10
• 5
• 2.5
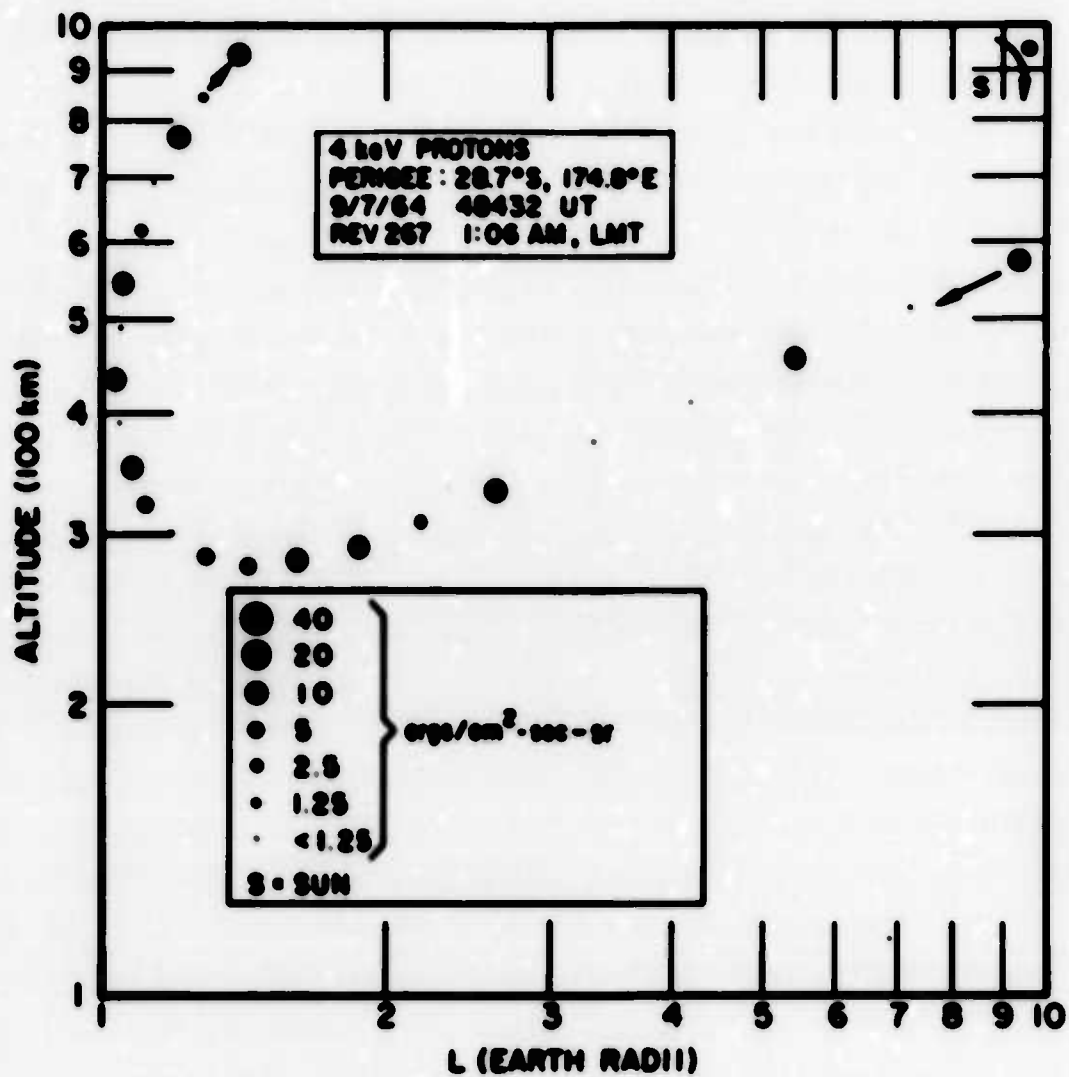· 1.25
· < 1.25

ergs/cm²-sec-sr

S = SUN

L (EARTH RADII)

Fig. 42.   Flux of 4 keV Protons on an Altitude-L Parameter
Plot for Orbit 267

The effect at altitude 500 km and L = 1.5 appears to be real and can be seen in all the perigee passes having these coordinates. In particular, perigee pass 66 (Fig. 38) is interesting, as both the descending and ascending portions of the pass are almost coincident in these coordinates. The points plotted are 6-sec averages and, hence, obscure rapid variations. Examination of the data at 460 km, however, reveals that the 4 keV proton flux decreased by a factor of 2 for 3 sec and then returned to its former value. As yet, we have no explanation for this effect.

Figure 43 presents the data from these 10 perigee passes, as a function of altitude, for L ≤1.5. The flux decreases nearly as rapidly as the inverse number density calculated from the Harris and Priester (1962) model atmosphere with an S index of 70 at 1:00 a.m., LT. This is consistent with a flux of protons incident upon the atmosphere and interacting with it.

Additionally, we have looked for a geographic ordering of the perigee data. In Fig. 44, the flux of 4 keV protons for altitudes less than 300 km has been plotted on a Mercator projection. The data here show no measurable flux (less than 1.25 ergs-cm^{-2}-sec^{-1}-sr^{-1}) of 4 keV protons in the South Atlantic anomaly and fluxes as high as 10 ergs-cm^2-sec-sr elsewhere.

Because electron fluxes were observed infrequently, only the real-time data were analyzed to find a suitable way of presenting the observations. An analysis was made of 4163 cycles of real-time data in which the Faraday cup measured electron fluxes greater than 8×10^7 particles-cm^{-2}-sec^{-1}-sr^{-1} in 265 cycles (5 percent of the time). Of these, 224 electron observations occurred between 15 September and 15 November 1964. Throughout the remainder of the year, electrons were observed only 1 percent of the time except in October when electrons were observed during 30 percent of the electron cycles. On 1 October 1964, the apogee of the satellite was on the sunlit side of the earth at 70 deg N latitude and was precessing northward at a rate of 2 deg/day, with equatorial crossings at local midnight and noon. Monthly correlations and anticorrelations between the incidence of electrons and various parameters were attempted, and the results were negative. The data do not correlate
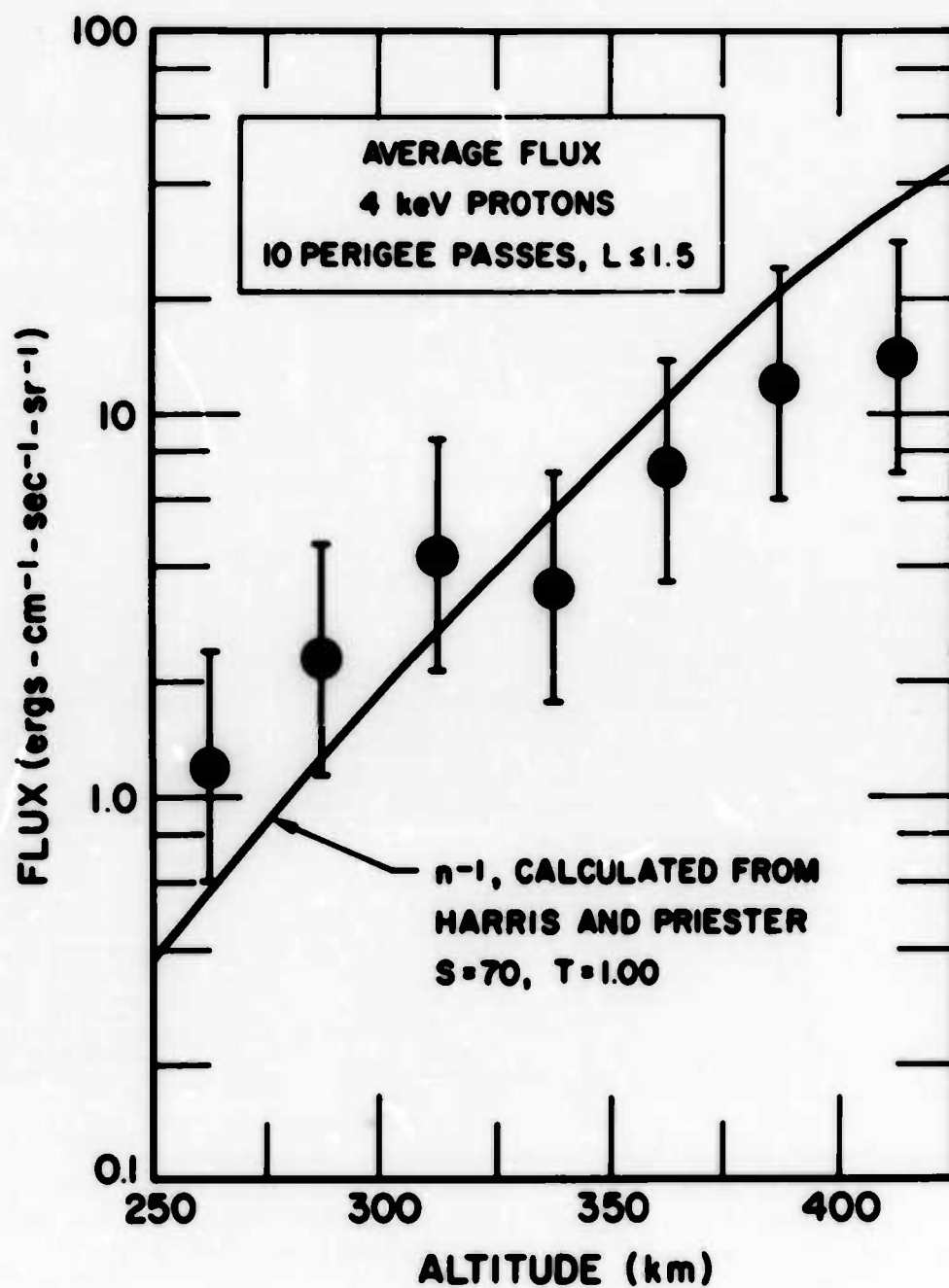
Fig. 43. Average Flux of 4 keV Protons from 10 Perigee Passes as a Function of Altitude
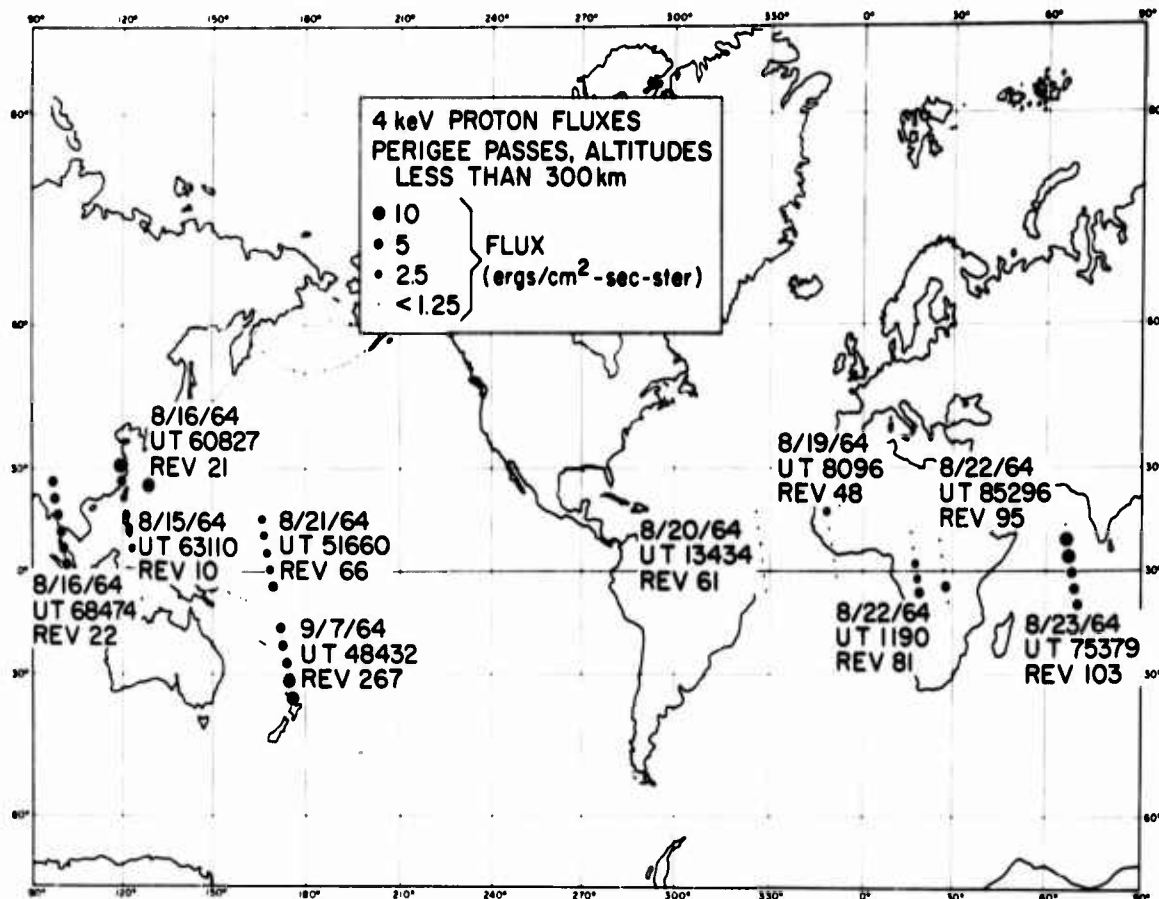
Fig. 44. Flux of 4 keV Protons from Perigee
Passes with Altitudes less than 300 km

with the locations of data acquisition, with the monthly A_p, with the percentage of time that the 3-hr K_p index was greater than 3o or less than 1-, or with altitude and altitude shadow combinations. These observations were not due to solar UV because no flux variations were observed either when the satellite passed from the earth's shadow to sunlight or from sunlight into the earth's shadow.

Frequently, the electron flux varied by two orders of magnitude from one cycle to the next and by one order of magnitude from second to second. Angular distributions were calculated for one orbit of tape-recorded data that showed that the fluxes peaked once for each satellite revolution at high latitudes, while at equatorial latitudes the angular distribution seemed to be doubly peaked. There are insufficient data for graphical presentation.

During the 15 September to 15 November 1964 period, the electron flux was nearly equally distributed between the day and night sides of the earth for $1.5 < L < 6$, whereas practically all of the electron observations for $L > 6$ were on the night side. In addition to this local time versus L dependence, the energy spectrum for the electrons observed near October 1964 differed from that observed throughout the remainder of the year. The statistics are extremely poor, as can be seen from Table VI. This table lists the number of orbits in each month in which 1, 4, 7, and 10 keV electrons were observed, the number of orbits in which any energy electrons were observed, and the total number of available orbits. The electrons had predominantly 7 and 10 keV energy during October, and 1 and 4 keV for the remainder of the year.

The foregoing observations were reported briefly in 1964 (Hilton, et al., 1964; Stevens, et al., 1964) and documented in 1966 (Hilton, et al., 1966).

Table VI. Incidence of Electron Observations with Flux Greater Than 8×10^7 Electrons-cm^{-2}-sec^{-1}

Month	Orbits with Electrons of Energy				Orbits with Electrons	Orbits of Data
	1 keV	4 keV	7 keV	10 keV		
August 1964	0	1	0	0	1	47
September	12	4	4	1	13	41
October	6	5	20	20	28	32
November	3	1	5	2	9	29
December	0	0	0	0	0	42
January 1965	0	0	0	0	0	8
February	0	3	2	1	4	31
March	4	2	0	0	4	14
April	2	0	0	0	2	4
May	2	0	0	0	2	6
June	0	1	0	0	1	7

B. OV3-3

The next successful launch of a Faraday cup detector was on the OV3-3 satellite, which was launched from Vandenberg Air Force Base in August 1966. Again the instrument was mounted on the spacecraft to look perpendicular to the spin direction.

The orbital parameters were similar to 1964-45A. Apogee was at 4488 km, perigee 364 km, and inclination 99 deg. Initially, perigee was 13.5 deg N, which precessed northward at 2 deg/day and occurred at 3:00 a.m. LT. The orbital period was 137 min.

The instrument functioned as expected at the start of the first two tape-recorded orbits, revs 3 and 6. That is, the four high-voltage monitors and the eight-point subcom low-voltage monitor gave the same values that were measured during calibration in the laboratory. Further, the five output voltages, which were proportional to the incident flux, appeared normal and were at the nominal values during the programmed calibration step.

In both these revolutions, however, the expected calibration voltages did not appear after the satellite had passed through perigee. The values of E1 through E5 before and after perigee in these two revolutions are shown in Table VII.

Table VII. Calibration Voltages

Outputs	Pre-Perigee (V)	Post-Perigee (V)
E1	0.55	0.55
E2	0.70	0.55
E3	2.00	0.55
E4	4.35	1.25
E5	4.40	2.50

We believe that this was due to an electronic failure in the preamplifier. It is curious that this failure apparently cured itself while the instrument was turned off during revs 4 and 5. Unfortunately, the failure on rev 6 was permanent, and the instrument never again calibrated properly.

During the 4 hours of normal operation on revs 3 and 6, there was no certain indication of any proton flux. Often there was a slight increase in the background level E5 as the positive DC grid voltage increased, from a background level corresponding to 2.3×10^5 cm^{-2} sec^{-1}-sr^{-1}-keV^{-1} at 0.80 keV to a background level corresponding to 5.3×10^5 cm^{-2}-sec^{-1}-sr^{-1}-keV^{-1} at 8.78 keV. An example of this effect is shown in Fig. 45. The satellite was near apogee, with coordinates of altitude 4470 km; latitude 20 deg S;
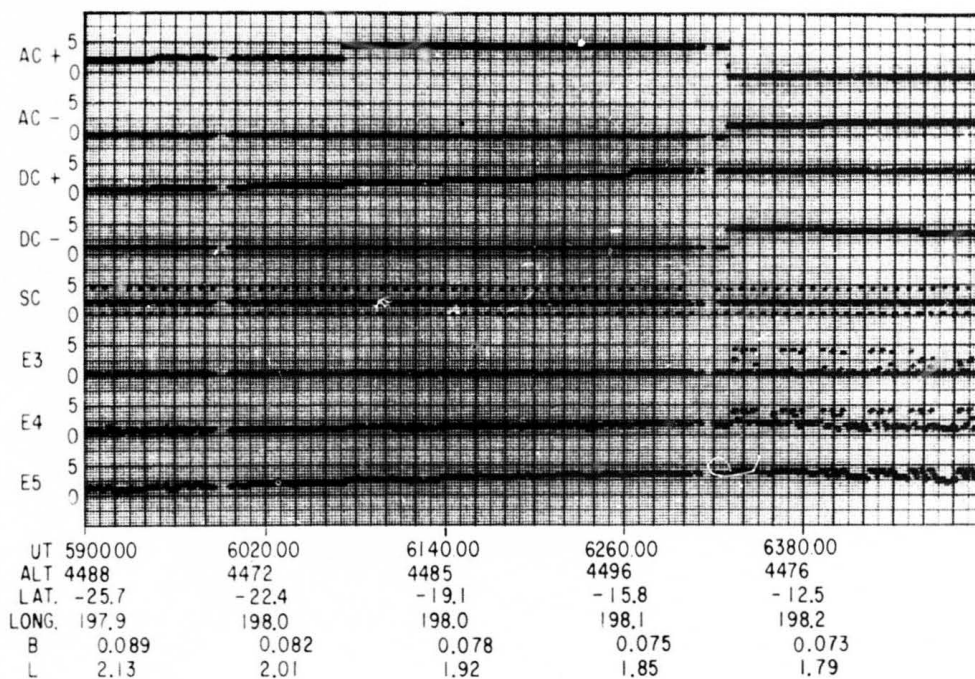
Fig. 45. OV3-3 Faraday Cup Data Showing a Slight
Increase in Background Level as +DC
Voltage Increases

longitude 198 deg E; B = 0.08 gauss, and L = 2.0. As can be seen, this apparent flux had no angular dependence. Similar outputs have been noted in the laboratory when the instrument was insufficiently outgassed. Hence, an upper limit to the proton fluxes on the two revs is between 2.3×10^5 and 5.0×10^5 cm^{-2} sec^{-1} $-sr^{-1}$ $-keV^{-1}$, depending upon energy.

The electron mode was sensitive to solar UV. This effect was to be expected and was due to the reflected UV that illuminated the backside of the negative high-voltage modulating grid. In general, we would expect the effect to decrease at higher voltages, because the ratio of the AC modulating voltage to the DC controlling voltage decreases. This effect is shown in Fig. 46. This sensitivity to UV in the electron mode had been recognized (Mozer, et al., 1962) and is an unfortunate characteristic of this instrument.

On one auroral zone crossing, however, auroral electron fluxes were observed. These data are shown in Fig. 47. In addition to the solar contamination, an isotropic flux can be seen in the 4.6 keV and 6.3 keV electron channels. If we refer to the calibration curves, we find that an output of 2.5 V in E4 corresponds to a flux of 3.4×10^6 cm^{-2} $-sec^{-1}$ $-sr^{-1}$ $-keV^{-1}$. At this time, Kp was 3, which is consistent with other auroral measurements.

It should be mentioned that, at altitudes below approximately 1000 km, there was a pronounced sagging of the positive high voltage. An example of this effect is shown in Fig. 48, where there is an approximate 30-sec period in the positive high-voltage monitor that is out of phase with the outputs in E5 and E4. The sagging of the high voltage is due presumably to a large flux of thermal electrons, and the effect has been reproduced in the laboratory with a current of about 2 μA. When the positive DC voltage drops below the AC modulating voltage, positive ions down to zero energy are accepted by the instrument.
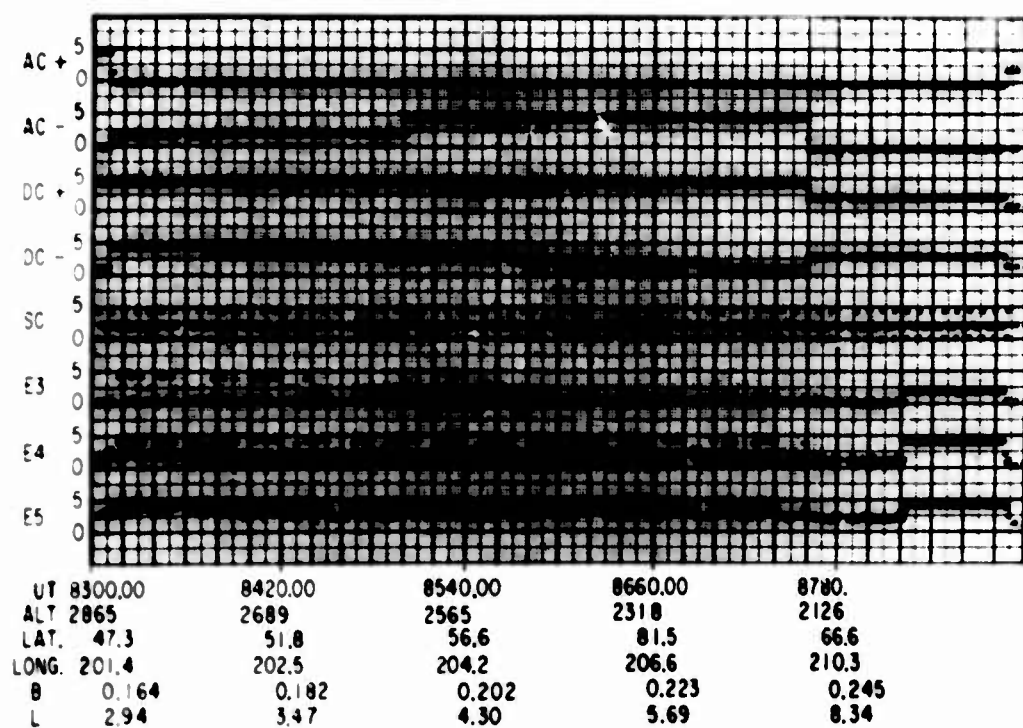
Fig. 46. OV3-3 Faraday Cup Data Showing Sensitivity
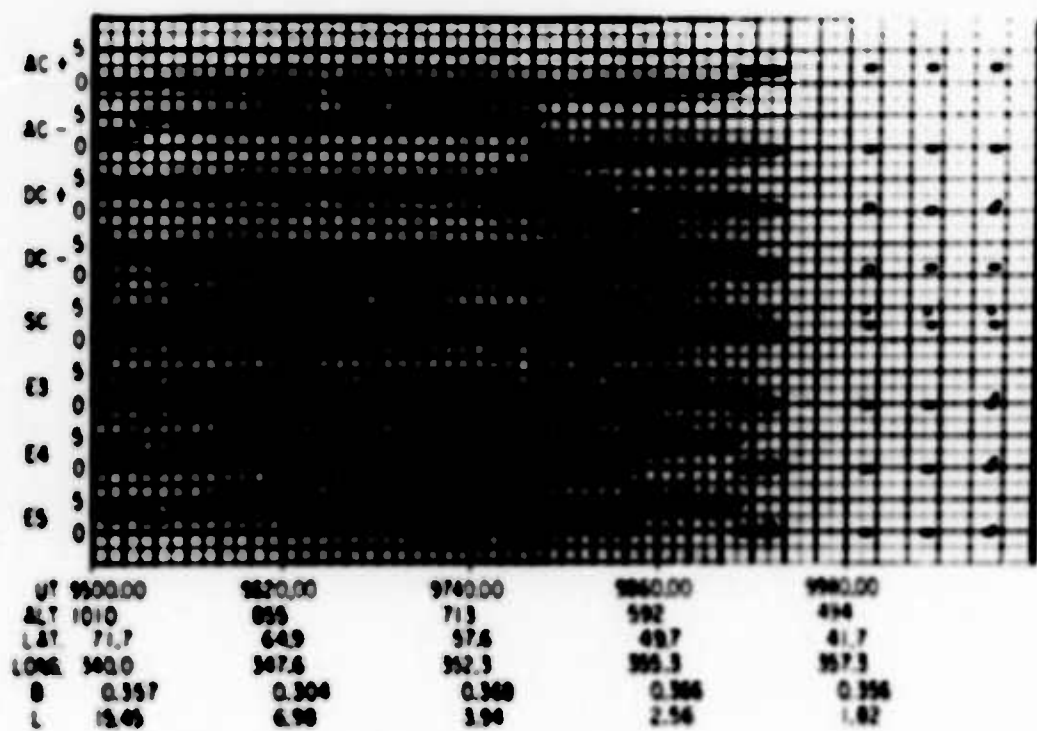to Solar UV in the Electron Mode

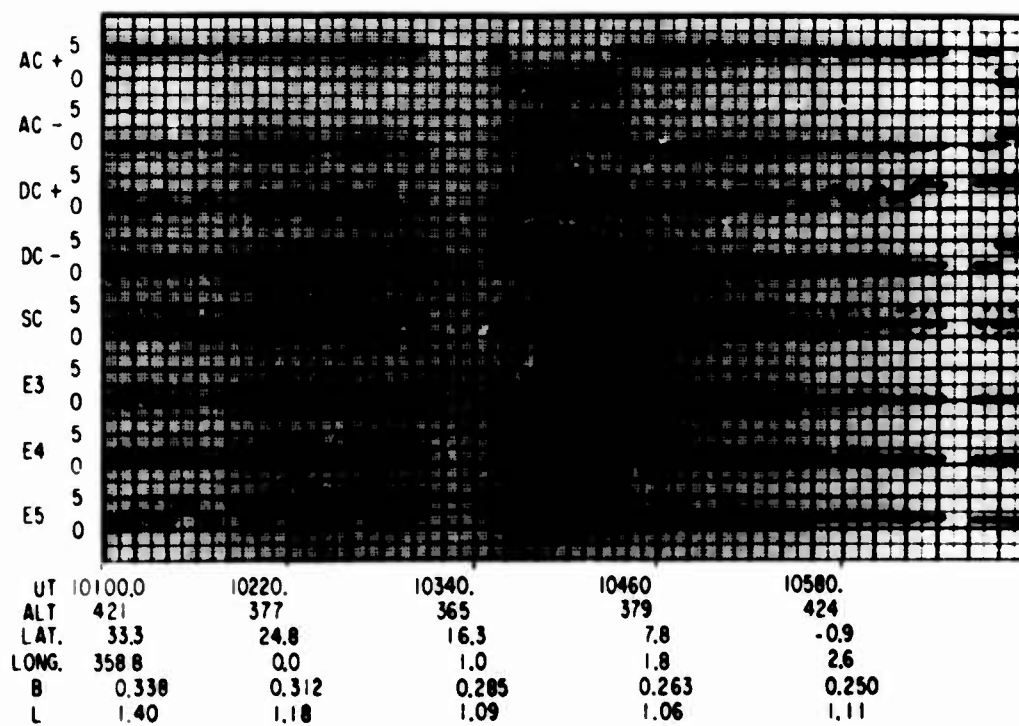**Fig. 47. OV3-3 Faraday Cup Data Showing Auroral Electrons at 9600 UT**

Fig. 48. OV3-3 Faraday Cup Data Showing a Sag in +DC Voltage as Large Outputs are Observed in E5 Due Presumably to Large Fluxes of Thermal Electrons

Additionally, an attempt was made to correlate the sagging of the positive DC voltage with the atmospheric ram. In Fig. 49, we have plotted the average value of the positive DC monitor voltage and the logarithm of the ram pressure vs time for one perigee pass - rev 277. The basis for the ram pressure calculation was the assumption of a CIRA model atmosphere (CIRA, 1965) with S = 150. This was multiplied by the velocity of the satellite and the sine of the angle between the assumed spin direction and the velocity vector. The asymmetry of the sag in the positive DC voltages is typical.

In summary, the presumed failure of the preamplifier is indicated by the lack of calibration output. Also, the sagging of the positive high-voltage supplies was ram-induced, which resulted in improved circuitry for the succeeding satellites.

C. OV1-14

Another Faraday cup detector was launched from Vandenberg Air Force Base on USAF satellite OV1-14 in April 1968. The orbit was highly elliptical, with an apogee of 9941 km, a perigee of 556 km, and an inclination of 100 deg. Initially, perigee was 4.4 deg S, which precessed northward at 0.75 deg/day and occurred at 1:20 a.m. LT. The orbital period was 208 min.

Failure of the spacecraft power system resulted in no data being received after rev 37, at which time the spin period had increased to 30 rpm, up from the normal 9 rpm. The instrument was turned on at rev 11; hence, we received four complete playback revs of usable data.

During these four revs, which represented 16 hours of data, the instrument operated normally and the values of the voltage monitors were as measured in the laboratory. As before, however, the positive DC high-voltage grid sagged at perigee due to a presumed flux of thermal electrons, and the instrument was still sensitive to solar UV in the electron mode.

Some 1200 sec of data taken during rev 16 playback, plus many features of the OV1-14 instrument, are shown in Figs. 50 and 51. The top four graphs show the four high-voltage monitors: AC+, AC-, DC+, and DC-. Next is the 8-point subcommutator. The final three graphs are the high-gain outputs; E3, E4, and E5.
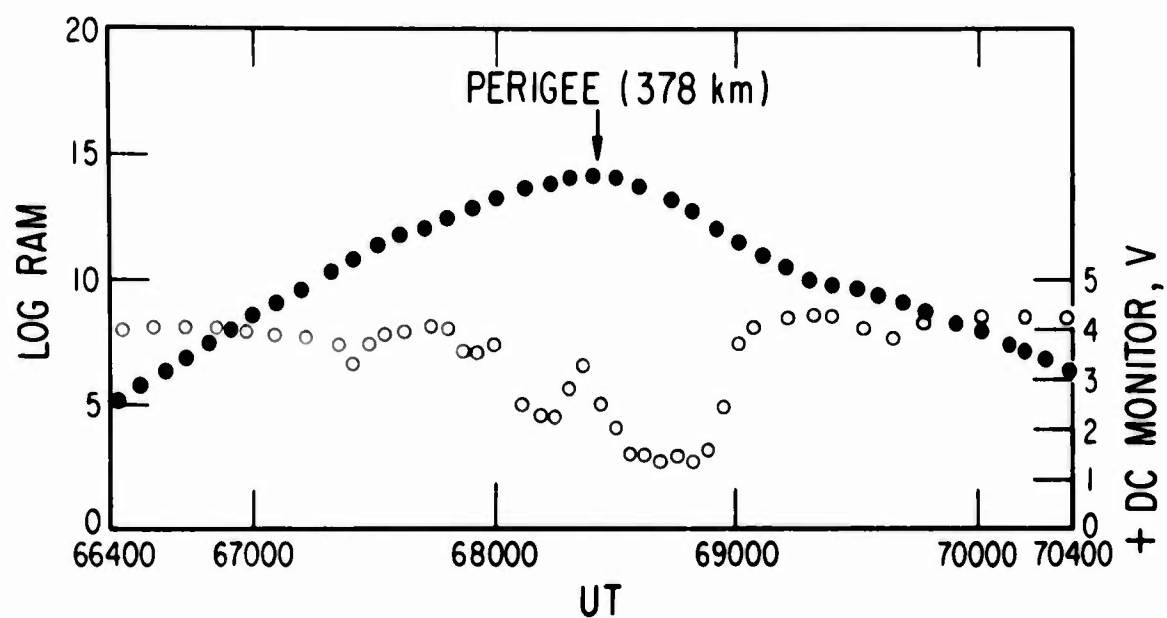
Fig. 49. OV3-3 Faraday Cup Data Showing the
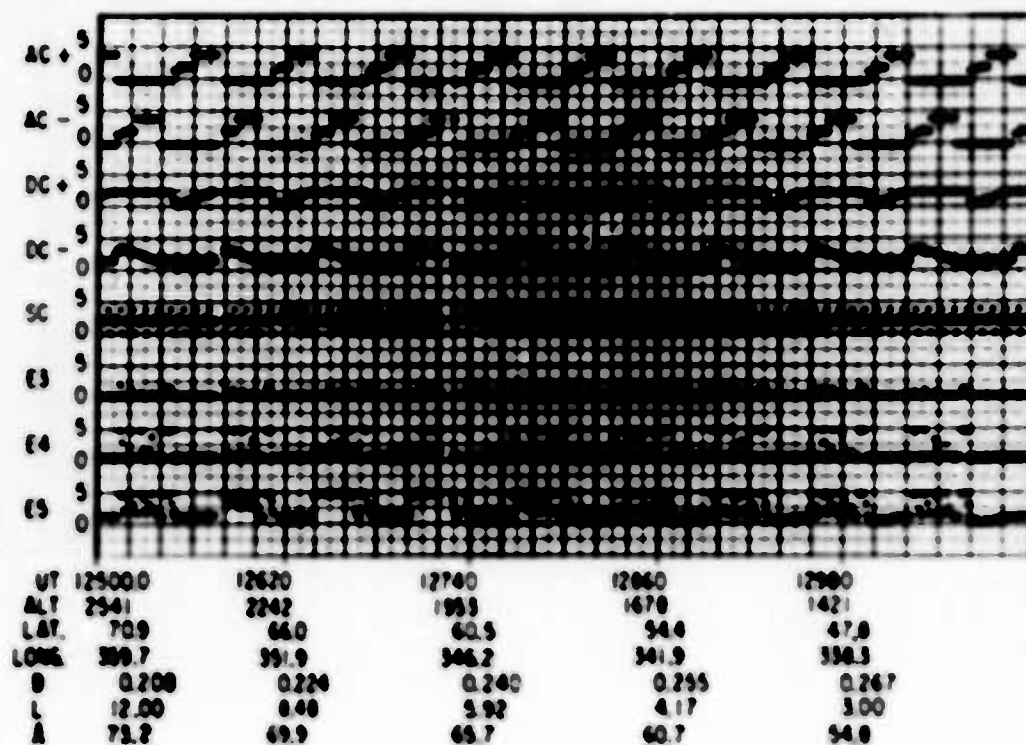Correlation of Ram Pressure with +DC
Voltage During Perigee

Fig. 50.   OV1-14 Faraday Cup Data Showing Auroral
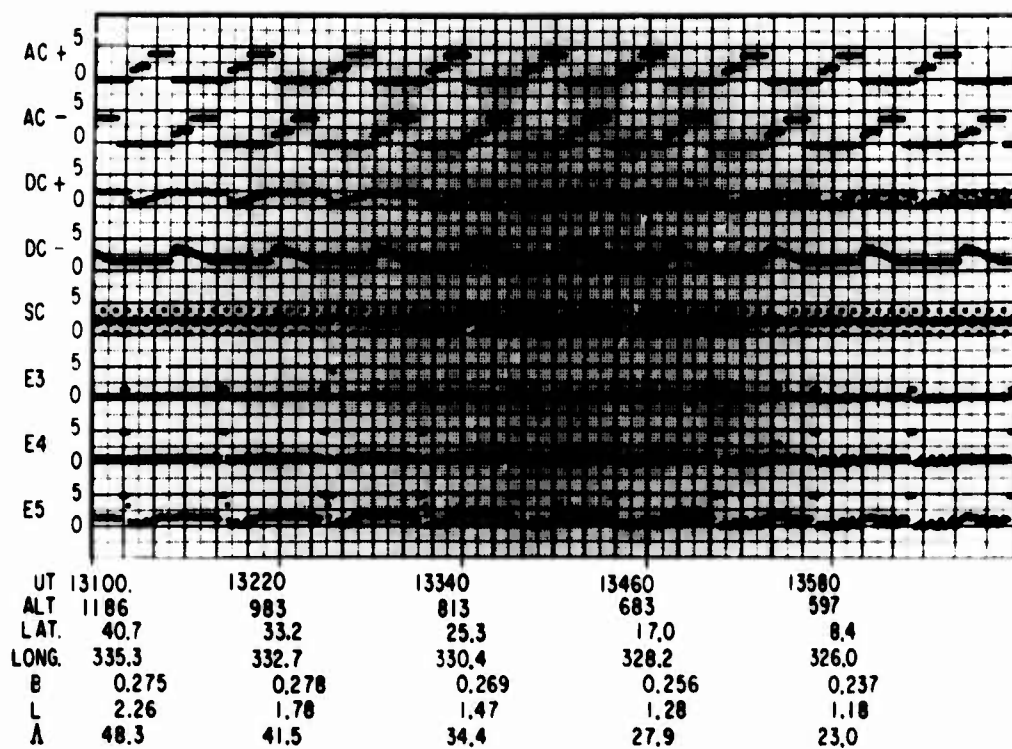Electrons at 12700 UT

Fig. 51. OV1-14 Faraday Cup Data Showing a Sag in +DC
Voltage as Large Outputs are Observed in E5
Due Presumably to Large Fluxes of Thermal
Electrons

Of the five voltage monitors, all but the DC+ monitor appear normal during this time period. The DC+ monitor begins to sag, with a once-per-spin period modulation, at approximately 13100 universal time (UT) and at an altitude of 1187 km, and continues to do so down to perigee altitude, 550 km, at 13700 UT. This sagging results in a negative output during the proton cycle as shown by the output of E5, E4, and even E3 during this period.

It is evident from these two graphs that there is no output during the proton mode of the instrument except during the time when the DC+ high voltage is sagging. In fact, no proton fluxes were observed for the 16 hr of data. Thus, these proton measurements do not agree with the results of 1964-45A. As will be shown below, the electron measurements agree with those of other satellites; hence, we believe the OV1-14 results are correct (Hilton and Stevens, 1968).

Another feature is the instrument's sensitivity to UV radiation as shown by the once-per-period sun-spike in the electron mode that continues up to 13100 UT, at which time the spacecraft entered the earth's shadow.

Finally, examination of the four electron cycles that began at 12560 UT shows a marked increase in the low-energy electron flux, which is clearly evident even in the presence of solar UV contamination. If we refer to the ephemeris listed at the bottom of Fig. 50, this flux occurs between L-values of 9 and 5 and is clearly auroral precipitation. This precipitation is seen on the four revs for which we have data.

The electron data have been examined and all shown in Fig. 52. Here is shown the extent of auroral electron precipitation as a function of magnetic time and invariant latitude. These data are from eight polar passes, four over each pole. The OV1-14 threshold for electrons is 5×10^7 electrons-cm^{-2}-sec^{-1}-sr^{-1}-keV^{-1}. Electron precipitation from the OV1-15 (SPADES) low-energy electrostatic analyzer, as well as from the OGO IV (Hoffman, 1969) and Aurora I (Burch, 1968) satellites, is presented for comparison. The agreement is extremely good and confirms the successful operation of this instrument.
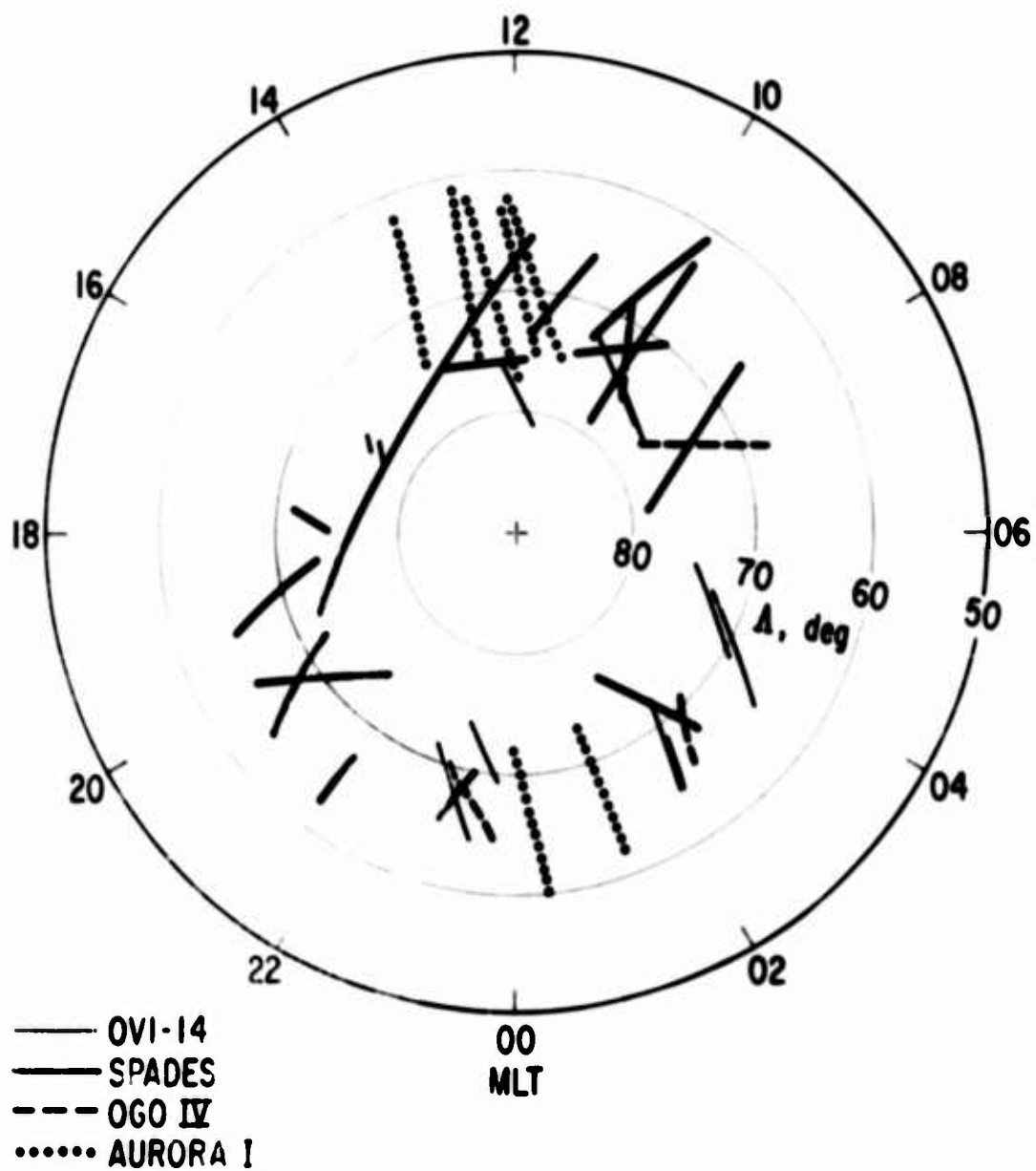
Fig. 52. Electron Auroral Zones Showing Data from the OV1-14 Faraday Cup and the OV1-15 Electrostatic Analyzer, as well as Data from OGO IV and Aurora I

In summary:

1. No fluxes of protons were observed; hence, those reported from 1964-45A were presumably in error.

2. The measured extent of the electron auroral zone is consistent with that measured by Aerospace on OV1-15, Goddard Space Flight Center on OGO IV, Rice University on Aurora I, and other experiments.

3. The sensitivity of the instrument to photo-electrons from solar UV and the sagging of the DC+ high-voltage grid to presumed thermal electrons were still present.

D. OV1-15

On 11 July 1968, the OV1-15 satellite (SPADES) was launched from Vandenberg Air Force Base into a near polar orbit at 1130 hr LT. Initially, the spin rate was 9 rpm, and the spin direction was perpendicular to the orbit plane. Apogee was at 1815 hr and perigee at 0158 hr (Carter, et al., 1969).

Measurement of particle heating sources was achieved with two electro-static analyzers and a Faraday cup detector. These three instruments were used to measure electrons and protons in the range from 1 to 10 keV. Much interesting data have come from the electrostatic analyzers (Hilton, et al., 1969; Cornwall, et al., 1970; Mizera, et al., 1970; Hilton, et al., 1970; Cornwall, et al., 1971; Mizera and Hilton, 1971; and Morse, et al., 1971). In this report, however, we have concentrated only on the results obtained by means of the Faraday cup detector.

Four typical auroral zone crossings are shown in Figs. 53 through 56. The normal programming of the instrument is seen in all four revs, with the absence of any detectable proton flux above threshold clearly evident. Finally, the occurrence of low-energy electrons at these auroral zone crossings is seen.

Fig. 53. OV1-15 Faraday Cup Data Showing Auroral
Electrons at 84920 UT

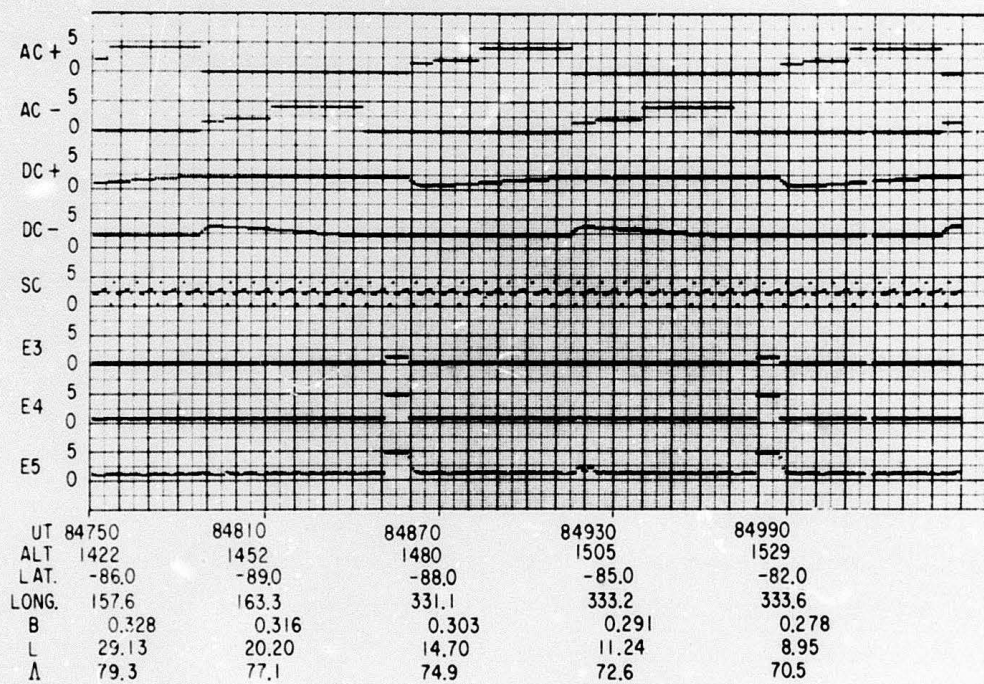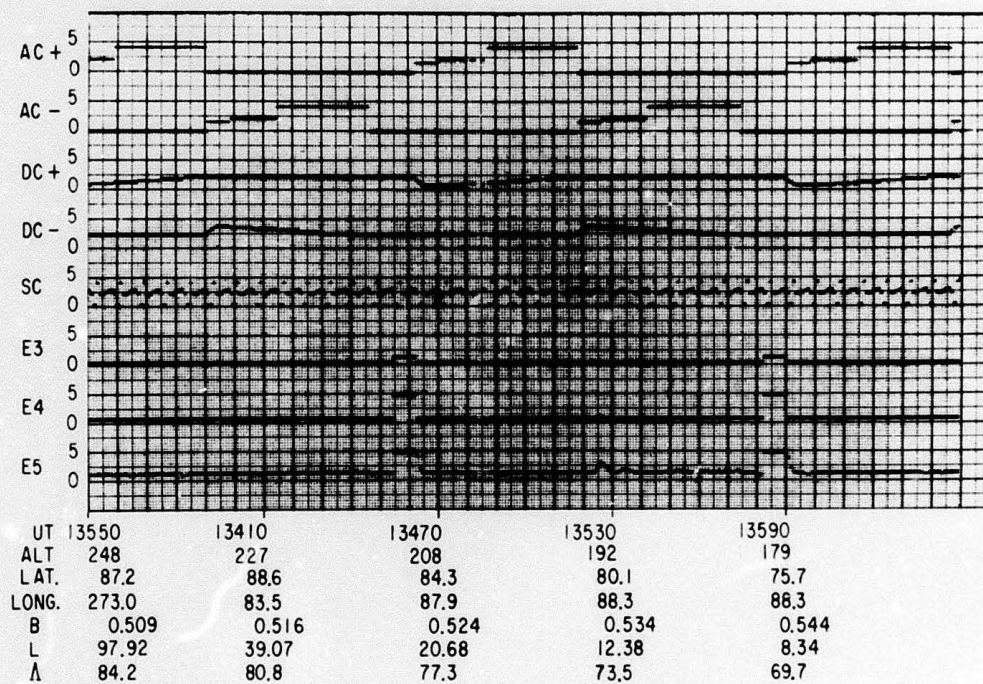| UT	13550	13410	13470	13530	13590
ALT.	248	227	208	192	179
LAT.	87.2	88.6	84.3	80.1	75.7
LONG.	273.0	83.5	87.9	88.3	86.3
B	0.509	0.516	0.524	0.534	0.544
L	97.92	39.07	20.68	12.38	8.34
Λ	84.2	80.8	77.3	73.5	69.7

Fig. 54. OV1-15 Faraday Cup Data Showing Auroral
Electrons at 13530 UT
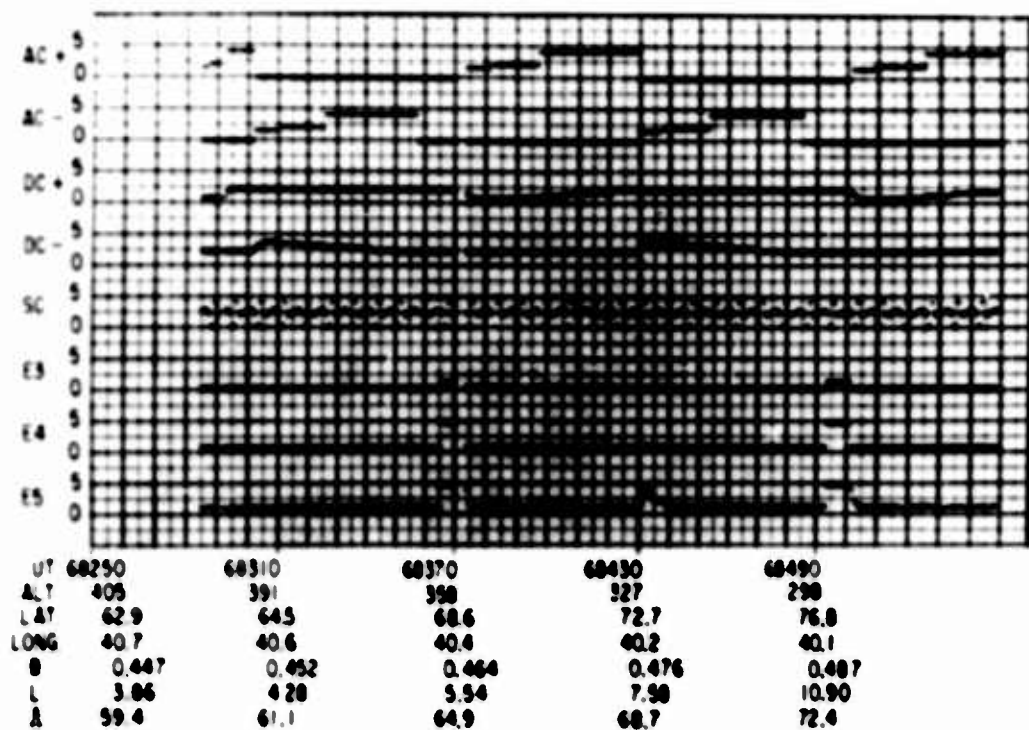
Fig. 55. OV1-15 Faraday Cup Data Showing Auroral
Electrons at 68430 UT

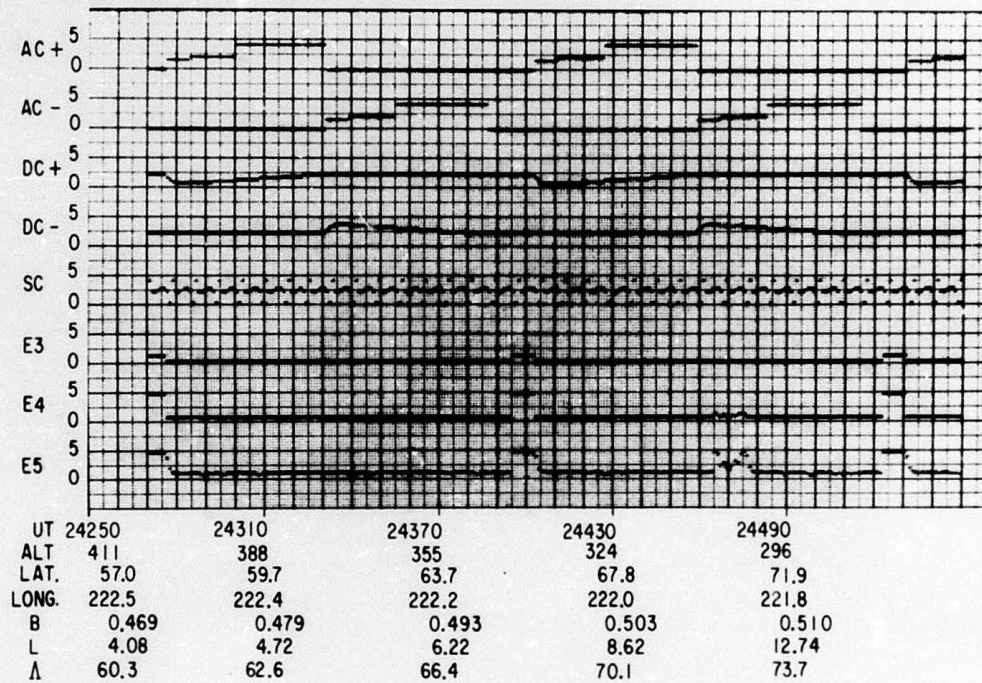| UT	24250	24310	24370	24430	24490
ALT	411	388	355	324	296
LAT.	57.0	59.7	63.7	67.8	71.9
LONG.	222.5	222.4	222.2	222.0	221.8
B	0.469	0.479	0.493	0.503	0.510
L	4.08	4.72	6.22	8.62	12.74
Λ	60.3	62.6	66.4	70.1	73.7

Fig. 56.   OV1-15 Faraday Cup Data Showing Auroral
Electrons at 24470 UT

These four auroral zone crossings, along with the magnetic coordinates
B, L, and λ at which the data were collected, are presented in Table VIII. In
addition, the flux measured in the lowest energy step (2.5 keV) of the electron
electrostatic analyzer is presented in Table VIII. The Faraday cup data are at
1.3 keV; hence, the agreement between these two instruments is reasonable.
The sensitivity of the Faraday cup was not sufficient for this environment.

The absence of large fluxes of low-energy protons was again consistent
with the measurements of OV1-14 and in disagreement with those of 1964-45A.

Table VIII. Five Auroral Zone Crossings

Revolution	Universal Time	Magnetic Time	Magnetic Coordinate			Differential Flux $(cm^{-2}-sec^{-1}-sr^{-1}-keV^{-1})$	
			B	L	λ	Faraday Cup at 1.2 keV	Electrostatic Analyzer at 2.5 keV
307	84920	20.1	0.29	11.8	73.1	2.0×10^{8}	1.9×10^{7}
352	13520	9.7	0.53	13.5	74.2	2.3×10^{8}	1.9×10^{7}
366	68430	22.8	0.48	7.6	68.7	3.4×10^{8}	7.4×10^{7}
382	24470	19.8	0.51	11.4	72.7	6.8×10^{8}	7.4×10^{7}

E. OV2-5

In September 1968, the last Faraday cup detector was launched from Cape
Kennedy on USAF satellite OV2-5. The orbit was nearly synchronous and
equatorial, with an apogee of 19308 n mi and a perigee of 18956 n mi.

Because of partial failure of the spacecraft telemetry system, only a small
amount of Faraday cup data was obtained. One interesting data acquisition was
received, however, and it will be discussed in the paragraphs that follow.

On 11 October 1968, we obtained almost one continuous hour of Faraday
cup data from 11400 to 14400 UT (1:50 to 2:50 LT). The instrument was in its
slow mode — 64 sec/step or 1024 sec/cycle. The outputs of the instrument for
the three cycles of this acquisition are shown in Fig. 57. At the top of each
of the three portions of the figure are the four high-voltage monitors, then
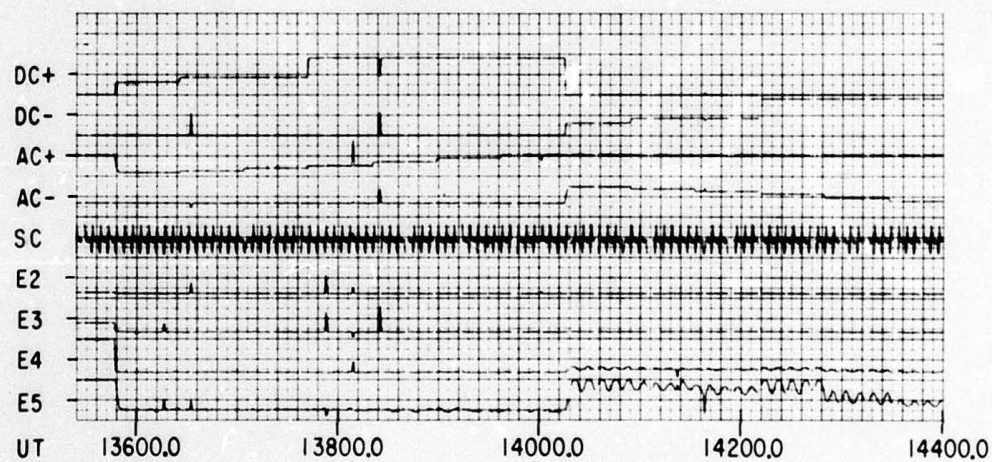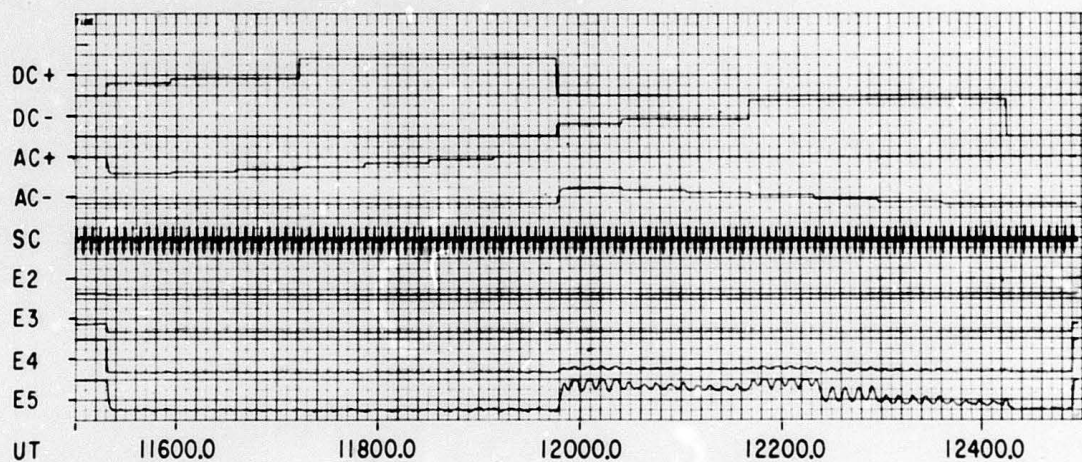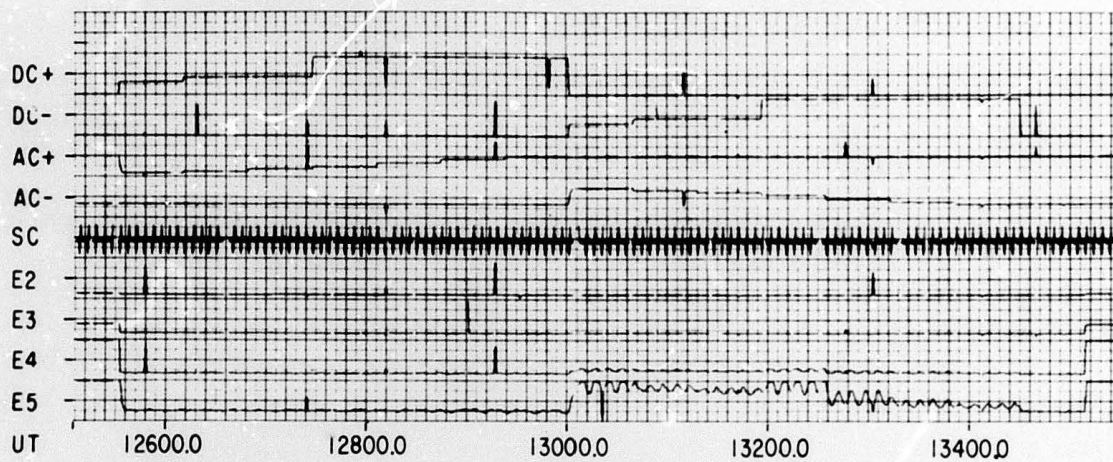the subcommutator monitor, and at the bottom the four output voltages.

Fig. 57. OV2-5 Faraday Cup Data Showing Low-Energy
Electrons at L = 6.6

Two things should be noticed in this acquisition. The first is the absence of any detectable proton flux above threshold, 2.5×10^6 protons-cm^{-2}-sec^{-1}-sr^{-1} at an energy of 0.74 keV. Secondly, the constancy of the electron spectrum on these three successive cycles, 17 min apart, is striking.

It should be stated that these measurements were taken at an exceptionally quiet time. For the 3-hr period during which these data were taken, K_p was 0_o. In fact, the maximum value of K_p for the preceding 12 hr was $1-$.

The electron spectrum obtained from these three data cycles is shown in Fig. 58. For comparison, an energy spectrum as measured by Schied, et al. (1970), on OGO-3 on 23 June 1966 is also shown. Several parameters that influence these data are presented in Table IX. The close agreement between these two electron spectra suggests perhaps a steady quiet time electron flux at synchronous altitudes. It is unfortunate that this one long acquisition contained the only complete cycle of the data received from OV2-5.

Table IX. Parameters that Influence the Electron Spectra

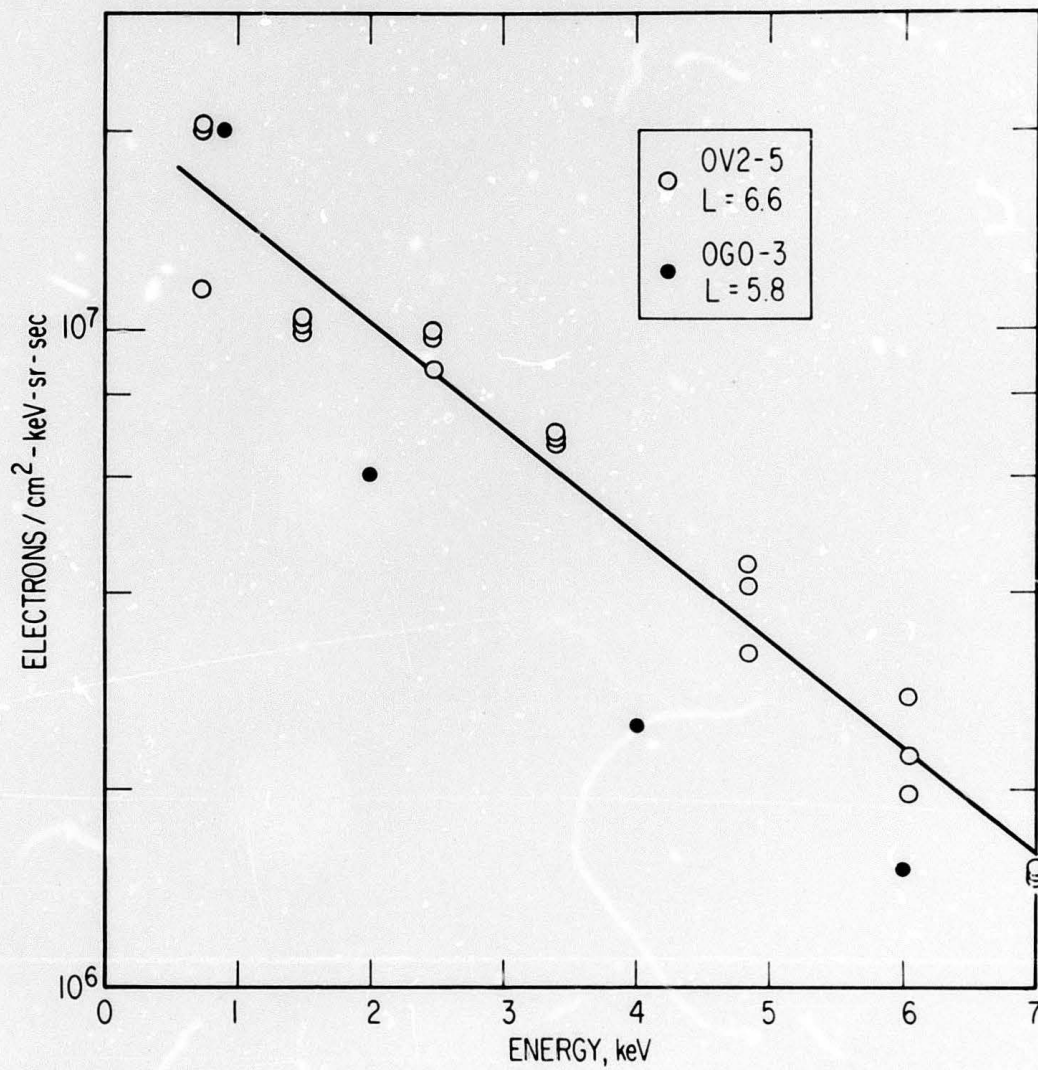| Parameter	OV2-5	OGO-3
Date	10-11-68	6-23-66
K_p	0_o	0_o
Max K_p in previous 12 hr	$1-$	2_o
Local time	2:00	0:30
L	6.6	5.8

Fig. 58.   Comparison of OV2-5 and OGO-3 Electron
Spectra at Synchronous Altitude

VII. CONCLUSIONS

A significant amount of effort has gone into this program since the initiation of the first Faraday cup detector in 1961 until the last Faraday cup detector was flown on OV2-5 in 1968.

Although chance played a large part in the failure of many satellites that would have affected the direction of this program, it is clear in retrospect that the study of low-energy-charged particles should have been broadened at an earlier date to include the development of other instrumentation, such as electrostatic analyzers.

The possible large fluxes of 4 keV protons, which were measured by the satellite 1964-45A, have continued to be a mystery. The two satellites OV1-14 and OV1-15, in similar orbits, did not encounter such fluxes. It appears, therefore, that the 1964 measurements were a characteristic of the time period, the instrument, or simply in error. As this report is being concluded, however, Heikkila (1970) on ISIS-1, reports large fluxes of soft particles near the equator. Thus, the resolution of this mystery is still in doubt.

PRECEDING PAGE BLANK

REFERENCES

Bader, M., "Preliminary Explorer 12 Data on Protons Below 20 keV,"
J. Geophys. Res. 67, 5007 (1962).

Bonetti, A., H. S. Bridge, A. J. Lazarus, B. Rossi, and F. Scherb,
"Explorer 10 Plasma Measurements," J. Geophys. Res. 68,
4017 (1963).

Bridge, H. S., A. J. Lazarus, E. F. Lyon, B. Rossi, and F. Scherb,
"Plasma Probe Instrumentation on Explorer X," Space Research III,
ed. W. Priester, North-Holland Publishing Company, Amsterdam,
Netherlands, p. 1113 (1963).

Burch, J. I., "Low-Energy Electron Fluxes at Latitudes Above the Auroral
Zone," J. Geophys. Res. 73, 3585 (1968).

Carter, V. L., B. K. Ching, and D. D. Elliott, "Atmospheric Density
Above 158 Kilometers Inferred from Magnetron and Drag Data From
the Satellite OV1-15 (1968-059A)," J. Geophys. Res. 74, 5083 (1969).

CIRA, 1965, Cospar International Reference Atmosphere 1965, North-
Holland Publishing Company, Amsterdam, Netherlands (1965).

Cornwall, J. M., H. H. Hilton, and P. F. Mizera, "Observations of
Precipitating Ring Current Protons," EOS, Trans. Amer. Geophys.
Union 51, 807 (1970).

Cornwall, J. M., H. H. Hilton, and P. F. Mizera," Observations of
Precipitating Protons in the Energy Range 2.5 keV≤ E≤200 keV,"
J. Geophys. Res. 76, to be published.

Elliott, D. D., M. A. Clark, and J. E. Blamont, "A. Satellite Search for
the 6300-A Tropical Arcs," Trans. Am. Geophys. Union 44, 37 (1963).

Frank, L. A., "Several Observations of Low-Energy Protons and Electrons
in the Earth's Magnetosphere with OGO 3," J. Geophys. Res. 72,
1905 (1967).

Freeman, J., "Detection of an Intense Flux of Low-Energy Protons or
Ions Trapped in the Inner Radiation Zone," J. Geophys. Res. 67,
921 (1962).

Gringauz, K. I., V. V. Bezrukikh, V. D. Ozerov, and R. E. Rybchinskii,
"A Study of Interplanetary Ionized Gas, Energetic Electrons and Solar
Corpuscular Radiation Using Three-Electrode Charged Particle Traps
on the Second Soviet Cosmic Rocket," Dok. Akad. Nauk SSSR 131,
1301 (1960).

Harris, I. and W. Priester, Theoretical Models for the Solar-Cycle-Variation of the Upper Atmosphere, NASA Goddard Space Flight Center and Institute for Space Studies (1962).

Heikkila, W. J., "Soft Particle Fluxes Near the Equator," J. Geophys. Res. 76, 1076 (1971).

Hilton, H. H., J. R. Stevens, and A. L. Vampola, "Observations of Large Fluxes of Low Energy Protons," Trans. Amer. Geophys. Union 45, 602 (1964).

Hilton, H. H. and J. R. Stevens, "Low-Energy Protons," Trans. Amer. Geophys. Union 49, 720 (1968).

Hilton, H. H., P. F. Mizera, W. A. Kolasinski, and J. R. Stevens, "Global Measurements of Low Energy Protons and Electrons at Low Altitudes," EOS, Trans. Amer. Geophys. Union 50, 284 (1969).

Hilton, H. H., P. F. Mizera, and J. R. Stevens, "High Latitude Phenomena of Low Energy Protons and Electrons," EOS, Trans. Amer. Geophys. Union 51, 405 (1970).

Hilton, H. H., P. F. Mizera, and J. R. Stevens, "A Comprehensive Description of the Auroral Oval," EOS, Trans. Amer. Geophys. Union 51, 807 (1970).

Hilton, H. H., J. R. Stevens, and A. L. Vampola, "Measurement of Fluxes of Low-Energy Protons and Electrons with a Faraday Cup Detector," Compilation of Scientific Results from the SSD/Aerospace Radiation Monitoring Satellite 1964-45A, prepared by S. C. Freden, Report TDR-669(6260-20)-5, The Aerospace Corporation (1966).

Hoffman, R. A., "Low-Energy Electron Precipitation at High Latitudes," J. Geophys. Res. 74, 2425 (1969).

Hoffman, R. A., L. R. Davis, and J. M. Williamson, "Protons of 0.1 to 5 Mev and Electrons of 20 kev at 12 Earth Radii during Sudden Commencement on September 30, 1961," J. Geophys. Res. 70, 5001 (1962).

McIlwain, C. E., "Direct Measurement of Particles Producing Visible Auroras," J. Geophys. Res. 65, 2727 (1960).

Mizera, P. F., J. B. Blake, H. H. Hilton, and M. K. Hudson, "High Energy Proton Losses into the Atmosphere," EOS, Trans. Amer. Geophys. Union 51, 808 (1970).

Mizera, P. F. and H. H. Hilton, "Atmospheric Heating by Precipitating Energetic Particles," Symposium on the Upper Atmosphere: Results and Interpretation of OV1-15 Data, compiled by F. A. Morse, Report TR-0059(6260-10)-6, The Aerospace Corporation (1971).

Morse, F. A., H. H. Hilton, and P. F. Mizera, "Polar Ionosphere: Measured Ion Density Enhancements and Concomitant Soft Electron Precipitation," J. Geophys. Res. 76, to be published.

Mozer, F. S., A. Lawrence, and G. S. Gayron, Flight-Type Faraday Cup Detector, Report TRD-930 (2260-23) TR-1, The Aerospace Corporation (1962).

Prag, A. B., F. A. Morse, and R. J. McNeal, "Nightglow Excitation and Maintenance of the Nighttime Ionosphere by Low Energy Protons," J. Geophys. Res. 71, 3141 (1966).

Schield, M. A. and L. A. Frank, "Electron Observations Between the Inner Edge of the Plasma Sheet and the Plasmasphere," J. Geophys. Res. 75, 5401 (1970).

Stevens, J. R., H. H. Hilton, and A. L. Vampola, "Observations of Low-Energy Electrons at Large L-Values," Trans. Amer. Geophys. Union 45, 602 (1964).

Vernov, S. N., V. V. Melnikov, I. A. Savenko, and B. I. Savin, "Measurements of Low-Energy Particle Fluxes from the Cosmos and Electron Satellites," Space Research VI, ed. R. F. Smith-Rose, Spartan Books, Washington, D. C., p. 746 (1966).